Enhancing Fault Ride Through the Capability of a Grid-Connected PMSG-based Wind Energy Conversion System

Gutema Gudunfa Jaldu

A Thesis Submitted to

The Department of the Electrical Power and Control Engineering

School of Electrical Engineering and Computing

Presented in Partial Fulfilment of the Requirement for the Degree of Masters in Electrical Power and Control Engineering (Control Engineering)

Office of Graduate Studies

Adama Science and Technology

Septemeber, 2024

Adama, Ethiopia

Enhancing Fault Ride Through the Capability of a Grid-Connected PMSG-based Wind Energy Conversion System

Gutema Gudunfa Jaldu

Advisor: Dr Endalew Ayenew

A Thesis Submitted to

The Department of the Electrical Power and Control Engineering

School of Electrical Engineering and Computing

Presented in Partial Fulfilment of the Requirement for the Degree of Masters in Electrical Power and Control Engineering (Control Engineering)

Office of Graduate Studies

Adama Science and Technology

September, 2024

Adama, Ethiopia

DECLARATION

I hereby declare that this Master Thesis entitled "**Enhancing Fault Ride Through the Capability of a Grid-Connected PMSG-based Wind Energy Conversion System**" is my original work. That is, it has not been submitted for the award of any academic degree, diploma, or certificate in any other university. All sources of materials that are used for this thesis have been duly acknowledged through citation.

________________________	____________	________________
Name of the student	Signature	Date

RECCOMENDATION OF ADVISOR

I, the advisor of this thesis, hereby certify that I have read the revised version of the thesis entitled "**Enhancing Fault Ride Through the Capability of a Grid-Connected PMSG-based Wind Energy Conversion System**" prepared under my guidance by **Gutema Gudunfa** submitted in partial fulfilment of the requirements for the degree of Masters of Science in control system engineering. Therefore, I recommend the submission of a revised version of the thesis to the department following the applicable procedures.

______________________	__________________	_________________________
Advisor	Signature	Date

APPROVAL OF BOARD OF REVIEWERS

I, the advisor of the thesis entitled "**Enhancing Fault Ride Through the Capability of a Grid-Connected PMSG-based Wind Energy Conversion System**" and developed by **Gutema Gudunfa**; hereby certify that the recommendation and suggestions made by the board of examiners are appropriately incorporated into the final version of the thesis.

Name of Advisor	Signature	Date

We, the undersigned, members of the Board of Examiners of the thesis by **Gutema Gudunfa** have read and evaluated the thesis entitled "**Enhancing Fault Ride Through the Capability of a Grid-Connected PMSG-based Wind Energy Conversion System**" developed by **Gutema Gudunfa**" and examined the candidate during open defence. This is, therefore, to certify that the thesis is accepted for partial fulfilment of the requirement of the degree of Masters of Science in control system engineering.

Chairperson	Signature	Date
Internal examiner	Signature	Date
External examiner	Signature	Date

Final approval and acceptance of the thesis are contingent upon the submission of its final copy to the Office of Postgraduate Studies (OPGS) through the Department Graduate Council (DGC) and the school graduate committee (SGC).

Department Head	Signature	Date
School Dean	Signature	Date
Office of postgraduate studies, Dean	Signature	Date

ACKNOWLEDGEMENT

I am profoundly thankful to the all-powerful God for allowing me steadfast resilience and direction during the arduous journey of my thesis. I extend my profound gratitude to my esteemed Major Advisor, Dr Endalew Ayenew, whose remarkable proficiency, motivation, and unwavering encouragement have significantly influenced the culmination of the thesis. His unwavering care and inspiration have been pivotal in steering me towards achievement. Lastly, I wish to convey heartfelt appreciation and blessings to my family and all individuals who offered help and encouragement throughout my thesis endeavours.

TABLE OF CONTENTS

DECLARATION i
RECCOMENDATION OF ADVISOR ii
APPROVAL OF BOARD OF REVIEWERS iii
ACKNOWLEDGEMENT iv
TABLE OF CONTENTS v
LIST OF TABLE ix
LIST OF FIGURES x
ABBREVIATION AND ACRONYMS xii
ABSTRACT xiv
CHAPTER ONE 1
INTRODUCTION 1
1.1 Background of the study 1
1.2 Statement of the Problem 3
1.3 Objective 4
1.3.1 General objective 4
1.3.2 Specific Objective 4
1.4 Motivation of the Study 5
1.5 Scope of the thesis 5
1.6 Limitation of the Thesis 5
1.7 Significance of the Study 5
1.8 Thesis Organization 6
CHAPTER TWO 7
LITERATURE REVIEW 7
2.1 Theoretical Background of Wind Energy Conversion Systems 7
2.1.1 Wind Turbines and Its Classification. 7
2.2 Wind Turbine Generators 10

2.2.1 Squirrel Cage Induction Generator (SCIG).. 10

2.2.2 Wound Rotor Induction Generator (WRIG)... 11

2.2.3 Double Feed Induction Generator (DFIG)... 11

2.2.4 Permanent Magnet Synchronous Generator (PMSG).. 12

2.3 Control Techniques for a Wind Turbines Generator System 12

2.3.1 Pitch angle Control... 13

2.3.2 Maximum Power Point Tracking Control (MPPT).. 13

2.4 Fault ride through capability and types of faults 13

2.4.1 Type of Faults... 14

2.5 Power Transformer 16

2.6 Review of the Related Work 18

CHAPTER THREE 20

METHODOLOGY 20

3.1 Introduction.. 20

3.2 Materials 20

3.3 Modelling of Wind Energy Conversion... 21

3.3.1 Modelling of Aerodynamic Wind Turbine 21

3.4 Modelling of Pitch Actuator 27

3.5 Modelling of Permanent Magnet Synchronous Generator 28

3.5.1 Modelling Permanent Magnet Synchronous Generator in a Synchronously Rotating a-b-c Axis Reference Frame 29

3.5.2 Modelling Permanent Magnet Synchronous Generator in a Synchronously Rotating d-q Axis Reference Frame 32

3.5.3 Power and Torque Characteristics Permanent Magnet Synchronous Generator. 33

3.6 Mathematical Modelling of Back-To-Back Converters... 34

3.6.1 Mathematical Model of Machine Side AC-DC Converter 35

3.6.2 Mathematical Model of Grid Side DC-AC Converter 37

3.6.3 Dc Link Model 39

3.6.4 Model of LCL Filter 41

3.7 Mathematical Modelling of the STATCOM and Its operation 46

3.8 Controllers Design 49

3.8.1 Pitch Actuator Controller 49

3.8.2 Convertor Controller 51

3.8.3 Inverter Controller 58

3.8.4 STATCOM Controller 63

CHAPTER FOUR 68

RESULTS AND DISCUSSION 68

4.1 INTRODUCTION 68

4.1.1 Randomly generated wind speed 69

4.2 Wind Turbine and Pitch with Controller 71

4.2.1 Mechanical power 71

4.3 Three -phase Stator Voltages and Current from the PMSG 71

4.3.1 DC Link voltage from the rectifier 72

4.4 Grid Side Convertor during Normal Operation and Its Result 73

4.4.1 Three -phase Voltage and Current from Inverter before the three -phase Faults. 74

4.4.2 Three-phase Voltage and current from the grid before the Three-phase Fault. ... 75

4.5 Grid Side Convertor During different types of faults Operation and Its Result 75

4.5.1 Three- phase Voltages and Current from Inverter with L-G three -Phase Faults.76

4.5.2 Three-phase Voltages and current from grid with L-G Three- phase Fault. 77

4.5.3 Three -phase Voltages and current from Inverter with L-L-G three-phase Faults. 78

4.5.4 Three-phase Voltages and current from grid with L-L-G Three-phase Faults. ... 78

4.5.5 Three -phase Voltage and current from Inverter with 3L-G Three -phase Faults. 79

4.6 Three -phase Voltages and current from grid with 3L-G Three -phase Faults........... 80
4.7 Grid Side Converter during Different types of faults with STATCOM..................... 81
CHAPTER FIVE 83
CONCLUSION AND RECOMMENDATION 83
5.1 Conclusion 83
5.2 Recommendation 83
REFERENCE 85

LIST OF TABLE

Table 2-1: Specification of 690V/33KV Step-up Transformer.. 17

Table 2-2: Specification of 33KV/230KV Step-up Transformer...................................... 17

Table 3-1: Constant value of coefficient of power (Manyonge et al., 2012)...................... 26

Table 3-2: Wind Turbine Parameters 27

Table 3-3: Specification of LCL Parameters. 46

Table 3-4 : Tuning formulae of Ziegler Nichols (Pramujati et al., 2015).......................... 56

Table 3-5 Specification of the Designed converter controller... 58

Table 3-6: Specification of the Designed Inverter controller 63

Table 3-7 : Tuned PI controller gains 65

Table 3-8: Tuned PI controller for the DC voltage regulator 66

Table 3-9: Tuned Current regulators with PI controllers.. 67

LIST OF FIGURES

Figure 1-1: Arrangement of a PMSG-WT based WECS (Muisyo et al., 202_) 3
Figure 2-1:The wind turbines that rotate vertically (VAWTs) (Raouf et al., 2023).............. 8
Figure 2-2:The vertically oriented wind turbines (VAWTs) (Raouf et al., 2023)................. 9
Figure 2-3: Squirrel cage induction generator (Vijayaprabhu et al., 2021) 10
Figure 2-4: wound rotor induction generator (WRIG) connected to the grid (Elmorshedy, 2016)... 11
Figure 2-5: Grid-connected wind-generating system based on DFIG connected the grid .. 12
Figure 2-6: PMSG structure representation connected to the grid 12
Figure 2-7: Symmetrical faults 15
Figure 2-8: Scheme of L-G fault 15
Figure 2-9: Scheme of L-L-G 16
Figure 2-10: Scheme of L-L-G 16
Figure 3-1: Flow chart of methodology work activities 21
Figure 3-2 d-q and α-β standard salient pole synchronous machine (Azevedo, 2013) 29
Figure 3-3:Three phase AC-DC Active rectifier.((Keshavarz, 2011). 35
Figure 3-4 : Three phase inverter (Zheng et al., 2018) 38
Figure 3-5 :Dc-link model (Zouheyr et al., 2021) 40
Figure 3-6: Dc-link Circuit 41
Figure 3-7: LCL filter grid-connected ((Gajewski & Pieńkowski, 2016)). 42
Figure 3-8: Simplified circuit that is linked to the grid using STATCOM (Hong et al., 2018) 47
Figure 3-9: Pitch control Using the PI Controller 49
Figure 3-10 :Control diagram for three-phase voltage and current of GSC(Pavan Kumar & Bhimasingu, 2021). 58
Figure 3-11: Phase Locked Loop (Pavan Kumar & Bhimasingu, 2021)............................ 59
Figure 3-12: Diagram of voltage and current control (Kumar & Bhimasingu, 2021)......... 61
Figure 3-13: Equivalent Circuit of voltage and current control (Kumar & Bhimasingu, 2021)... 61
Figure 3-14: Diagram of the current control (Kumar & Bhimasingu, 2021) 62
Figure 3-15: Block Diagram for voltage control 63
Figure 3-16 : VSC-based STATCOM architecture 64
Figure 3-17: PI controller for the AC voltage regulator 65

Figure 3-18: PI controller for the DC voltage regulator 66
Figure 3-19: Current regulators with PI controllers 67
Figure 4-1: Block diagram of the overall system 69
Figure 4-2: Wind turbine modelling 70
Figure 4-3 : Power Coefficient Simulink 70
Figure 4-4: Wind Speed randomly generated 71
Figure 4-5: Mechanical power based randomly generated wind speed.............................. 71
Figure 4-6: PMSG connected to Rectifier 72
Figure 4-7: Dc Voltage from Rectifier and Connected to Inverter 73
Figure 4-8: Grid Side Convertor during Normal Operation 74
Figure 4-9:Three-phase AC voltage and current from the Inverter 74
Figure 4-10 :Three phase AC voltage and current from the grid...................................... 75
Figure 4-11: Grid Side Convertor during different types of faults Operation 76
Figure 4-12: three phase AC voltages and current from the inverter with L-G Fault 77
Figure 4-13: Three phase AC voltages and current from the grid with L-G Fault 77
Figure 4-14:Three phase AC voltage and current from the inverter with L-L-G Fault..... 78
Figure 4-15: Three phase AC voltage and current from the grid with L-L-G Fault 79
Figure 4-16: Three-phase AC voltage and current from the inverter with 3L-G Fault 80
Figure 4-17:Three-phase AC voltage and current from the grid with 3L-G Fault 80
Figure 4-18: Three phase voltage and current from the grid with STATCOM 81
Figure 4-19: Grid Side Convertor during different types of faults with STATCOM 82

ABBREVIATION AND ACRONYMS

2L-G	Line- Line-to-ground
3L-G	Line- Line -Line-to-ground
AC	Alternative Current
BC	Before the birth of Christ
DC	Direct current
DFIG	Doubly-fed Induction Generators
DVR	Dynamic Voltage Restorer
FACTS	Flexible Alternative Current Transmission System
FLC	Fuzzy Logic Controller
FRT	Fault ride through capability
GSC	Grid side converter
HAWTs	Horizontal axis wind turbines
IGBT	Insulator gate bipolar transistor
L-G	Line- to- ground
MOSFET	Metal-Oxide-Semiconductor Field-Effect Transistor
MPPT	Maximum Power Point Tracking
PI	Proportional integral
PCC	Point of common coupling
PLL	Phase lock loop
PMSG	Permanent Magnet Synchronous Generator
RENs	Renewable Energy Systems
RSC	Rotor Side Convertor
STATCOM	Static Synchronous Compensator

SVC	Static VAR Compensator
SCIG	Squirrel Cage Induction Generator
Var	Volt-ampere reactive
VSC	Voltage-Sourced Converter
WECS	Wind Energy Conversion Systems
WRG	Wound Rotor Induction Generator
WRIG	Wound Rotor Induction Generator
WT	Wind Turbine
VAWTs	Vertical Axis Wind Turbines

ABSTRACT

In response to the growing need for additional electricity beyond traditional energy sources, the significance of harnessing renewable energy sources has greatly increased worldwide. From these sources, wind energy conversion systems have become the primary contributors to power generation systems. Due to the escalating severity of global environmental and climate issues and the rapid rise in fuel costs and electricity demand, the renewable energy source, wind energy, this has become one of the most speedily expanding energy sources. A PMSG is a crucial generator that is used in wind energy conversion systems, including machine side and grid side converters using PI controller connected to the grid systems. The production of wind farms experiences fluctuations due to the irregular nature of wind speeds. Also due to nature and unnatural three-phase faults happened in wind turbines linked to the grid. This will cause the generator to produce an unbalanced three-phase voltage and current. During normal operation 690 V generated from PMSG. This 690 V AC converted to 690 V DC by using Rectifier. Again this 690V DC voltage is converted to 690 V AC and by using two step-up transformers this voltage is updated to 230 kV. The grid voltage is 230KV and when L-G, 2L-G 3L-G types of fault happened to the system, voltage from the grid is minimized to around 200 kV, 150 kV, and 80 kV respectively. These deviations, in turn, give rise to a system stability issue caused by the violation of the voltage. So, fault ride-through capability is very necessary for the stability of power generation plants. To overcome these different types of faults in the power system STATCOM PI controller is designed. This STATCOM returns the voltage to normal operation (230 kV) by injecting and absorbing reactive power. The simulation of voltage control PMSG has been designed on MATLAB/Simulink software.

Keyword; *2L-G, 3L-G, FRT ,L-G, MATLAB/Simulink, PI, PMSG, STATCOM***,**

CHAPTER ONE

INTRODUCTION

1.1 Background of the study

Energy is essential for the growth and prosperity of countries. However, as energy consumption increases, the availability and cost of basic energy resources have become a global challenge. While coal may seem abundant, oil and natural gas reserves are anticipated to decrease over the long run. Additionally, conventional carbon-based energy resources have harmful environmental consequences, such as global warming and climate change. To create an environmentally friendly energy supply people are paying close attention to renewable energy sources like wind, solar, small hydropower, wave, tidal, biomass, and geothermal power. Wind energy is a fresh and affordable alternative source of energy with great potential. Variable wind turbines are used because they can take the most power from the wind and control reactive power independently, making them a valuable tool for meeting our energy needs (Gambhir et al., 2015).

Adding too much wind power to a power system without careful planning can disrupt voltage and frequency control, power quality, reliability, and other critical functions, impacting the overall performance pertaining to the electrical grid. Researchers are developing new methods to control the speed, power, torque, and frequency of wind turbines. This is a rapidly growing field with the potential for significant advances. It requires a deep understanding of power systems, machines, power electronics, and control theory. Modelling wind farms can help us understand how they work and how they affect the overall power system. Researchers have developed a variety of methods for modelling wind turbines, generators, transformers, and control and protection systems (Kouadria et al., n.d.2015).

Wind energy conversion system (WECS) is devices that change wind energy into mechanical. Wind turbines are a type of WECS that generate electricity from wind power. Windmills are another type of WECS that use wind power to power machines or perform tasks such as Moving water or crushing grains. Wind turbines are thought to have originated in Persia around 200 BC (Tamaarat, 2019). for systems that convert wind energy the most concepts is choosing the right wind generator. To select the best generator topology, factors such as cost, controllability, protection, and integration cost must be considered. WECS generators that are frequently utilized are the Permanent Magnet Synchronous Generator

(PMSG), Doubly Feed Induction Generator (DFIG), and Squirrel Cage Induction Generator (SCIG). In the primary stages of wind energy development, squirrel cage induction generators were connected to wind turbines through shafts and gearboxes (Moness & Moustafa, 2016).

Currently, the most widely utilized form of systems that convert wind energy is those furnished with squirrel cage induction generators (SCIG). The SCIGs are relatively simple and inexpensive to build. They are robust and reliable. However, SCIGs have several limitations, including: They don't start themselves. So they need an external power source to start up, they have a relatively low efficiency, especially at low wind speeds and they can generate reactive power, which can burden the grid (de Azevedo & Barros, 2021).

In the 1990s, the wind industry began using DFIGs, which are variable-speed generators that can harness power from various wind speeds and involve employing power electronics to regulate the electrical output of wind turbines. DFIGs require AC power for both the stator and rotor.to generate reactive power Var as a high-speed generator; a doubly fed induction generator requires the gearbox and additional auxiliary components (Navarrete et al., 2019).

Through a back-to-back converter, a doubly-fed induction generator (DFIG) is connected to the grid. Because it allows control over both the active and reactive power generated by DFIG, this converter is essential to preserving the grid's stability. DFIGs are widely utilized in wind energy conversion systems due to their many advantages over other generator types, including increased grid stability, variable speed operation, and power reliability (Gatavi et al., 2019).

Now days the wind industry is increasingly using permanent magnet synchronous generators (PMSGs), which are low-speed generators. PMSGs do not require gearboxes because they are low-speed generators, and they can be easily controlled using variable speed converters. There are several benefits to PMSGs not having a gearbox, including increased dependability, lower maintenance costs, and improved efficiency (Gatavi et al., 2019).A grid side converter (GSC) and a rotor side converter (RSC) are the two main parts of an AC/DC/AC converter. They are the converters on the rotor side. In order to regulate the injection of both active and reactive electricity into the grid, the rotor side converter (RSC) regulates the rotor current and the grid side converter (GSC) controls the voltage of the DC link.

(Berhanu et al., 2018). A STATCOM is a apparatus that connects to an electric power system in parallel and can provide or absorb the reactive power. The total of reactive power that the STATCOM provides or absorbs can be transformed to control certain aspects of the electric power system. It is a device that uses power electronics to provide or absorb from reactive power to voltage regulation and recover the stability of an electrical power system. (Muisyo et al., 2020).

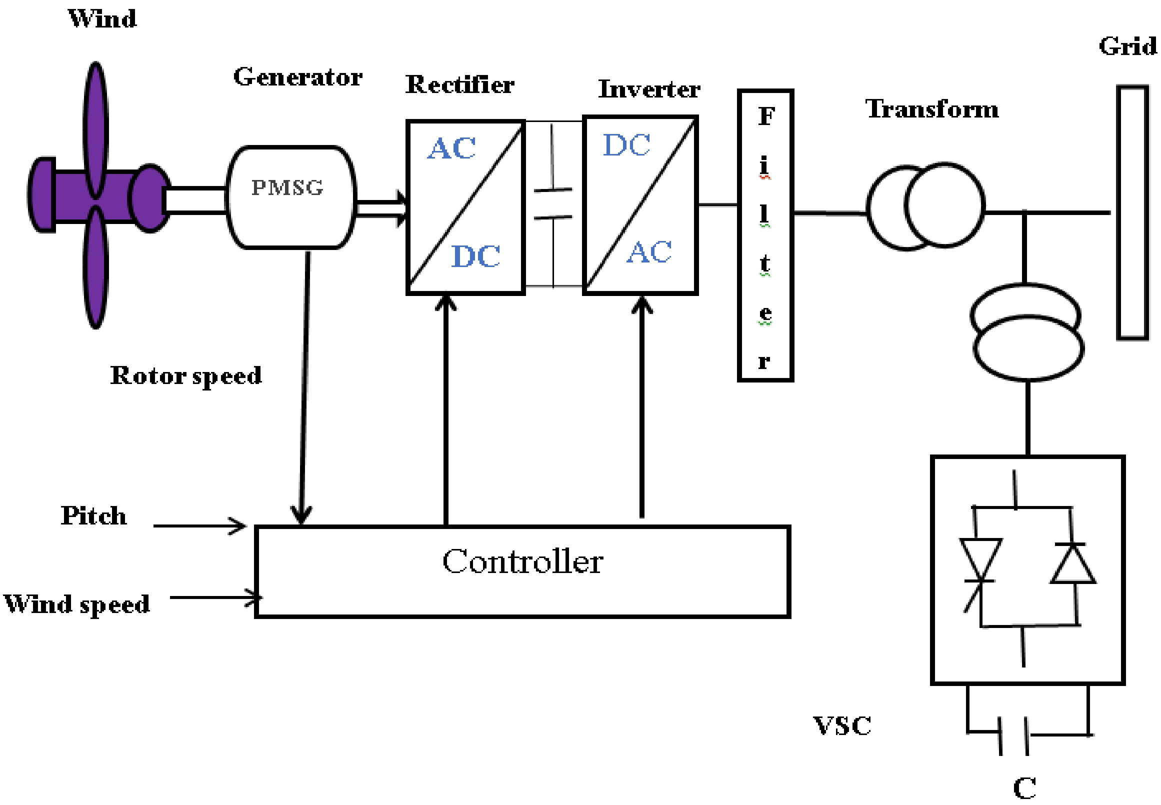

Figure 1-1: Arrangement of a PMSG-WT based WECS (Muisyo et al., 202_)

1.2 Statement of the Problem

Energy is essential to the growth and prosperity of countries. However, as energy consumption increases, the availability and cost of basic energy resources have become a global challenge. Wind energy can be converted into mechanical or electrical energy using wind energy conversion systems (WECS). Wind turbines are a type of WECS that generate electricity from wind power. During this active power and reactive power is produced. Also connected to the grid during normal operation, however, different types of faults will happen in normal operation, due to different factor that such natural factor and man-made factor the voltage of the grid connected system is fluctuated. So, this is the great problem in wind energy conversion systems. Also, unbalanced voltage has different disadvantage in wind energy conversion which is coupled to the grid. Such as generator and transmission line losses, voltage instability, overloading of equipment, Harmonics, and Reduced active power output of overall of the system .so in order to overcome above disadvantage in wind energy conversion system connected the grid, voltage control is very necessary. Voltage control is important for several causes, such as: keeping the voltage stable at the common coupling point (PCC).Reducing power losses in the transmission and distribution system, enhancing the grid's power quality. By controlling the voltage output of a PMSG-based WECS, the grid operator can improve the overall performance and reliability of the power system. In order to overcome this fault STATCOM is required. STATCOMs can provide rapid reactive power support to maintain voltage levels within acceptable limits during faults. This helps prevent voltage collapse and supports the system until the fault is cleared. So, this thesis' primary goal is to solve problems arising from the overflow of reactive power by using STATCOMs (Voltage source converters) and STATCOMs enable generators to remain connected and operational during faults, enhancing the overall fault ride-through capability of the system.

1.3 Objective

1.3.1 General objective

The primary goal of this thesis is to Enhance Fault Ride through the Capability of a Grid-Connected PMSG-based Wind Energy Conversion System for voltage control during a power system phase fault

1.3.2 Specific Objective

The thesis aims to achieve the following specific goals:

- Wind turbine modelling using a PMSG as the care of research
- Modelling of MSC and GSC bidirectional converters
- Modelling of LCL Filter for the system
- Controlling of MSC and GSC bidirectional converters using the PI controller by decoupling three phases into a d-q axis.
- Applying STATCOM to recover the faults that may occur in the system.
- Analysis system before the fault, during the fault, and after STATCOM.
- Build a Simulink model of the system, connecting blocks to represent the different components and their interactions.

1.4 Motivation of the Study

In recent times, wind energy has experienced significant growth as an energy source, with the majority of various technologies for converting wind energy now employing permanent magnet synchronous generator (PMSG)-based configurations. The PMSG are pivotal in grid operations, drawing considerable interest due to their variable speed, converting a large portion of wind energy into electrical power, high density of power and enhance high efficiency. Due to natural and man-made different kinds of faults will happen in the system. At that time wind turbine linked to the grid is disconnected and the voltage required to the system is minimized. Because of this, the three-phase voltage from the grid e is unstable. To maintain system stability, it is necessary to regulate voltage requiring the creation of suitable wind energy models and control systems by using STATCOM to overcome this fault and return to normal operation.

1.5 Scope of the thesis

The thesis investigates the modelling, analyse performances, and control methods for a permanent magnet synchronous generator (PMSG) used in a wind energy conversion system (WECS) linked to the grid by using a bidirectional converter which is implemented in MATLAB/Simulink 2023a. The thesis also designs optimal controllers for the WECS connected to the grid to enhance fault ride-through capability.

1.6 Limitation of the Thesis

The thesis uses MATLAB/Simulink to simulate the system but does not test the system in the tangible. So, deploying the system in the real world is difficult and expensive because it takes more time and money than simulating it in MATLAB/Simulink. This is the main limitation of this thesis

1.7 Significance of the Study

The primary goal of the thesis is to control Voltage in wind energy conversion linked to the electrical grid by using STATCOM. So, if Voltage is controlled it has the following advantage.

- ➢ It gives guide on how to use STATCOM to regulate reactive power to maintain grid voltage stability.
- ➢ It enhances comprehension of the operating a wind turbine with variable speed, along with the modelling and control principles of generators and converters.

- PMSG-based WECS can insert or consume reactive power to help control the voltage where the system connects to the grid. This can help to prevent voltage sags and swells, which can damage other equipment linked to the grid.

- The reactive power generation can source of losses in the grid's transformers and transmission wires. By controlling voltage, PMSG-based WECS can help to reduce these losses and restore the grid's overall efficiency.

- Voltage control can help to increase the power transfer capacity of the grid.

- PMSG-based WECS can use reactive power control to improve the grid stability. This is because oscillations in the grid can be dampened out and kept from becoming unstable by using reactive power.

1.8 Thesis Organization

There are five chapters in the thesis. The primary chapter offers a concise introduction to wind energy conversion system, encompassing an overview, statement of the problems, objectives, motivation importance, range, and the organization of this thesis.

Chapter Two explores the review of the literature. Exploring prior research on wind turbine PMSG Based linked to the grid and fault ride-through capability. It draws upon existing literature on different types of generators and types of wind turbines.

Chapter three encompasses the methodology by providing detailed insights into the process utilized in the system for converting wind energy. This chapter delves into deriving the mathematical representation of wind turbines based PMSG, mathematical of the grid side and the machine side converter with the controller, and Mathematical model of STATCOM and its controller to overcome faults in the grid system.

Chapter four examines the simulation outcomes of the system during normal operation connected to the grid, during three-phase faults, after STATCOM, and evaluates the finds

Chapter five explores the conclusions reached and offer recommendations for future endeavours aimed at enhancing the system.

CHAPTER TWO

LITERATURE REVIEW

2.1 Theoretical Background of Wind Energy Conversion Systems

A conversion of wind energy is a complicated process. That turns wind power into electricity. With wind turbines, electricity is produced in two stages. First, the rotor rotates due to the wind, producing mechanical energy from wind. Second the mechanical energy is converted to electrical energy via the generator. Wind speed is critical for maximizing power output (Ofualagba & Ubeku, 2008).

2.1.1 Wind Turbines and Its Classification.

The wind turbines harnesses of the wind's kinetic energy through the rotor equipped including two or more blades. These blades are connected mechanically to an electrical generator, allowing for the conversion of the captured energy into electricity. There are two main design configurations for wind turbines: These consist of the horizontal and vertical axis configurations. These configurations represent distinct and different approaches to the wind turbine design (Ofualagba & Ubeku, 2008). Choosing the quantity of wind turbine blades is a complex design decision. Two-blade systems are generally cheaper compared to three-blade systems. However, Wind turbines with two blades must rotate at a faster rate.to generates power compared to their three-blade counterparts.

According to Betz's law, proposed by German physicist Albert Betz in 1919, a wind turbine is capable of converting 59% of the kinetic energy emanating from the wind into mechanical energy (Zorich & Garberville, 2023).

The Horizontal Axis Wind Turbines (HAWTs)

The majority prevalent kinds of wind turbines are those with a horizontal axis. They typically consist of a tower with a horizontal axis rotor at its top which is comprised of dual or three long, thin blades that look like an airplane propeller. The blades are oriented to directly confront the wind and spin, converting the kinetic energy of the wind into mechanical energy.. The energy in mechanical form is used to turn a generator, which produces electricity (Alabdali et al., 2020).

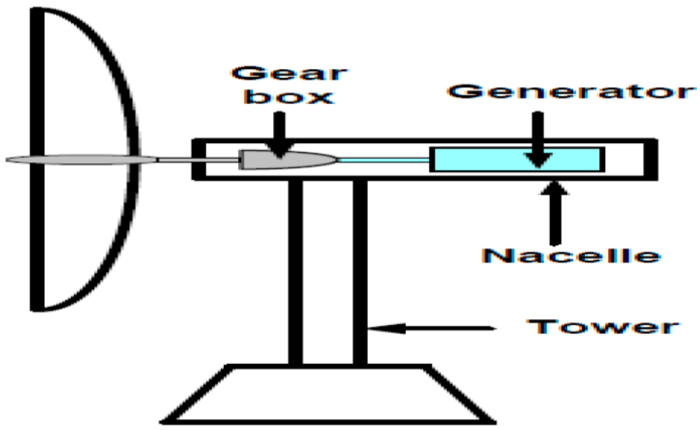

Figure 2-1:The wind turbines that rotate vertically (VAWTs) (Raouf et al., 2023)

The Vertical Axis Wind Turbines (VAWTs)

The wind turbines that rotate vertically (VAWTs) (VAWTs) feature shorter, broader and curved blades resembling the beaters found in an electric mixer. Unlike HAWTs, VAWTs can be mounted on towers or on buildings, and they can generate electricity even when the wind is not blowing directly at them. However, they are not as common as HAWTs because they are less efficient and can be more difficult to maintain Generally, most commercial wind turbines use a horizontal axis design because horizontal axis turbines tend to perform (Mathew & Philip, 2012) rm better than vertical axis turbines in capturing wind power. Horizontal axis turbines are the dominant type used commercially.

However, vertical axis wind turbines (VAWTs) are much less common even though some recent developments are leading to new possibilities for VAWT technology. Researchers and wind turbine manufacturers are exploring improved VAWT designs that provide benefits over horizontal axis turbines (Alabdali et al., 2020).

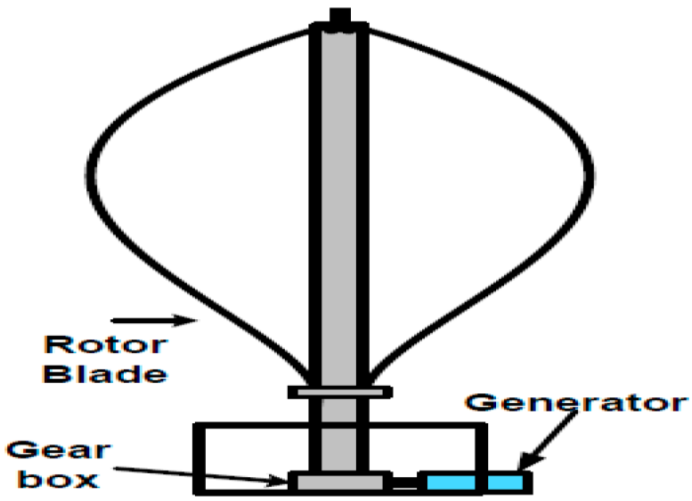

Figure 2-2:The vertically oriented wind turbines (VAWTs) (Raouf et al., 2023)

Off-Grid and On-Grid Wind Turbine

Both off-grid and on-grid wind turbines are used in various applications. The off-grid system, often referred to as a backup system, operates independently of the grid. It relies on storage batteries or alternative energy source like generators. These features render the off-grid system additional costly, intricate, and fewer adoptable compared to the system that runs on the grid. It is typically employed to power residences distant farming equipment, signs for traffic and gates. The on-grid connected system is referred to by different names, including gird-connected, grid-tried, grid direct or integrated grid systems. The on-grid system is commonly employed in urban areas where the houses are connected to utility networks. Its primary advantage lies in primary the eliminating the need for battery storage and avoid the cost associated with battery and regulator. The on-grid system ceases operation during the fault failure (Algaddafi et al., n.d.2016). so, in order to solve this condition fault ride through capability is needed in this thesis by considering on grid wind turbine.

Fixed and variable speed wind turbines

Wind turbines are classified into fixed speed and variable speed varieties based on their speed. Permanent magnet synchronous generators (PMSG) and double feed induction generators (DFIG) are the two types of generators employed in these variable speed wind turbines. In the latter case, the generator terminal is scaled at 30% of rated power within an AC/DC/AC converter and is directly connected to the grid. In contrast, PMSG-based systems require two full-scale back-to-back converters to connect the generator to the grid. In this thesis PMSG is considered because of, favoured for its precise control, great effectiveness and little maintenance needs and suitability for gearless design. (El Kassoumi et al., 2022)

2.2 Wind Turbine Generators

In wind energy conversion systems various three-phase generators can be linked to wind turbines. There are different varieties of generators utilized in wind turbines. The two common categories of generators used in WTS are asynchronous (induction) generators and synchronous generators. Squirrel cage induction generators (SCIG) and wound rotor induction generators (WRIG) fall into the category of asynchronous (induction) generators. On the other hand, wound rotor generator (WRG) and PMSG belong to the synchronous generators group (Babu & Divya, 2017).

2.2.1 Squirrel Cage Induction Generator (SCIG)

The SCIG is a significantly superior option among variable-driven wind power turbines, as it operates seamlessly in tandem through the power conversion to regulate both the generated voltage and frequency for standalone loads. The capability to generate additional power from the wind is restricted due to the potential overloading of the generator to achieve high power output, the adjustment of the blade pitch angle is more necessary. Despite these limitations, the SCIG endures as a viable alternative energy source that is simple in design structure, reduced maintenance needs, and impressive power-to-weight ratio, rendering it resilient. Nevertheless, when compared to DFIG for flexible speed operation, it necessitates a greater number of power converter switches, resulting in increased switching losses (Vijayaprabhu et al., 2021).

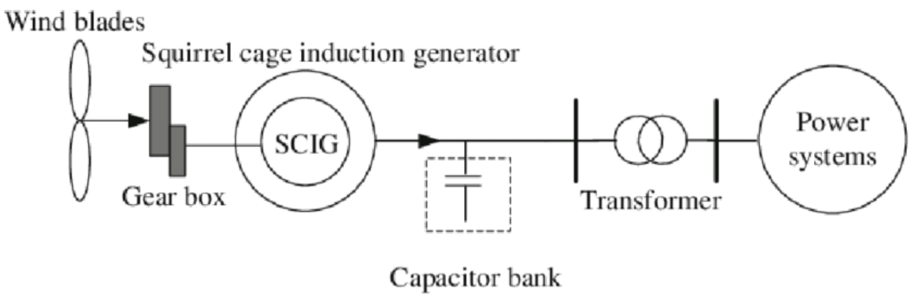

Figure 2-3: Squirrel cage induction generator (Vijayaprabhu et al., 2021)

2.2.2 Wound Rotor Induction Generator (WRIG)

This type of turbine operates on the flexible speed principle .As seen in the diagram, in this design, the WRIG is directly connected to the grid. The generator's slip and power output are controlled by the rotor resistance that can be adjusted. In this configuration, a reactive power compensator eliminates the requirement for reactive power, while a soft starter reduces inrush current. However, the drawback of this configuration includes speed range, inadequate control over both active power and reactive power, and dissipation of slip power as losses in the variable resistance (Babu & Divya, 2017).

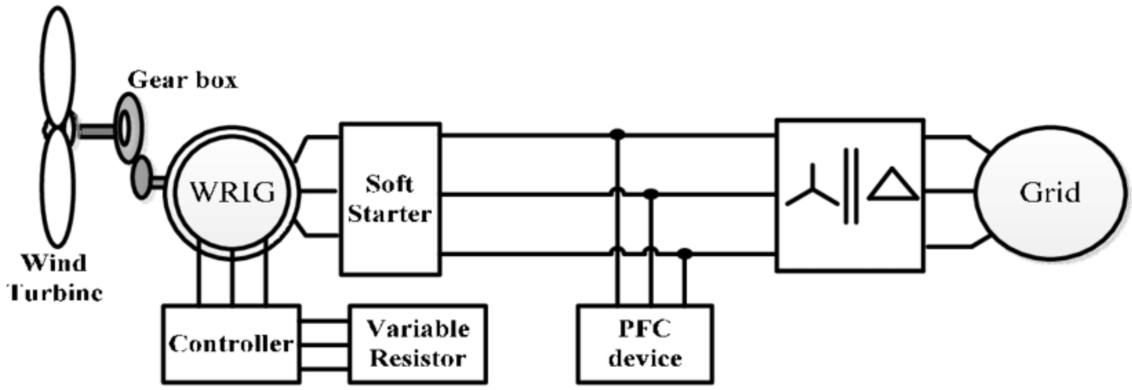

Figure 2-4: wound rotor induction generator (WRIG) connected to the grid (Elmorshedy, 2016)

2.2.3 Double Feed Induction Generator (DFIG)

The DFIG is extensively employed in variable -speed technologies for converting wind energy.It holds a significant position among generators utilized in wind energy application. According to picture below, in this type, the rotor is connected to the grid by a bidirectional frequency converter, whereas the stator is directly attached to the grid. Connecting back-to-back power converter to the rotor circuit limits its power rating to 30% of the generator’s rated power. Despite this, DFIG based WECS faces drawbacks including the necessity of rotor slip rings and expensive gearboxes additionally, implementing multi-pole low speed DFIG configuration possess technical challenges (Elmorshedy, 2016).

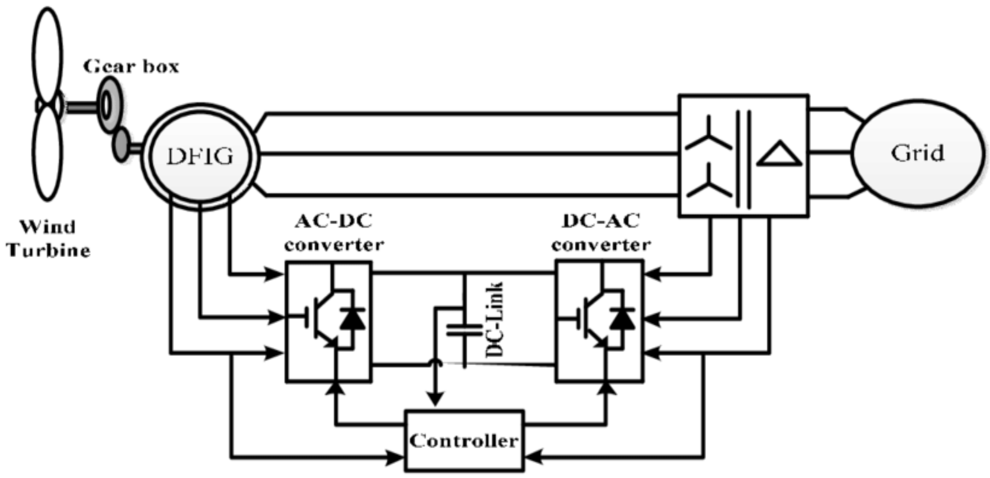

Figure 2-5: Grid-connected wind-generating system based on DFIG connected the grid

(Elmorshedy, 2016)

2.2.4 Permanent Magnet Synchronous Generator (PMSG)

A PMSG drive eliminates the need for a gearbox due to its lack of rotor current at minimal rotational speeds. Being gear less, this drive facilitates the creation of small wind turbines for consumers, offering high efficiency and low maintenance costs. The principle behind the PMSG involves generating torque through wind power. This generated torque is then transferred to the generator's rotor shaft. The acceleration of the rotor of the rotor's mechanical rotation relies on the difference between the generator's electrical torque as well as the mechanical torque (Vijayaprabhu et al.,2021). since the speed range is maximized, eliminating the need for shifting gears, while both active and reactive power are fully contrivable , maintenance is less since it is brushless (Vijayaprabhu et al.,2021). In this thesis due to the above advantage PMSG is selected.

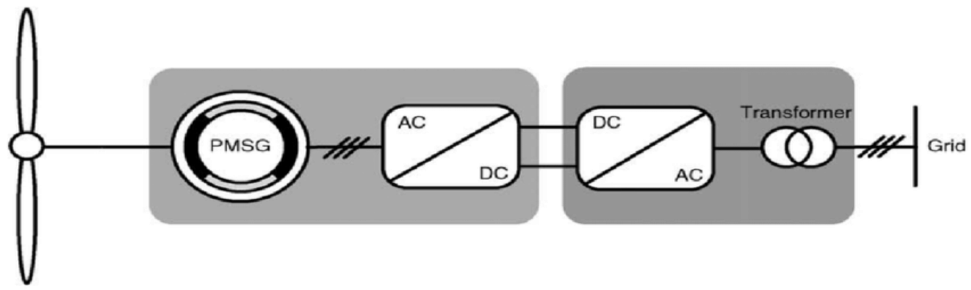

Figure 2-6: PMSG structure representation connected to the grid

2.3 Control Techniques for a Wind Turbines Generator System

Control strategies for generator wind turbine systems play a crucial role in optimizing energy extraction, ensuring grid stability, and prolonging lifespan of the equipment**.** By designing the following control strategies wind turbine generators can operate efficiently, reliably, and safely, making significant contribution to renewable energy generation and grid integration.

2.3.1 Pitch angle Control

From wind turbines**,** variables wind turbines are widely preferred within wind turbines systems due to their superior efficiency and enhanced control capabilities over a wide range. However, the stochastic and intermittent nature of wind speeds to variability in the energy conversion process. To optimize energy extraction from wind turbines, pitch angle control is serves as a crucial mechanism. This control strategy enables the system to operate with heightened efficiency and reliability, particularly in turbulent weather conditions characterised by stochastic behaviour. Moreover, it aids in stabilizing output power at both higher and lower wind speeds. Modifying the pitch angle of the blades in response to wind speed variation is essential for maximizing energy conversion efficiency, allowing the turbine to adapt to changing wind conditions effectively. (Habtamu et al., 2021).

Changes in wind speed variability result in fluctuation in the active power output of technologies for converting wind energy. This variation of active power has impact on the reactive power output, thereby affecting the voltage at the common point connection. Utilizing support from wind energy conversion systems can be advantageous and necessary to address system contingencies and maintain the normal operation of the power systems. Reactive power requirements, specified by most transmission systems are mandated for conversion systems of the wind turbines to ensure compliance with both transient and steady-state conditions when connecting to their respectively grids (Raouf et al., 2023).

2.3.2 Maximum Power Point Tracking Control (MPPT).

In wind energy conversion system, employing a MPPT control is crucial due to its significant role in optimizing the extraction of high energy from the PMSG unrelatedly of wind speed. The principle of the maximum power point tracking controller revolves around executing an MPPT method, enabling the system to attain and continuously track the maximum power point (Zebraoui & Bouzi, 2018).

2.4 Fault ride through capability and types of faults

Electric power supply must remain continuous, making any factors leading to the losses of a generation unit undesirable. The main aim of employing fault ride through (FRT) techniques to avoid the losses of generation unit is significant both from an economic and technical standpoint (Alhammad & Habiballah, 2021).

Fault ride through capability describes the capacity of an electrical system to remain operational and stable during and after a fault event, such as a short circuit or voltage disturbance. This capability is crucial for maintaining the reliability and stability of the grid voltage (Shuaibu et al., 2021).

2.4.1 Type of Faults.

A fault is referring to the disruption that interferes with the regular current supply to the intended destination. Power system faults are categorized into two types. Hence, faults can transpire at the connection points of any active and passive electrical apparatus. Active electrical equipment encompasses synchronous and asynchronous machines, as well as grid equivalents. Inactive electrical devices comprise transformers, transmission lines and loads (Alhammad & Habiballah, 2021).

- **I.** Faults in Open circuit.
- **II.** Faults in Short circuit. This type of fault is known as shunt fault. This paper is mostly focused on this type of fault.

I. Faults in Open Circuit

A rise in voltage and drop in current in the faulted phase are characteristics of open circuit faults. Consequently, by keeping an eye on each phase’s voltage, they can find faults in the open circuit that occur if the voltage value increases. Current flow stops when there is an open circuit fault, which happens infrequently**.** This kind of fault is known as a series fault (Alhammad & Habiballah, 2021).

II. Faults in short circuit

During Faults in a Short circuit, the voltage droops and the failed phase current will always increase. The beginning of a short circuit problem is indicated if the current value increases. The most dangerous failures are short circuits, where the current increases significantly over the instrumentation’s nominal current. Short circuit faults are frequent occurrences and can be classified into two primary categories; symmetrical and non-symmetrical faults.

1, Symmetrical Faults

A Symmetrical fault is characterized by balance and equal impact on all-phases. About 5% of faults in the Systems with three phases are symmetrical, making symmetrical faults the most serious since they affect all three phases.

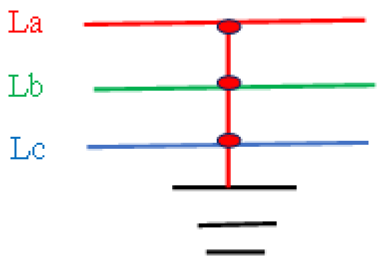

Figure 2-7: Symmetrical faults

2, Asymmetrical Faults

An asymmetrical fault disrupts balance and impacts individual phases distinctly, resulting in uneven voltage drops of varying intensities depending on the fault's nature. Such faults may manifest as line L-G, line to line, (L-L-G) faults. Analysing asymmetrical faults poses challenges, with three-phase systems having roughly 95% of the problems exhibiting this characteristic. Subsequent sections will offer further insights in to the specific types of the asymmetrical faults.

1. **Line -To -Ground Fault**.

The most frequent types of faults are L-G fault, which is brought on by a conductor coming into connection with a ground structure. It is discovered that L-G defects account for 70% of all faults.

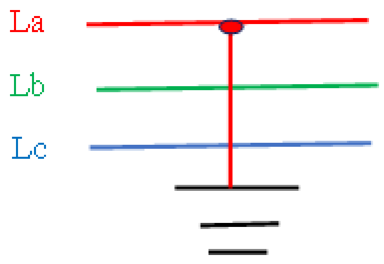

Figure 2-8: Scheme of L-G fault

2. Line -To -Line Fault.

A line -to-line (L-L) problem occurs when one phase comes into contact with another phase L-L faults account for 15% of all faults.

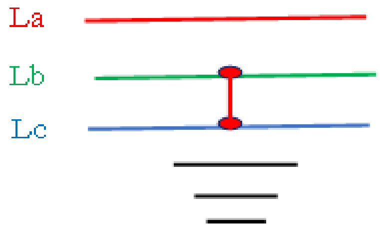

Figure 2-9: Scheme of L-L-G

3. 2 L-Ground Fault.

This type of asymmetrical fault is happened when two phases touch the ground. This type accounts for 10% of all faults (Alhammad & Habiballah, 2021).

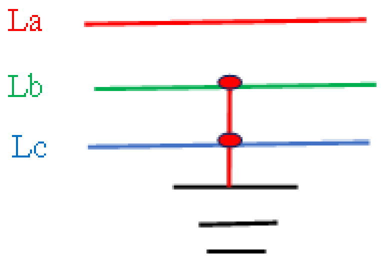

Figure 2-10: Scheme of L-L-G

2.5 Power Transformer

A transformer is static apparatuses which have the capable of transferring and transforming electrical energy from one or multiple circuits to another, utilizing magnetic coupling and the principle of electromagnetic induction. Power transformers are extensively employed in both the electrical and electronics sectors. Their integration into power systems enables the choices of optimal and cost-effective voltage levels for various requirements, such as using high voltage for long-distance electrical power transmission. A transformer comprises two inductive coils .namely the first and secondary coils. These coils are electrically isolated but magnetically linked through a low-reluctance path. The laminated core produces an alternating magnetic flux when an alternating voltage is given to the primary coil. The primary current flows due to the closed circuit formed by the coil. Consequently, self-induction occurs in the primary and the secondary coil experiences induction through the influences of the primary coil (known as mutual induction). This mutual induction leads to the emergence of magnetic flux in the secondary coil. If the secondary circuit is linked to a load, electric energy can be transferred as a whole, completing the process of electrical energy conversion (Syahputra & Arrozak, 2017). In this thesis two types of transformers in this thesis which are 690V/33KV and 33KV/230KKV.

Table 2-1: Specification of 690V/33KV Step-up Transformer

Value	Primary winding	Secondary winding
Voltage	690V	33KV
Frequency	50hz	50hz
Resistance (pu)	0.0012	0.0012
Inductance(pu)	0.0057	0.0057
Magnetization Resistance(Ω)	500	500
Inductance Resistance(Ω)	500	500
Nominal power	1.5MW	1.5MW

Table 2-2: Specification of 33KV/230KV Step-up Transformer

Value	Primary winding	Secondary winding
Voltage	33kV	230KV
Frequency	50hz	50hz
Resistance (pu)	0.0005	0.0005
Inductance(pu)	-0.00149	-0.00149
Magnetization Resistance(Ω)	500	500
Inductance Resistance(Ω)	500	500
Nominal power	1.5MW	1.5MW

2.6 Review of the Related Work

In current times, there has been significant attention in PMSG-based wind turbine control systems, leading to active involvement of researchers in activities related to PMSG modelling, design, and control. Because PMSG has higher efficiency, faster response, no need for slip rings or brushes, and a Simplified control system. The following literature reviews summarizes the research conducted in the field of PMSG-based wind turbine control systems: for instance, in (Hemeida et al., 2018). This paper discusses the use of STATCOM to recover the system's fault ride-through capability in this paper the possibility of a short circuit from the three phases to ground faults for 100ms has been considered in various locations throughout the system. This study examines the FACTS devices' dynamic performance. Specifically the STATCOM and VSC is analysed in the context of stabilizing a wind farm integated with a multi-machine power system. The result of this paper is the comparison between Fuzzy Logic Controller (FLC) and conventional controllers for SVC and STATCOM reveals that the FLC provides better dynamic performance during transient faults. Specifically, the FLC is shown to have less overshoot and better damping of oscillations, with a reduced settling time. Their dynamic performances under such conditions are evaluated and compared in this research work. However, the paper's limitation is they consider only Three-phase to ground short circuit faults. However, they didn't consider other types of faults such as breaks in circuits, faults from a line to ground, and faults between two lines Also, one of the challenges with DFIGs is their sensitivity to grid disturbances. If there is a fault or disturbance in the grid, such as a voltage dip or a sudden change in frequency, the DFIG may experience instability or even trip offline.

Alhammad & Habiballah's paper provides a comprehensive overview of fault ride-through capabilities, including the different types of FRT and the most public renewable energy systems (RENs) where FRT procedures are used. To better understand fault ride-through (FRT) capabilities, this paper introduces and discusses different categories of faults in power system and its impact on the quality of power. The paper concludes by discussing the devices employed for the identification of faults in the protective system (Alhammad & Habiballah, 2021). But here are some of the disadvantages of using protective devices such as fuses, relays, and circuit breakers when wind energy is connected to the grid, increased cost, Complexity, Reduced reliability, and reduced power quality. To overcome this limitation using STATCOM is better to enhance the power quality and steadiness of the wind energy system. It is a voltage-sourced converter (VSC) that can insert or consume reactive power into the grid.

(Shuaibu et al., 2021)This paper review articles on FRT capabilities of DFIG-based wind turbines (WTs) to identify limitations and propose a technique that incorporates fault current limiting capabilities into FRT. in this paper the possibility of the most common faults in power systems are shunt faults has been considered in various locations throughout the system, Also, the methods that improve the topology or optimize the control scheme of DVR to incorporate fault current limiting (FCL) capability is discussed in this. But the limitation of using Dynamic Voltage Restorer has disadvantage over quality of power due to Complexity, Limited capacity, reduced reliability. The main drawback of wind turbines based on DFIG that are connected to the grid is that it is very difficult to improve their performance using flux weakening control because the stator is linked to the grid directly (Shuaibu et al., 2021).

(AlGhamdi, 2023**)** In this work, the fault ride-through (FRT) capabilities of a wind turbine that employs a switching reluctance generator (SRG) are improved by the employment of a dynamic voltage restorer (DVR). The wind turbine may detach from the grid due to voltage sag, swell, and poor line voltage in the grid. The DVR is used to inject voltage at the point of common coupling (PCC) into the grid voltage during grid outages in order to raise an SRG's stator voltage.) However, the limitation of this paper is SRGs require more complex control algorithms to manage phase currents and minimize torque ripple, which can complicate the design and operation and SRGs typically experience higher torque ripple, which can lead to mechanical stress and reduced smoothness in power generation, necessitating additional measures to mitigate this issue. Also using Dynamic Voltage Restorer has disadvantage over quality of power due to Complexity, Limited capacity, reduced reliability. Therefore, this thesis examines the use of STATCOM to introduce reactive power into the system during a failure in order to improve fault ride through capability in wind energy conversion systems that are connected to the grid.

CHAPTER THREE

METHODOLOGY

3.1 Introduction

The strategy and methods used in this thesis are covered in this chapter. It provides an in-depth look at modelling and controlling a PMSG-based wind turbine system. Specifically, it outlines the mathematical modelling of the wind turbine components. It then discusses modelling the PMSG, involving both the converter on the rotor and grid side. It also describes how to use PI Controllers with STATCOM devices to adjust reactive power and enhance fault ride using the capabilities of grid-connected WEC S.

Finally, it details the Simulink model created in MATLAB to simulate the wind turbine system. This includes incorporating an appropriate control system. The goal is to control reactive power connected to the grid using a PMSG wind turbine with its associated control strategies.

In summary, this chapter attention to explaining the research approach, mathematical modelling of key components, PMSG modelling, control techniques, and simulation model used to analyse and test the PMSG wind turbine system in MATLAB/Simulink.

3.2 Materials

The MATLAB/Simulink software package will be utilized to simulate and analyse the system model for this thesis. MATLAB is a general-purpose computing platform with a wide range of toolboxes. It includes high-level mathematical functions for numerical solutions and graphical user interfaces. Simulink provides tools for model-based design and simulation. Together, MATLAB and Simulink will enable testing and analysis of the system model. Additionally, Microsoft Office will be employed for the majority of the documentation, while Math Type will be utilized specifically for the creation of equations and formulas

The following methods and techniques will be utilized to achieve the goals for the research:

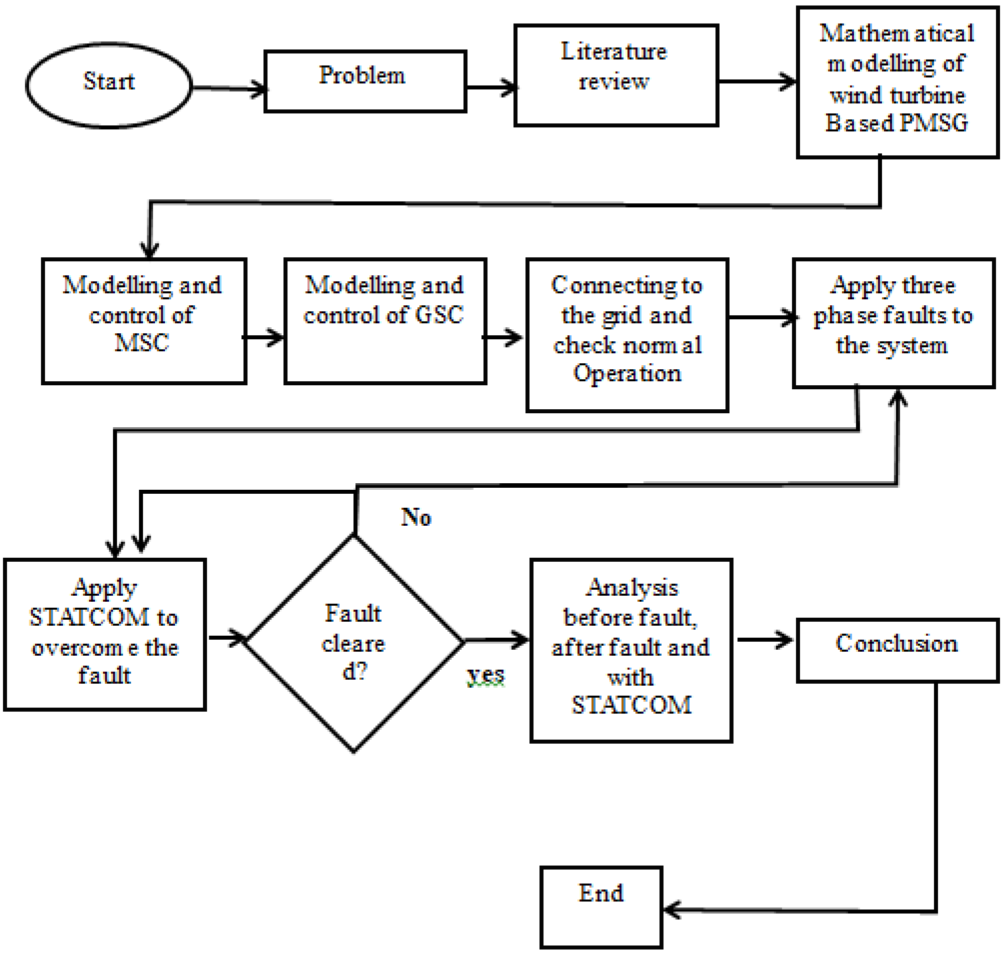

Figure 3-1: Flow chart of methodology work activities

3.3 Modelling of Wind Energy Conversion

The WECS consists of three components; these are generator (wind turbines), the power electronics, and the load. These components are individually modelled as and understand and optimize the overall system's performances. This means each part is analysed separately to assess its function and contribution to the energy conversion processes.

3.3.1 Modelling of Aerodynamic Wind Turbine

The kinetic energy of an object is equal to the work done (W) in moving it from a state of rest to a certain distance under the influence of a force (F) when constant acceleration, represented by "a," is applied to an object with the mass (m) and initial velocity (v). (Stuff, 2011).

$$W = E = Fs. \tag{3.1}$$

Where s is displacement .

Newton's second law of motion states that an object's force is equal to its mass times its acceleration (Georgievich, 2022).

$$F = ma \tag{3.2}$$

From Equations (3.1) and (3.2) we can derive kinetic energy as follows

$$E = \ mas \tag{3.3}$$

In the kinematics energy of solid motion formula $v^2 = 2as + u^2$, where u represents the starting velocity of the object, its follow that (Manyonge et al., 2012).

$$a = \frac{{v_f}^2 - {u_i}^2}{2s} \tag{3.4}$$

When, the starting velocity is equal to zero. Then Equation (3.3) becomes

$$E = \frac{1}{2} m v^2 \tag{3.5}$$

This formulation of kinetic energy assumes a constant mass for a solid. However, when we consider the wind, which is essentially in air motion, both velocity and density can vary. Consequently, there is no fixed mass in this case. In this paper, we will make assumption that the density of air is relatively stable. Even when there are changes in attitude and temperature the kinetic energy law given in Equation (3.5) will be applied. Therefore, using the given Equation (3.5), one can calculate the kinetic energy (measured in joules) within the air with mass m traveling at velocity (wind speed).

The power P in the wind is determined by the rate of change of kinetic energy.. Specifically (Stuff, 2011)

$$P = \frac{dE}{dt} = \frac{1}{2} \frac{dm}{dt} {v_w}^2 \tag{3.6}$$

since $$\rho = \frac{m}{v}, m = \rho v \tag{3.7}$$

Where m is mass and v is volume and density.

$$\frac{dV}{dt} = \frac{dAh}{dt} = A \frac{dh}{dt} = Av \tag{3.8}$$

The mass flow rate is derived from

$$\frac{dm}{dt} = \frac{d\rho v}{dt} = v\frac{d\rho}{dt} + \rho\frac{dv}{dt} \tag{3.9}$$

When density is constant then

$$\frac{dm}{dt} = \rho\frac{dv}{dt} \tag{3.10}$$

But, $V = Ah$, so derivate of volume is

$$\frac{dV}{dt} = \frac{dAh}{dt} = A\frac{dh}{dt} = Av \tag{3.11}$$

From Equations (3.8), (3.9), (3.10) the mass flow rate is equal to

$$\frac{dm}{dt} = \rho Av \tag{3.12}$$

From Equations (3.6) and (3.12), so the power of wind is calculated

$$P = \frac{1}{2}\rho A v_w{}^3 \tag{3.13}$$

Mechanical power generated by a wind turbine (P_{wind}) harnessed by the through blades measured in watts is defined as the disparity between the wind powers encountered up-stream and downstream.

$$P_w = \frac{1}{2}\rho A v_w \; (v^2{}_{us} - v^2{}_{us}) \tag{3.14}$$

Where P_w Mechanical power is generated by a wind turbine, v_{us} is represents the speed of wind upstream at the entry point of rotor blades, measured in m/ s and v_{us} is represents the speed of wind downstream near the rotor blades' exit, measured in meters per second. Equation (3.9) means the flow rate of mass we can rewrite this equation as follows.

$$\rho A V_w = \rho A(\frac{v_{us+} v_{ds}}{2}) \tag{3.15}$$

Where, V_w the average velocity of the turbine rotor blades is determined by taking the mean of the velocities at both the entry and exit points.

From Equations (3.14) and (3.15) the power output of the wind turbine. is derived as follows

$$P_w = \frac{1}{2}\rho A(v_{us} - v_{ds})(\frac{v_{us} + v_{ds}}{2}) \tag{3.16}$$

$$\begin{aligned} P_w &= \frac{1}{2}\rho A\left[\frac{v_{us}}{2}(v^2{}_{us} - v^2{}_{ds}) + \frac{v_{ds}}{2}(v^2{}_{us} - v^2{}_{ds})\right] \\ &= \frac{1}{2}\rho A\left[\frac{v^3{}_{us}}{2} - \frac{v_{us}v^2{}_{ds}}{2} + \frac{v_{ds}v^2{}_{us}}{2} - \frac{v^3{}_{ds}}{2}\right] \\ &= \frac{1}{2}\rho A\left[\frac{v^3{}_{us} - v_{us}v^2{}_{ds} + v_{ds}v^2{}_{us} - v^3{}_{ds}}{2}\right] \\ &= \frac{1}{2}\rho A v^3{}_{us}\left[\frac{1 - (\frac{v_{ds}}{v_{us}})^2 + (\frac{v_{ds}}{v_{us}}) - (\frac{v_{ds}}{v_{us}})^3}{2}\right] \\ &= \frac{1}{2}\rho A v^3{}_{us} C_P \end{aligned} \tag{3.17}$$

Where the power coefficient is defined

$$C_P = \frac{1 - (\frac{v_{ds}}{v_{us}})^2 + (\frac{v_{ds}}{v_{us}}) - (\frac{v_{ds}}{v_{us}})^3}{2} \tag{3.18}$$

$$C_p = \frac{(1 + \frac{v_{ds}}{v_{us}}) - (\frac{v_{ds}}{v_{us}})^2 - (\frac{v_{ds}}{v_{us}})^3}{2}$$

By rearranging

$$\begin{aligned} &= \frac{(1 + \frac{v_{ds}}{v_{us}}) - (\frac{v_{ds}}{v_{us}})^2(1 + (\frac{v_{ds}}{v_{us}}))}{2} \\ &= \frac{(1 + \frac{v_{ds}}{v_{us}})(1 - (\frac{v_{ds}}{v_{us}})^2)}{2} \end{aligned} \tag{3.19}$$

Equation (3.19) defines C_p as the portion of wind energy from the upstream that the rotor blades harness.The parameter that is widely known as the Betz limit was derived in 1919 by a German physicist by the name of Albert Betz. The power coefficient varies according to the ratio of the wind turbine tip speed. Let be the difference between the wind speed upstream (v_{us}) and downstream (v_{ds}) of the turbine. So

$$\lambda = \frac{v_{ds}}{v_{us}} \tag{3.20}$$

or $$\lambda = \frac{Tip \text{ speed of blades}}{wind \text{ speed}} \tag{3.21}$$

Where λ symbolize the wind turbine's tip speed blade.

The turbine's rotating speed and blade length define the speed at the tips of the blades, which is expressed in meters per second. i.e.

$$Tip\ speed\ of\ blades = \frac{turbine's \text{ rotational speed(w) x R}}{wind \text{ speed}} \tag{3.22}$$

Where R represents the turbine's radius and w is measured in radius per second .by substituting the expression in Equations (3.19) and (3.22) results in

$$C_p = \frac{(1+\lambda)(1-\lambda^2)}{2} \tag{3.23}$$

Derive the expression for the differentiation of the C_p concerning λ and set it equal to zero to determine the value of the λ at which C_p reaches it maximum.

$$\begin{aligned} \frac{dC_p}{d\lambda} &= \frac{d}{d\lambda}\left(\frac{((1-\lambda^2)*(1+\lambda)}{2}\right) \\ &= \frac{d}{d\lambda}\left(\frac{1-\lambda^2-\lambda-\lambda^3}{2}\right) \\ &= \frac{-2\lambda+\lambda-3\lambda^3}{2} \\ &= -2\lambda+\lambda-3\lambda^3 = 0 \\ \lambda &= \text{-}1 \quad \text{and } \lambda = \frac{1}{3} \end{aligned} \tag{3.24}$$

When we substitute the value of this λ in Equation (3.23) which means -1 and 0.333, then we get 0 and $16/27 = 0.5925$ respectively. This upper limit is $16/27 = 0.5925$. according to Betz limit, it stipulates that wind turbines cannot exceed converting greater than λ (59.3%) of the wind's kinetic energy in to mechanical energy for the rotor rotation. represented as C_p max =0. 593. However it is significant to note that wind turbines are unable to work at this maximum threshold. Wind turbines typically operate at efficiencies below the theoretical maximum known as the Betz limit.in fact even the best designed wind turbines achieved efficiencies in the range of 0.35 to 0.45, which is significantly lower than the Betz limit 0.593. When the rotor of wind turbines rotates at the slow pace, a significant portion of the wind tends to flow via the gaps between the blades, resulting in the minimum power extraction. Conversely, if the rotor spins too rapidly, rotating the blades function as a solid barrier, impeding the flow of wind and diminishing power mining. The turbines need to be designed to purpose at the most effective wind tip speed ratio λ to increase the generation of power from the Wind stream. In theory, the greater values of λ are advantageous for the optimal functioning of the generator. However, there are drawbacks associated with high λ .it results in the erosion of the blades' leading edges, primarily due to the impact of airborne sand particles. This necessitates the application of erosion-resistant coatings, which may elevate energy production costs. Increased the value of values of λ also contribute to issues such as noise generation, vibration, diminished rotor efficiency resulting from the drag and tip losses, and the risk of turbine failure with excessively higher rotor speed (Manyonge et al., 2012).

Pitch angle (β) and tip speed ratio (λ) can be employed in the following equation to express the power factor.

$$C_p(\lambda,\beta) = c_1(\mathrm{c}_2 \frac{1}{\lambda_i} - \mathrm{c}_3\,\beta - \mathrm{c}_4)\,\mathrm{e}^{\frac{-c_5}{\lambda t}} + c_6\lambda \tag{3.25}$$

$$\frac{1}{\lambda t} = -\frac{0.035}{1+\beta^3} + \frac{1}{\lambda + 0.08\beta} \tag{3.26}$$

The power coefficient (cp) is the primary critical parameter in power control scenarios. It is a nonlinear function that changes depending on the type of turbine and is somewhat impacted by wind speed. The power coefficient depends on the angle of the pitch and tip speed ratio, whereas the wind turbine's tip speed is dependent on variables such the rotor speed, the radius of the blades, and the wind speed. Within the framework of this thesis, the following values are utilized.

Table 3-1: Constant value of coefficient of power (Manyonge et al., 2012).

C_1	C_2	C_3	C_4	C_5	C_6
0.5176	116	0.4	5	21	0.0068

The rotational speed also yields the rotor torque.

$$T_m = \frac{P_m}{w_r} \tag{3.27}$$

Where T_m is represented by rotor torque, P_m mechanical power, w_r rotor speed (Rashid et al., 2018). These parameters are controlled or regulated by using a wind turbine blade pitch mechanism.

Table 3-2: Wind Turbine Parameters

Parameters	Symbols	Values and units
Air Density	ρ	$1.223\, kg / m^3$
Power coefficient	c_p	0.48
Rated wind speed	v_w	9-10 m/s
Radius	R	40m
Tip speed ratio	λ	8.1
Coefficients	$c_1 - c_6,$	$0.5176,\ 116, 0.4, 5, 21, 0.0068,$
Mechanical power	p_m	1.5MW

3.4 Modelling of Pitch Actuator

One of the most adaptable and popular control strategies for modifying a wind turbine's output power and speed is the pitch actuator, which rotates a blade along its longitudinal axis when the wind speed exceeds the rated threshold. Electrical or hydraulic control is available for pitch actuator systems. In an electric actuator step-up, each blade can be adjusted using a servo motor. In this thesis, a DC servo motor is utilized as the actuator. The dynamic relationship between the measured angle of the pitch (β) and the pitch demand (β_{de}) given by the pitch controller is outlined by the actuator model. This is the expression for the change in pitch angle.

$$\frac{d\beta}{dt} = \frac{\beta_{de} - \beta}{\tau_\beta} \quad (3.28)$$

Where $\beta_{de}, \beta, \tau_\beta$ are the pitch demand, measured pitch angle and time constant pitch actuators respectively. From the equation we can derive the following equation as,

$$\frac{d\beta}{dt}\tau_{\beta} = \beta_{de} - \beta$$
$$\frac{d\beta}{dt}\tau_{\beta} + \beta = \beta_{de} \qquad (3.29)$$

Through the application of Laplace transformation, and rearrangement of this equation, the statement can be rephrased as follows

$$s\beta\tau_{\beta} + \beta = \beta_{de}$$
$$\frac{\beta}{\beta_{de}} = \frac{1}{s\tau_{\beta} + 1} \qquad (3.30)$$

The pitch control's effectiveness is influenced by the time constant of the actuator .it can be determined using the initial parameters of the wind turbine.

3.5 Modelling of Permanent Magnet Synchronous Generator

DFIG and PMSG represent the leading technologies in wind power generation Employed in most wind energy conversion. A DFIG is an induction generator that interfaces with the grid via a dual-convertor. This converter enables the management of both the active and reactive power produced by DFIG, playing a essential role in preserving the grid stability. DFIGs are commonly used in wind energy conversion systems because they offer several advantages over other types of generators, including Variable speed operation, Power quality and improved grid stability. Since the stator of a DFIG is linked directly to the grid, any faults in the grid can have an important impact on the DFIG (Gatavi et al., 2019).

PMSG offers several advantages compared to DFIG, such as the ability to function without the gearbox, low maintenance expenses, and the capability to harness maximum power from variable speeds. Consequently, PMSG was selected for this thesis due to its favourable attributes. The two-phases synchronous reference frame serves as the foundation for the dynamic model of PMSG, and the q-axis is 90 degrees ahead of the d-axis with respect to the direction of rotation. The a-b-c three phase frame and the d-q rotating reference frame are continuously aligned thanks to a phase lock loop (PLL).(Azevedo, 2013).

3.5.1 Modelling Permanent Magnet Synchronous Generator in a Synchronously Rotating a-b-c Axis Reference Frame

The standard assumptions that form the basis for the modelling of PMSG in power systems and in converter system analysis typically including the following

- The stator windings are arranged sinusoidal along the air gap, especially with the regard to their common interaction with the rotor.
- The presences of the stator slots do not significantly alter the inductance of the rotor based on its position.
- The impact of magnetic hysteresis and saturation effects is insignificant.
- The stator wind is exhibiting symmetry
- The inclusion of damping windings is not taken into account.
- Power losses are assumed to be constant so the windings' capacitance can be ignored and the resistances stay constant.

The PMSG model is presented as shown and follows the figure below. To model PMSG the transformation Clark and Park transformations are very necessary and are presented in the next section.

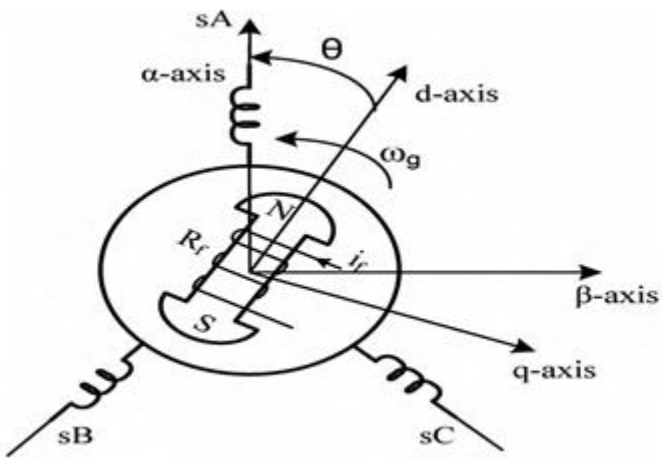

Figure 3-2 d-q and α-β standard salient pole synchronous machine (Azevedo, 2013)

3.5.1.1 Clark and Park Transformation

For deploying vector control, the Clark and park transformation are fundamental techniques. Essentially, the stationary quantities (a-b-c) are essentially converted in to the

($\alpha-\beta$) an orthogonal stationary quantities by the Clark transformation while the ($\alpha-\beta$) quantities are transformed to the d-q rotational quantities by the transformation of the park .in this thesis three reference frames were taken in to consideration.

1. In a reference frame of the three-phase, the quantities X_a X_b X_c represent three-phase electrical voltage or current that lies in the same plane, each spaced apart by an angle of 120^o
2. Stationary reference frame is described as orthogonal when its two axis X_α (along the α axis) and X_β (along the X_d axis) are at a right angles to each other .these axis also situated use the same plane as the frame for the three phases of reference
3. In a reference frame of the orthogonal rotating, the X_d is positioned at an angle θ (rotating angle) relative to the axis, while the X_q is perpendicular to the X_d along the q-axis (Abdul & Altahir, 2020). this transformation can be direct transformation and reverse transformation.

Direct Transformation

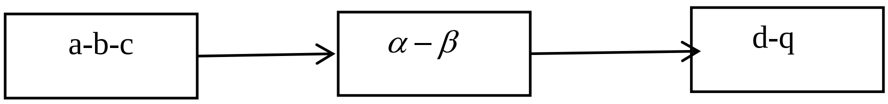

$$\begin{pmatrix} X_\alpha \\ X_\beta \end{pmatrix} = \frac{3}{2} \begin{pmatrix} 1 & -\frac{1}{2} & -\frac{1}{2} \\ 0 & \frac{\sqrt{3}}{2} & \frac{\sqrt{3}}{2} \end{pmatrix} \begin{pmatrix} X_a \\ X_b \\ X_c \end{pmatrix} \tag{3.31}$$

$$\begin{pmatrix} X_d \\ X_q \end{pmatrix} = \begin{pmatrix} \cos(\theta) & \sin(\theta) \\ -\sin(\theta) & \cos(\theta) \end{pmatrix} \begin{pmatrix} X_\alpha \\ X_\beta \end{pmatrix} \tag{3.32}$$

$$\begin{pmatrix} X_d \\ Xq \end{pmatrix} = \begin{pmatrix} \cos\theta & \cos(\theta-120^o) & \cos(\theta+120^o) \\ \text{-}\sin\theta & \text{-}\sin(\theta-120^o) & \text{-}\sin(\theta+120^o) \end{pmatrix} \begin{pmatrix} X_a \\ X_b \\ X_c \end{pmatrix} \tag{3.33}$$

Reverse Transformation.

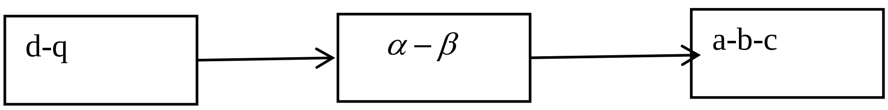

$$\begin{pmatrix} X_{\alpha} \\ X_{\beta} \end{pmatrix} = \begin{pmatrix} \cos\theta & \text{-}\sin\theta \\ \sin\theta & \sin\theta \end{pmatrix} \begin{pmatrix} X_d \\ X_q \end{pmatrix} \tag{3.34}$$

$$\begin{pmatrix} X_a \\ X_b \\ X_c \end{pmatrix} = \begin{pmatrix} 1 & 0 \\ -\frac{1}{2} & \frac{\sqrt{3}}{2} \\ -\frac{1}{2} & \frac{\sqrt{3}}{2} \end{pmatrix} \begin{pmatrix} X_{\alpha} \\ X_{\beta} \end{pmatrix} \tag{3.35}$$

$$\begin{pmatrix} X_a \\ X_b \\ X_c \end{pmatrix} = \begin{pmatrix} \cos\theta & \text{-}\sin\theta \\ \cos(\theta - \frac{2}{3}\pi) & \text{-}\sin(\theta - \frac{2}{3}\pi) \\ \cos(\theta + \frac{2}{3}\pi) & \text{-}\sin(\theta + \frac{2}{3}\pi) \end{pmatrix} \begin{pmatrix} X_d \\ X_q \end{pmatrix} \tag{3.36}$$

Where

- X depicts voltage or current in rotational, orthogonal, and stationary reference frames.
- θ is represents the angle between the d-q and $\alpha - \beta$ reference frame (Abdul & Altahir, 2020)

The following equation represents the electrical dynamics behaviour of PMSG described in terms of the phase variable.

$$\begin{aligned} v_{as} &= \frac{d\lambda_{as}}{dt} + R_s I_{as} \\ v_{bs} &= \frac{d\lambda_{bs}}{dt} + R_s I_{bs} \\ v_{cs} &= \frac{d\lambda_{cs}}{dt} + R_s I_{cs} \end{aligned} \tag{3.37}$$

Where

v_{as} , v_{bs} , v_{cs} represented three-phase voltage stator side.

I_{as} , I_{bs}, $I_{cs,}$ represent three-phase current stator side.

R_s Represent resistance in three phases

λ_{as} , λ_{bs} , λ_{cs} represent the three phase flux linkages are determined both three phase current and permanent magnets, and they are expressed the through the following equation.

$$\lambda_{as} = \lambda_{ra} + L_{aa}i_{as} + L_{ab}i_{bs} + L_{ac}i_{cs} \tag{3.38}$$

$$\lambda_{bs} = \lambda_{rb} + L_{ab}i_{as} + L_{bb}i_{bs} + L_{ac}i_{cs} \tag{3.39}$$

$$\lambda_{cs} = \lambda_{rc} + L_{ac}i_{as} + L_{cb}i_{bs} + L_{cc}i_{cs} \tag{3.40}$$

or

$$\begin{pmatrix} \lambda_{as} \\ \lambda_{bs} \\ \lambda_{cs} \end{pmatrix} = \begin{pmatrix} \lambda_{ra} \\ \lambda_{rb} \\ \lambda_{rc} \end{pmatrix} + \begin{pmatrix} L_{aa} & L_{ab} & L_{ac} \\ L_{ab} & L_{bb} & L_{bc} \\ L_{ac} & L_{cb} & L_{cc} \end{pmatrix} \begin{pmatrix} i_{as} \\ i_{bs} \\ i_{cs} \end{pmatrix} \tag{3.41}$$

Where

L_{aa}, L_{bb}, L_{cc}, are self -inductances.

L_{ab}, L_{ac}, L_{bc}, are ,mutual inductances.

λ_{ra}, λ_{rb} λ_{rc} are the flux linkages of the rotor from the permanent magnet.

$$\begin{aligned} \lambda_{as} &= \lambda_r \cos\theta \\ \lambda_{bs} &= \lambda_r \cos(\theta - \frac{2\pi}{3}) \\ \lambda_{cs} &= \lambda_r \cos(\theta + \frac{2\pi}{3}) \end{aligned} \tag{3.42}$$

The reliance on results from the stator's self-inductance reaching its highest value when the rotor's q-axis lines up with the phase axis. However, when the q-axis is positioned between them, the mutual inductance increases (Viera Valencia & Garcia Giraldo, 2019).

3.5.2 Modelling Permanent Magnet Synchronous Generator in a Synchronously Rotating d-q Axis Reference Frame

By apply the transformation of the park converts the three-phase reference frame into a d-q reference frame. Through this transformation method, dynamic AC Parameters are converted into DC variables that remain constant over time by applying inverse park transformation we drive Equation (3.28), where X represents any of the variables such as flux linkage, current, and voltage.

$$\begin{pmatrix} X_{qs} \\ X_{ds} \\ X_{os} \end{pmatrix} = \begin{pmatrix} \cos\theta & \cos(\theta - \frac{2\pi}{3}) & \cos(\theta + \frac{2\pi}{3}) \\ \sin\theta & \sin(\theta - \frac{2\pi}{3}) & \sin(\theta + \frac{2\pi}{3}) \\ \frac{1}{2} & \frac{1}{2} & \frac{1}{2} \end{pmatrix} \begin{pmatrix} X_{as} \\ X_{bs} \\ X_{cs} \end{pmatrix} \tag{3.43}$$

Where, X represents current or voltage. Using this transformation, the equation for voltage on the d-q axis can be formulated as follows.

$$T_e = 1.5p(\lambda_r \, \mathrm{i}_{qs} - (\mathrm{L}_{ds} - \mathrm{L}_{qs})) \tag{3.44}$$

$$v_{ds} = R_s i_{ds} + L_d \frac{di_{ds}}{dt} - w_g i_{qs} L_q \tag{3.45}$$

$$v_{qs} = R_s i_{qs} + L_q \frac{di_{qs}}{dt} + w_g i_{ds} L_d + w_g \lambda_r \tag{3.46}$$

Where, v_{ds} and v_{qs} are the voltages in the stator of the d-q position frame, i_{ds} i_{qs} are the current in the stator of the reference frame of d-q. L_d , L_q are the inductance in the d-q axis reference frame, w_g is the speed of angular of the generator. λ_r is flux linkage in the rotor

3.5.3 Power and Torque Characteristics Permanent Magnet Synchronous Generator

The active and reactive powers at any given moment are expressed as follows (Paul et al., 2015).

$$P_{inpabc} = \begin{pmatrix} v_{as} & v_{bs} & v_{cs} \end{pmatrix} \begin{pmatrix} i_{as} \\ i_{bs} \\ \mathrm{i}_{cs} \end{pmatrix} \tag{3.47}$$

$$Q_{abc} = \frac{1}{\sqrt{3}} (\mathrm{v}_{bc} \mathrm{i}_a + \mathrm{v}_{ac} \mathrm{i}_b + \mathrm{v}_{ab} \mathrm{i}_c) \tag{3.48}$$

Where Q_{abc} , P_{inpabc} , reactive power and active power in a-b-c reference frame respective

The electromagnetic torque of PMSG can be described in the following manner.

$$T_e = \frac{3}{2} p(\lambda_r \, i_{qs} - (L_{ds} - L_{qs}) i_{qs} i_{ds}) \tag{3.49}$$

Where, p is the poles number.

If we consider non-salient, the electrical torque can be determined by specifying that the inductance of the PMSG for direct axis inductance (L_{ds}) equal to the inductance for the quadrature axis (L_{qs}) or $L_{qs} = L_{ds}$. Then electromagnetic torque of PMSG and power out generator will be as follows (Viera Valencia & Garcia Giraldo, 2019).

$$T_e = \frac{3}{2} p(\lambda_r \, i_{qs}) \tag{3.50}$$

$$= P_e w_g \tag{3.51}$$

Finally, using the given equation, the machine's active and reactive power is determined within a fixed reference frame and a synchronously spinning reference frame (Muluneh &Teame, 2021).

$$\begin{aligned} P_{\alpha\beta} &= \frac{3}{2}(V_\alpha i_\alpha + V_\beta i_\beta) \\ Q_{\alpha\beta} &= \frac{3}{2}(V_\alpha i_\beta - V_\beta i_\alpha) \\ P_{dq} &= (V_d i_d + V_q i_q) \\ Q_{dq} &= (V_d i_q - v_q i_d) \end{aligned} \tag{3.52}$$

Where $P_{\alpha\beta}$, $Q_{\alpha\beta}, P_{dq}$ and Q_{dq} is denote active and reactive power in $\alpha - \beta - 0$ the reference frame of the stationery and d-q synchronously rotating reference respectively.

3.6 Mathematical Modelling of Back-To-Back Converters

In a flexible-speed wind turbine electric generation system, there are three primary components. They are the wind turbine itself, the generators and the power converter. The power converter comprises two main sections. The generator rectifier and the inverter grid or load interface. Various power electronic components are employed in AC/DC and DC/AC power conversion processes within these converters (Oğuz et al., 2013). Power electronic converters manipulate voltage/ current waveform produced by PMSG according to the requirement of the grid. Since the output voltage of PMSG varies with wind speed, it is necessary to use an AC to DC converter, as a Machine Side Converter and DC to AC converter known as the Grid Side Converter for linking the generator to the grid (Van & Hai, 2013).

3.6.1 Mathematical Model of Machine Side AC-DC Converter

The bidirectional AC-DC converter operating in three phases is a critical component of energy storage systems, given its ability to facilitate power flow in both directions and synchronize with the system, making it indispensable for the bidirectional AC-DC converter must achieve high efficiency to mitigate issues related to poor power quality, including high AC voltage distortion, poor power factor, and high overall harmonic distortion, fluctuations in DC ripple and pulsations in the DC Voltage (Akter et al., 2015).

An active rectifier is a type of AC-DC converter that employs actively controlled switches, such as MOSFET and IGBTs, rather than diodes or thyristors, to rectify voltage and current. It offers main two advantages, the regulation of the output voltage (DC -link) and decrease of harmonics in the AC inputs. This converter has a bidirectional nature, allowing the DC side to function as either an output or an input (Keshavarz, 2011).

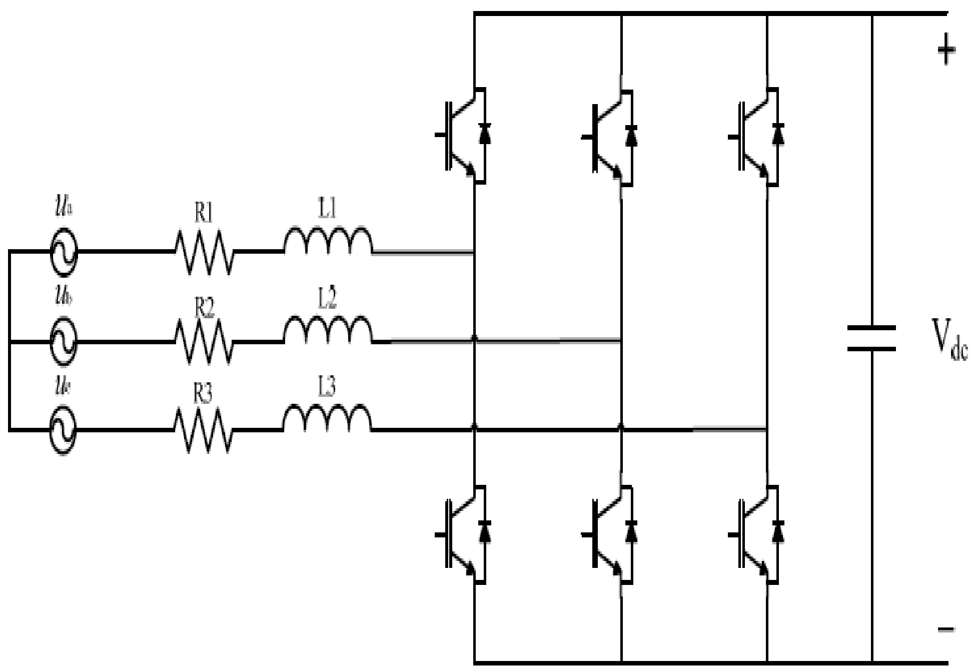

Figure 3-3:Three phase AC-DC Active rectifier.((Keshavarz, 2011).

The line voltages and current in the three-phase system can be represented mathematically as follows.

$$V_a = v_m \cos(wt) \quad (3.53)$$

$$V_b = v_m \cos(wt - 120^\circ) \quad (3.54)$$

$$V_c = v_m \cos(wt - 240^\circ) \quad (3.55)$$

$$I_a = I_m \cos(wt + \varphi) \quad (3.56)$$

$$I_c = I_m \cos(wt + \varphi - 240^\circ) \quad (3.57)$$

$$I_b = I_m \cos(wt + \varphi - 120^\circ) \quad (3.58)$$

The a-b-c – model of rectifier refers to a representation that describes its behaviour using three phases (a-b-c). In this model, rectifier's operation is characterised and analysed based on these three phases.

Assumption

- R1, R2, R3 are equal to R
- L1, L2, L3 are equal to L

$$\begin{bmatrix} V_a \\ V_b \\ V_c \end{bmatrix} = R \begin{bmatrix} I_a \\ I_b \\ I_c \end{bmatrix} + L \frac{d}{dt} \begin{bmatrix} I_a \\ I_b \\ I_c \end{bmatrix} + \begin{bmatrix} V_{sa} \\ V_{sb} \\ V_{sc} \end{bmatrix} \quad (3.59)$$

As well $$c \frac{dv_d}{dt} = S_a I_a + S_b I_b + S_c I_c - I_{load} \quad (3.60)$$

where S_a, S_b, S_c are switching function in a-b-c reference frame

$$V_{sa} = \left(\frac{2S_a - (S_b + S_c)}{3}\right) V_{dc} \quad (3.61)$$

$$V_{sb} = \left(\frac{2S_b - (S_a + S_c)}{3}\right) V_{dc} \quad (3.62)$$

$$V_{sc} = \left(\frac{2S_c - (S_a + S_b)}{3}\right) V_{dc} \quad (3.63)$$

The voltage between the two phases is determined

$$V_{Sab} = (S_a - S_b) V_{dc} \quad (3.64)$$

$$V_{Sbc} = (S_b - S_c) V_{dc} \quad (3.65)$$

$$V_{Sac}=(S_c-S_a)V_{dc} \quad (3.66$$

$$V_{Sca}=(s_c-s_a)V_{dc}\begin{bmatrix}V_a\\V_b\\V_c\end{bmatrix}=R\begin{bmatrix}I_a\\I_b\\I_c\end{bmatrix}+L\frac{d}{dt}\begin{bmatrix}I_a\\I_b\\I_c\end{bmatrix}+\begin{bmatrix}V_{sa}\\V_{sb}\\V_{sc}\end{bmatrix} \quad (3.67)$$

By utilizing the Clark transformation voltage equation can be defined in the $\alpha-\beta$ coordinates as follow

$$\begin{bmatrix}V_\alpha\\V_\beta\end{bmatrix}=R\begin{bmatrix}I_\alpha\\I_\beta\end{bmatrix}+L\frac{d}{dt}\begin{bmatrix}I_\alpha\\I_\beta\end{bmatrix}+\begin{bmatrix}V_{s\alpha}\\V_{s\beta}\end{bmatrix} \quad (3.68)$$

$$c\frac{dv_d}{dt}=\frac{3}{2}(S_\alpha I_\alpha+S_\beta I_\beta)-I_{load} \quad (3.69)$$

The voltage equations for the active rectifier, expressed in d-q coordinates, can be described as follows

$$\begin{aligned}V_d&=Ri_d+L\frac{d_{id}}{dt}-wLi_q+v_{sd}\\V_q&=Ri_q+L\frac{d_{iq}}{dt}+wLi_d+v_{sq}\\c\frac{dv_d}{dt}&=\frac{3}{2}(S_dI_d+S_qI_q)-I_{load}\end{aligned} \quad (3.70)$$

3.6.2 Mathematical Model of Grid Side DC-AC Converter

A grid side Inverter is composed of three phases with each phase incorporating two modules comprising IGBTs paired with freewheeling diodes. The IGBTs, together with a freewheeling diode, form a bidirectional semiconductor switch capable of facilitating energy flow in both directions (Mrcela et al., 2016). Following the generation of wind power, the electricity is initially transformed into direct DC voltage using a rectifier on the machine side The insulated gate bipolar transistor (IGBT) is then controlled by the grid-connected inverter to convert the DC voltage to AC voltage. This process might cause harmonics to arise during the modulation process. After being filtered, AC voltage is ultimately supplied to the power grid by considering L_1 and L_2 which indicate the inductance of the filter on the side of the inverter and the side grid respectively represents the capacitance in the filter. While R_c denoted the series damping resistance located on the capacitor side (Zheng et al., 2018).The representation of the mathematical inverter is as follow.

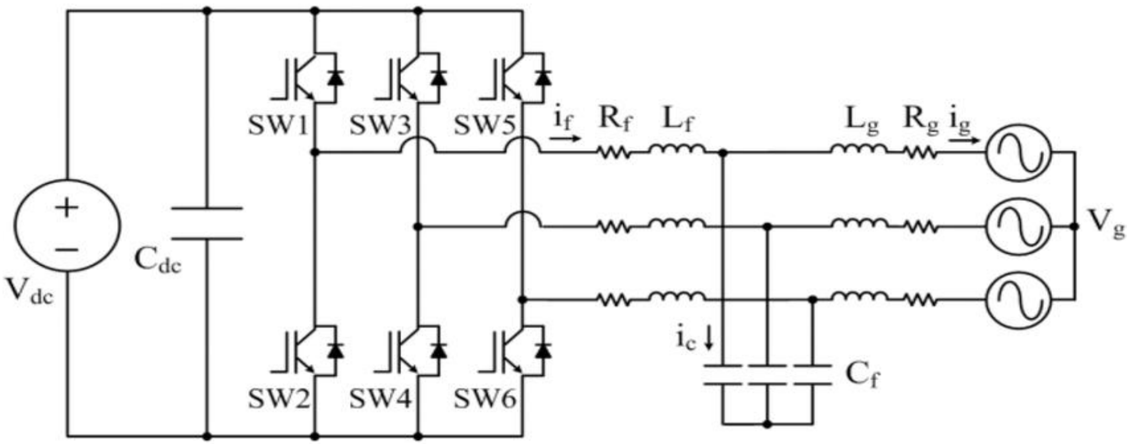

Figure 3-4 : Three phase inverter (Zheng et al., 2018)

$$\begin{aligned} L_1 \frac{di_{1abc}}{dt} &= V_{iabc} - Vc_{abc} - R_c(i_{1abc} - i_{2abc}) \\ L_2 \frac{di_{2abc}}{dt} &= Vc_{abc} - V_{gabc} + R_c(i_{1abc} - i_{2abc}) \\ C \frac{dvc_{abc}}{dt} &= (i_{1abc} - i_{2abc}) \end{aligned} \tag{3.71}$$

Where

- i_{1abc} i_{2abc} is represent the currents from the inverter output and output current from the grid -connected respectively.
- $V_{iabc}, Vc_{abc}, V_{gabc}$ are represent the inverter output voltage, capacitor voltage and grid-connected voltage respectively

As per the equal power work Clark transformation outlined in Equation (3.38), the inverter system operating in the abc -stationary coordinate reference frame can be converted in to a two-phase $\alpha\beta$ reference frame of the stationary. This transformation aims to simplify the controller's complexity.

$$T = \frac{2}{3}\begin{pmatrix} 1 & -\frac{1}{2} & -\frac{1}{2} \\ 0 & \frac{\sqrt{3}}{2} & -\frac{\sqrt{3}}{2} \end{pmatrix} \tag{3.72}$$

After the Clark transformation, the model can be model can be stated in the state equation form, illustrating the precise relationships among the variables of the inverter system.

$$\begin{aligned}
&L_1\frac{di_{1\alpha}}{dt}=V_{i\alpha}-Vc_{\alpha}-R_c(i_{1\alpha}-i_{2\alpha})+V_{i\alpha}\\
&L_1\frac{di_{1\beta}}{dt}=V_{i\beta}-Vc_{\beta}-R_c(i_{1\beta}-i_{2\beta})+V_{i\beta}\\
&L_2\frac{di_{2\alpha}}{dt}=Vc_{\alpha}-Vg_{\alpha}+R_c(i_{1\alpha}-i_{2\alpha})\\
&L2\frac{di_{2\beta}}{dt}=Vc_{\beta}-Vg_{\beta}+R_c(i_{1\beta}-i_{2\beta})\\
&\frac{dVc_{\alpha}}{dt}=\frac{1}{C}(i_{1\alpha}-i_{2\alpha})\\
&\frac{dVc_{\beta}}{dt}=\frac{1}{C}(i_{1_\beta}-i_{2_\beta})
\end{aligned}\tag{3.73}$$

Where

- $i_{1\alpha}, i_{1\beta}$ and $i_{2\alpha}, i_{2\beta}$ represent the component of the inverter output currents and the currents connected to the grid in the $\alpha\beta$ coordinate system.
- $V_{i\alpha}, V_{i\beta}$ and Vc_{α}, Vc_{β} represent the component of the inverter voltages outputs and the capacitor voltages in the $\alpha\beta$ coordinate system.
- Vg_{α}, Vg_{β} represent the component of the voltage connected to the grid in the $\alpha-\beta$ coordinate system (Zheng et al., 2018).

3.6.3 Dc Link Model

In Figure 3-4 the connection between converters on the machine and grid sides is shown to include shunt capacitance representing the dc-link.

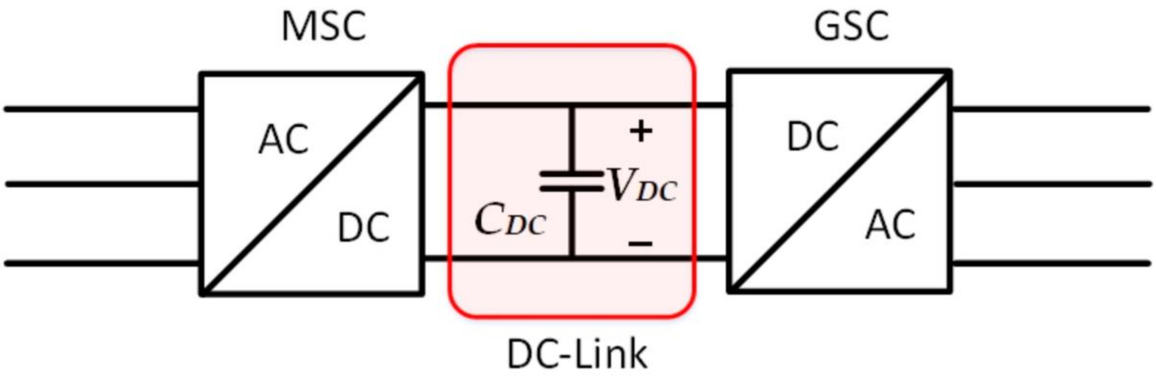

Figure 3-5 :Dc-link model **(**Zouheyr et al., 2021)

The Dc-link's energy storage capacity (E_{dc}) can be approximated using the following method (Awwad, 2022).

$$E_{dc} = 0.5C_{dc}(u_{dc}{}^{2}) \tag{3.74}$$

Where

- ➢ E_{dc} represents the energy stored in the Dc-Link.
- ➢ C_{dc} represents the capacitor that is stored in the Dc-Link.
- ➢ u_{dc} represents the voltage in the Dc-link.

One can select the dc-link capacitance by considering the maximum permissible voltage ripple. The switching frequency and the Dc-link capacitor size both affect the voltage ripple (Δu_{dc}). The dc-link capacitor (C_{dc}) expression is as follows.

$$C_{dc} \geq \frac{P_{no}}{4\sqrt{3}\pi f u_{dc} \Delta u_{dc}} \tag{3.75}$$

Where

- ➢ P_{no} is the voltage source converter's nominal power.
- ➢ f Represents the AC power supply's basic frequency.

The power transmitted through DC bus, as illustrated in Figure (3.5), is therefore described by (Zouheyr et al., 2021).

$$P_c = P_g - P_m \tag{3.76}$$

Where

- ➢ P_c is the power that the capacitor uses.
- ➢ P_g is the power supplied by generator side converter.
- ➢ P_m is the power absorb by the machine side converter.

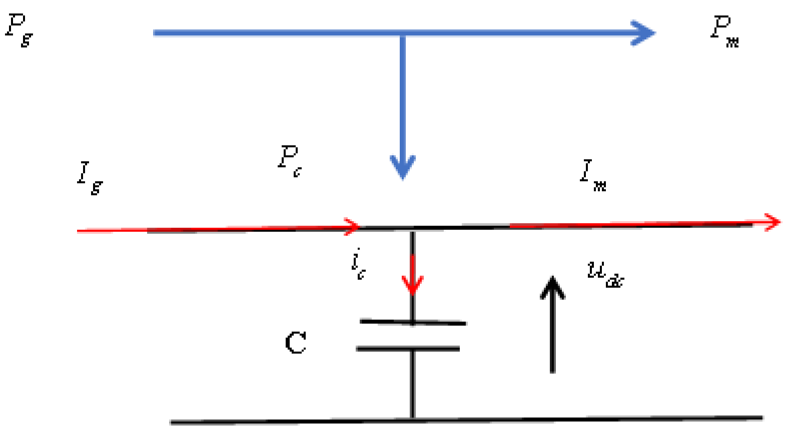

Figure 3-6: Dc-link Circuit

The power absorbed by the capacitor (P_c) can be described using the linearized form

$$P_c = u_{dc} c \frac{du_{dc}}{dt} \tag{3.77}$$

The expression for the DC bus voltage is delivered from Equations (3.55) and (3.56) as follow

$$\frac{du_{dc}}{dt} = \frac{1}{c} \frac{P_g - P_m}{u_{dc}} \tag{3.78}$$

3.6.4 Model of LCL Filter

A DC -AC converter linked to the power grid utilizes PWM to produces a sinusoidal waveform with extra harmonics in its output. Various conversion technologies exist, catering to low current application as well. Nonetheless, the inclusion of the filter is crucial. Filters are commonly utilized to dampen the harmonics present in the generated AC voltage. Their function includes diminishing high-frequency switching and safeguarding the load from transient voltage fluctuations. Various types of filters are utilized in DC-AC converters, including the L filter, LC filter .RC filter and LCL filter (Hasan et al., 2021).

To improve power quality and minimize current harmonics in the output of the GSC (Grid side converter), both LCL and L grid filters are employed. Comparatively the LCL grid filter demonstrates superior performances over the conventional L grid filter. The LCL filters offers the benefit of effectively decoupling the GSC from the AC grid.

The description provided for the LCL grid filter focuses on the analysis of a single-phase circuit with a real three phase filter setup. Figure (3-7) illustrates the equivalent single-phase circuit of the LCL filter (Gajewski & Pieńkowski, 2016).

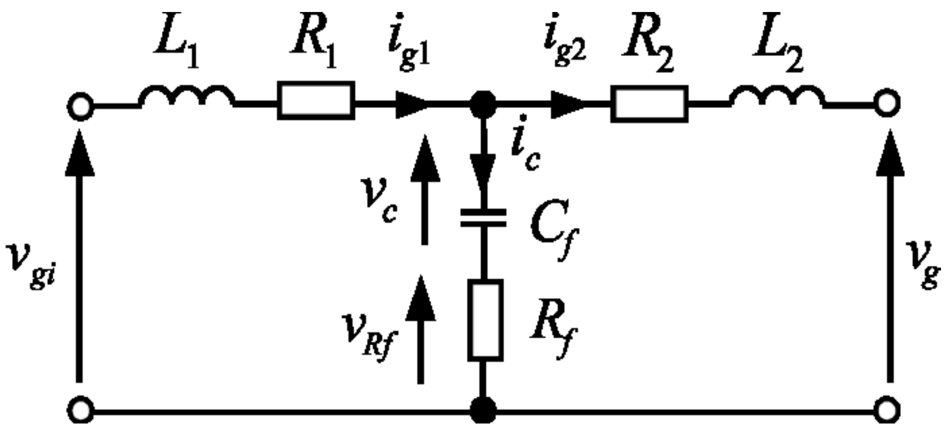

Figure 3-7: LCL filter grid-connected ((Gajewski & Pieńkowski, 2016)).

Where,

- V_{gi} is the voltage of the output of the grid connected GSC.
- V_g is the voltage grid
- R_1 and L_1 are resistance and inductance of the filter on the grid-side converter
- R_2 and L_2 are Show the filter's resistance and inductance on the side of the grid.
- i_{g1} is the phase current output from the conversion grid side.
- i_{g2} is the phase current output from the grid side.
- i_c is the current flowing through the filter capacitor.

- R_f and C_f are the resistance and capacitance responsible for damping in the filter.
- V_f denotes the voltage that is applied across the filter capacitor.

The state equations of the LCL grid filter can be represent in the following the equation.

$$\begin{bmatrix} \frac{di_{g1}}{dt} \\ \frac{di_{g2}}{dt} \\ \frac{dv_c}{dt} \end{bmatrix} = \begin{bmatrix} -\frac{R_f + R_1}{L_1} & \frac{R_f}{L_1} & -\frac{1}{L_1} \\ \frac{R_f}{L_2} & \frac{R_2 + R_f}{L_2} & \frac{1}{L_2} \\ \frac{1}{c_f} & \frac{1}{c_f} & 0 \end{bmatrix} \begin{bmatrix} i_{g1} \\ i_{g2} \\ v_c \end{bmatrix} + \begin{bmatrix} \frac{1}{L_1} & 0 \\ 0 & -\frac{1}{L_2} \\ 0 & 0 \end{bmatrix} \begin{bmatrix} v_{gi} \\ v_g \end{bmatrix} \tag{3.79}$$

The process for designing the LCL grid filter is out lined as follows.to begin, the initial stage involves determining the values of the The base capacitance (Cb), base impedance (Zb), and base inductance (Lb), for the filter through the calculation.

$$Z_b = \frac{V^2{}_n(rms)}{S_n} \tag{3.80}$$

$$L_b = \frac{Z_b}{w_g} \tag{3.81}$$

$$C_b = \frac{1}{w_g Z_b} \tag{3.82}$$

Where

- V_n is the phase converter voltage under normal conditions.
- S_n is the apparent power rating of the converter under normal conditions.
- w_g is the frequency of the grid in angular measure.

The selection of the filter capacitance, C_f, is made with the condition in that it remains below 5% of the base capacitance (Reznik et al., 2014).

$$Cf \le 0.05 C_b I_n = \frac{S_n}{3V_n} L_1 = \frac{V_{dc}}{6 f_{sw} I_{\max rip}} \tag{3.83}$$

The amplitude of the current ripple denoted as $I_{\max rip}$, in the GCS output phase current can be adjusted within range of 10% to 25% of the nominal converter phase current I_n (Gajewski & Pieńkowski, 2016).

$$I_{\max} = \sqrt{2}(0.1-0.25).I_n \tag{3.84}$$

Where $$I_n = \frac{S_n}{3V_n} \tag{3.85}$$

The derivation of the inductance for both the converter side (L_1) and the grid filter (L_2) can be performed as follows.

$$L_1 = \frac{V_{dc}}{6 f_{sw} I_{\max rip}} \tag{3.86}$$

$$L_2 = rL_1 \tag{3.87}$$

Where

- f_{sw} is the switching frequency of GSC
- V_{dc} is the dc link converter's mean voltage.
- r is the inductance L_2 to the inductance (L_1) ratio.

The damping resistance can be computed as follows

$$R_f = \frac{1}{3 f_r c_f} \tag{3.88}$$

Where

- f_r is the frequency at resonance, which is derived as,

$$f_r = \frac{1}{2\pi}\sqrt{\frac{L_1 + L_2}{L_1 L_2 c_f}} \tag{3.89}$$

Considering the following value

- Grid voltage =690v
- Rated power= 1.5MW

- Grid frequency =50hz
- Switching frequency of the grid =10KHZ

$$z_{base} = \frac{690}{1.5x10^6}^2 = 0.32\Omega$$

$$I_{base} = \frac{0.32\Omega}{2*3.14*50} = 1.01mA$$

$$C_{base} = \frac{1}{2*3.14*50*0.32} = 995.22\mu F$$

$$Cf \leq 0.05C_b = 0.05*995.22\mu F$$
$$C = 49.76\mu F$$

$$I_n = \frac{S_n}{3V_n} = \frac{1.5*10^6}{3*690} = 724.64A$$

$$I_{\max} = \sqrt{2}(0.1-0.25).I_n = I_{\max} = \sqrt{2}*0.25*724.64 = 256.2A$$

$$L_1 = \frac{V_{dc}}{6f_{sw}I_{\max rip}} = \frac{690}{6*256.2*10^4} = 44.89\mu H$$

$$L_2 = rL_1 = 0.2*44.89\mu H = 8.98\mu H$$

$$f_r = \frac{1}{2\pi}\sqrt{\frac{L_1+L_2}{L_1L_2c_f}} = f_r = \frac{1}{2\pi}\sqrt{\frac{44.89\mu H + 8.98\mu H}{44.89\mu H * 8.98\mu H * 49.76\mu F}} = 8.26KHz$$

$$R_f = \frac{1}{3f_rc_f} = \frac{1}{3*8.26KHz*49.76\mu F} = 0.82\Omega$$

Table 3-3: Specification of LCL Parameters.

Parameters	Calculated value
Voltage from inverter(V)	690V
Rated power(W)	1.5MW
Grid frequency(Hz)	50hz
Switch frequency(Hz)	10Khz
Base impedance**(Ω)**	0.32Ω
Base current(A)	1.01mA
Nominal current(A)	724.64µA
Filter capacitance(F)	49.76µF
Damping resistance(Ω)	0.82Ω
Resonant frequency(Hz)	8.26Khz
Inductance (L1)	44.89µH
Inductance (L2)	8.89µH

3.7 Mathematical Modelling of the STATCOM and Its operation

A STATCOM serves as a reactive compensation device connected in parallel, capable of either producing or absorbing reactive power to control specific parameters within an electrical power system. By employing self-commutated pulse width modulation (PWM) converters alongside a suitable control system, STATCOM implementation achieves a faster response time than the fundamental power cycle. Because STATCOM is a self-energized reactive power compensation device, reactive power is not supplied or absorbed by any conventional passive elements. By controlling the injection of reactive power from STATCOM at the linked point, controllable power electronics can be used to manage the system voltage. When the bus voltage is low, the STATCOM adds reactive power to the system; conversely, when the bus voltage is high, it subtracts reactive power from the system.

Let V1 and V2 stand for the corresponding grid voltage and STATCOM terminal voltage. The equivalent reactance of the compensator and filter output transformer is denoted by X. The actual and reactive power (P and Q) between the grid bus and STATCOM is expressed as follows (Tarafdar Hagh et al., 2008).

$$P = \frac{V_1 * V_2}{X} \sin \sigma \tag{3.90}$$

$$Q = \frac{V_1 (V_1 - V_2 \cos \sigma)}{X} \tag{3.91}$$

Where σ denotes the angle difference between V1 and V2

In order to accomplish the necessary reactive power exchange to power systems, STATCOM modifies V2 and σ .In order to balance reactive power and preserve the reliability of the power grid, STATCOM, which is linked to the grid in parallel, may produce three-phase sinusoidal voltage amplitudes and phase angles with a quick, adjustable fundamental frequency. A simplified circuit with a STATCOM linked to the grid is seen in Figure 3-8.
Figure 3-8 illustrates the equivalent circuits' model of the STATCOM. In this model, resistances R represent the combined losses due to the transformer winding resistance and the inverter conduction. L denotes the transformer's Leakage inductance (Han et al., 2006).

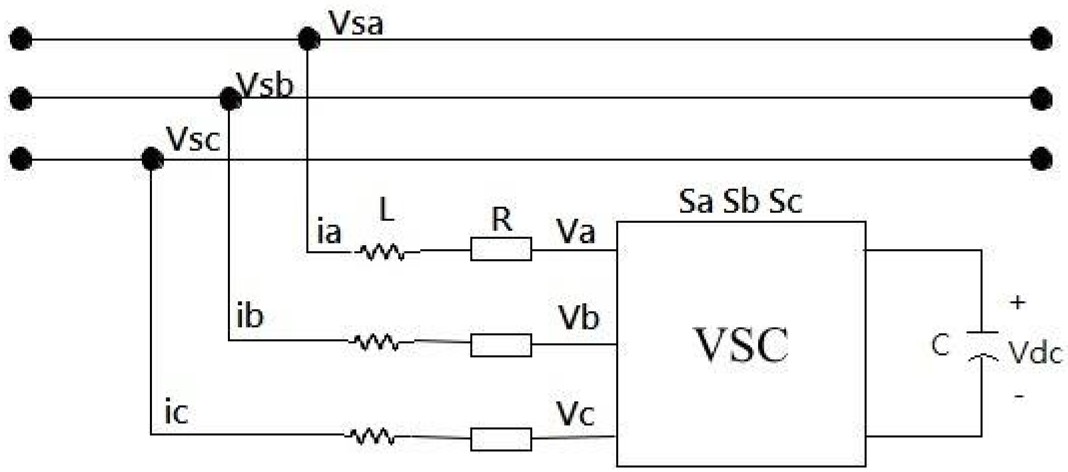

Figure 3-8: Simplified circuit that is linked to the grid using STATCOM (Hong et al., 2018)

- v_a, v_b, *and* v_c are the three-phase AC voltages following the Voltage Source Converter (VSC);
- V_{sa}, V_{sb}, *and* V_{sc} are the voltages at the power grid's connected point;

- $i_a,\ i_b,\ and\ i_c$ are the compensating currents in three phases and
- $s_a,\ s_b,\ and\ s_c$ represent the three-phase switching statuses, as illustrated in Figure (3-8)

The dynamic time-domain model of the circuit can be obtained using Kirchhoff's law:

$$\begin{aligned}\frac{di_a}{dt} &= \frac{V_a}{L} + \frac{Ri_a}{L} - \frac{V_{sa}}{L}\\ \frac{di_b}{dt} &= \frac{V_b}{L} + \frac{Ri_b}{L} - \frac{V_{sb}}{L}\\ \frac{di_c}{dt} &= \frac{V_c}{L} + \frac{Ri_c}{L} - \frac{V_{sc}}{L}\\ \frac{dV_{dc}}{dt} &= \frac{(s_a i_a + s_b i_b + s_c i_c)}{C}\end{aligned} \qquad (3.92)$$

To simplify the computation, the three-phase voltage and current in an a-b-c reference frame are transformed into the d-q0 rotating reference frame using the Park Transform matrix P as follows:

,

$$P = \begin{pmatrix} \cos wt & \cos(wt - 120^o) & \cos(wt + 120^o) \\ \sin wt & s\,in(wt - 120^o) & \sin(wt + 120^o) \\ \frac{1}{2} & \frac{1}{2} & \frac{1}{2} \end{pmatrix} \qquad (3.93)$$

That's, $i_{dq0} = P * i_{abc}$ where $i_q\ and\ i_q$ can be easily controlled in an orthogonal *d-q* coordinate system as follows:

$$\begin{aligned}\frac{di_d}{dt} &= \frac{S_d V_{dc}}{L} - \frac{Ri_d}{L} - \frac{V_{sd}}{L} + wi_q\\ \frac{di_q}{dt} &= \frac{S_q V_{dc}}{L} - \frac{Ri_q}{L} - \frac{V_{sq}}{L} + wi_d\\ \frac{dV_{dc}}{dt} &= \frac{3}{2C}(S_d I_d + S_q i_q)\end{aligned} \qquad (3.94)$$

The state variables are $i_d,\ i_q,\ and\ V_{dc}$, and the control system's inputs are $S_d\ and\ S_q$. The control system's outputs (designated as) are the $y_1\ and\ y_2$ PWM modulator's input values:

$$\begin{aligned}y_1 &= i_d - i_{dref}\\ y_2 &= i_q - i_{qref}\end{aligned} \qquad (3.95)$$

Where, i_{dref} *and* i_{qref} , denotes the references respectively.

3.8 Controllers Design

In a wind energy conversion system linked to the grid, controllers are essential for regulating voltage during various types of three phase faults. These faults can happen due to a variety of causes such as short circuits. When a fault is occurs, it can cause disturbance in the grid voltage, affecting the stability and consistency of the entire power system. Controllers are needed to mitigate the effects of these faults and continue the voltage within acceptable limits. Here is the controller applied in the system.

3.8.1 Pitch Actuator Controller

Pitch angle control is frequently used with turbines to regulate the blades' rotating speed and, consequently, the turbine's output. The actuator's transfer function, derived from Equation (3.30) is also displayed in Figure 3-9, which displays the output signal of the PI controller as B_d , the required pitch angle and PI Controller can be represented in the following manner (Hwas & Katebi, 2012).

$$\begin{aligned} B_d &= K_p e(t) + K_i \int e(t)dt \\ x &= K_i \int e(t)dt \end{aligned} \tag{3.96}$$

Where $$e(t) = w_{m\mathrm{Re}f} - w_m \tag{3.97}$$

Let $$\frac{dx}{dt} = K_i e(t) \tag{3.98}$$

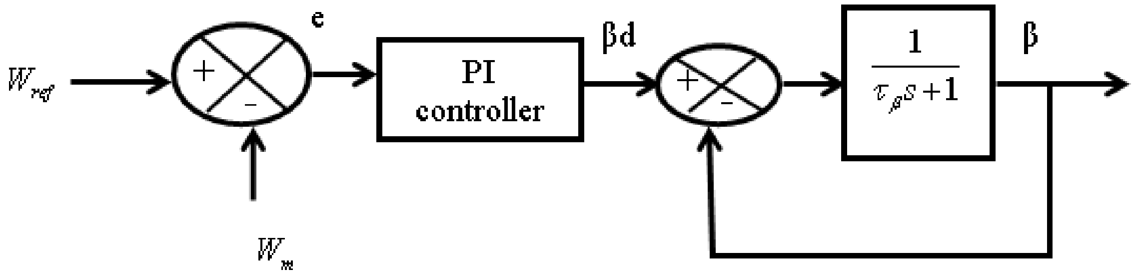

Figure 3-9: Pitch control Using the PI Controller

Derived from Equations (3.97) and (3.98), the partial differentiation of B_d concerning e is as follows

$$\frac{d\beta_d}{dt} = K_p + \frac{dx}{dt}$$
$$= K_p + \frac{dx/de}{de/dt} \quad (3.99)$$
$$= K_p + K_i \frac{e}{de/dt}$$

The difference in the within the range e an adjustable slip synchronous generator is extremely narrow. Additionally, since K_p is much larger than Ki, Equation (3.100) can be written

$$K_p = \frac{d\beta_d}{de} \quad (3.100)$$

By simplifying the internal closed loop system of the actuator in Figure (3-8) to moving forward and presuming to control a time constant of ($\tau_\beta = 1\sec$). For the actuator, we derived the following transfer function. The rate of change of the desired blade pitch angle ($d\beta_d$) is equal to the desired blade pitch angle (β_d) itself. This indicates a direct relationship between the desired blade pitch angle (β_d) and the actual blade angle of the pitch (β), considering the simplified forward path of the actuator.

$$\frac{\beta}{\beta_d} = \frac{1}{s+2} K_P = \frac{2\beta}{wm\_ref - w_m} \quad (3.101)$$

In the steady state S approach to zero and $\beta_d = 2\beta$. From Equations (3.86), (3.88), (3.89), the values of the K_i and K_p are determined as follows(Hwas & Katebi, 2012).

$$K_P = \frac{2\beta}{wm\_ref - w_m} \quad (3.102)$$

$$K_i = \frac{1}{w_{m\,ref} - w_m} * \left(\frac{2\beta}{w_{mref} - w_m} - Kp\right) * \frac{d\Delta w}{dt} \quad (3.103)$$

From designed wind turbine B=0.0997,In direct-drive systems, The PMSG's rotor and the wind turbine's rotor are directly connected. This means: $w_t = w_m$ =0.414rad/sec and w_{mref} =1,737 rad/sec then the value of designed controller is as follow.

$$K_P = \frac{2\beta}{wm\_ref - w_m} = \frac{2*0.0997}{1.737-0.414} = 0.15$$

$$K_i = \frac{1}{1.737-0.414} * (\frac{2*0.0997}{1.737-0.414} - 0.15) * 0.1323 = 0$$

3.8.2 Convertor Controller

Using a converter controller in a rectifier connected to a PMSG offers several benefits, particularly in applications such as wind turbines and other renewable energy systems. Converter controllers can implement MPPT algorithms to ensure that the PMSG operates at its optimal power output regardless of varying wind speeds or other environmental conditions. From Equation (3.70) the convert the given dynamic equations into Laplace transform, we need to organize them into a standard format.From the given following equation transfer function.

The given dynamics equation is

$$V_d = Ri_d + L\frac{d_{id}}{dt} - wLi_q + v_{sd} \tag{3.104}$$

$$V_q = Ri_q + L\frac{d_{iq}}{dt} + wLi_d + v_{sq} \tag{3.105}$$

To derive transfer function using Laplace transform where v_d is input and i_q, i_d are the outputs, we need consider the equation in both direct and quadrature axes. The given equation is for the direct axes. Typically, the quadrature axes are also provided, but we will assume as it has a similar form for this purpose.

Given from Eequations (3.104) and (3.105)

$$V_d = Ri_d + L\frac{di_d}{dt} - wLi_q + v_{sd} \tag{3.106}$$

We need the quadrature axis equation.

$$V_q = Ri_q + L\frac{di_q}{dt} + wLi_d + v_{sq} \tag{3.107}$$

By applying the Laplace transform to both equations.

- For the direct axis:

$$V_d(s) = Ri_d(s) + Lsi_d(s) - wLi_q(s) + v_{sd}(s) \quad (3.108)$$

- For the quadrature axis:

$$V_q(s) = Ri_q(s) + Lsi_q(s) + wLi_d(s) + v_{sq}(s) \quad (3.109)$$

Expressing $i_d(s)$ in terms of $V_q(s)$ and $V_d(s)$:

- For the direct axis equation:

$$V_d(s) = (R + Ls)i_d(s) - wLi_q(s) + v_{sd}(s) \quad (3.110)$$

By rearranging:

$$i_d(s) = \frac{V_d(s) - v_{sd}(s) + wLi_q(s)}{R + Ls} \quad (3.111)$$

- Forthe quadrature axis

$$V_q(s) = Ri_q(s) + Lsi_q(s) + wLi_d(s) + v_{sq}(s) \quad (3.112)$$

$$i_q(s) = \frac{V_q(s) - v_{sq}(s) - wLi_d(s)}{R + Ls} \quad (3.113)$$

- Substitute $i_q(s)$ from the quadrature equation into the direct axis equation to get relation between $i_d(s)$ and the inputs.

  First, isolate $i_q(s)$ in terms of $i_d(s)$:

$$i_q(s) = \frac{V_q(s) - v_{sq}(s) - wLi_d(s)}{R + Ls} \quad (3.114)$$

  Now substitute this in to the direct axis equation for $i_d(s)$

$$i_d(s) = \frac{V_d(s) - v_{sd}(s) + wL(\frac{V_q(s) - v_{sq}(s) - wLi_d(s)}{R + Ls})}{R + Ls} \quad (3.115)$$

- By rearranging Equation (3.115) and solving for the $i_d(s)$

$$i_d(s) = \frac{V_d(s) - v_{sd}(s)}{R + Ls} + \frac{wL}{R + Ls} * \frac{V_q(s) - v_{sq}(s) - wLi_d(s)}{R + Ls} \quad (3.116)$$

$$= \frac{V_d(s) - v_{sd}(s)}{R + Ls} + \frac{wL(V_q(s) - v_{sq}(s))}{(R + Ls)^2} - \frac{(wL)^2 i_d(s)}{(R + Ls)^2} \quad (3.117)$$

- By collecting like terms and solving this equation for $i_d(s)$ as follow equation based on Equation (3.109)

$$i_d(s) + \frac{(wL)^2 i_d(s)}{(R + Ls)^2} = \frac{V_d(s) - v_{sd}(s)}{R + Ls} + \frac{wL(V_q(s) - v_{sq}(s))}{(R + Ls)^2} \quad (3.118)$$

$$(1 + \frac{(wL)^2}{(R + Ls)^2}) i_d(s) = \frac{V_d(s) - v_{sd}(s)}{R + Ls} + \frac{wL(V_q(s) - v_{sq}(s))}{(R + Ls)^2} \quad (3.119)$$

- By solving this equation for $i_d(s)$, rearranging and simply as follows equation based on equation (3.112)

$$i_d(s) = \frac{(R + Ls)V_d(s) - v_{sd}(s) + wL(V_q(s) - v_{sq}(s))}{(R + Ls)^2 + (wL)^2} \quad (3.120)$$

Looking at Equation (3.114) the transfer function from $V_d(s)$ to $i_d(s)$ is

$$\frac{i_d(s)}{V_d(s)} = \frac{(R + Ls)}{(R + Ls)^2 + (wL)^2} \quad (3.121)$$

- For solving $i_q(s)$

  - Using the equation $i_q(s) = \frac{V_q(s) - v_{sq}(s) - wLi_d(s)}{R + Ls}$

  - Substitute the expression of $i_d(s)$ into this equation.

This process follows similarly, and after simplification, the transfer function for $i_q(s)$ will be:

$$\frac{i_q(s)}{V_q(s)} = \frac{-wL}{(R + Ls)^2 + (wL)^2} \quad (3.122)$$

These procedures must be followed in order to apply a proportional-integral (PI) controller to the specified transfer function of a converter.

- Understand the given transfer function or Plant given from equation (3.115)

$$G(s) = \frac{i_d(s)}{V_d(s)} = \frac{(R + Ls)}{(R + Ls)^2 + (wL)^2} \tag{3.123}$$

- Determine the PI Controller

    - The PI controller has the form:

$$G_c(s) = K_{pd} + \frac{K_{id}}{s} \tag{3.124}$$

In this case, (K_{id}) is the integral gain and (K_{pd}) is the proportionate gain. Nonetheless, by merging the controller, the closed-loop transfer function of the system with the PI controller can be discovered. This is the closed-loop transfer function ($T_d(s)$):

$$T_d(s) = \frac{G_c(s)G(s)}{1 + G_c(s)G(s)} \tag{3.125}$$

$$= \frac{(K_{pd} + \frac{K_{id}}{s})\frac{R + Ls}{(R + Ls)^2 + (wL)^2}}{1 + (K_{pd} + \frac{K_{id}}{s})\frac{R + Ls}{(R + Ls)^2 + (wL)^2}} \tag{3.126}$$

By simplifying the numerator and denominator, as well as by rearranging this equation we can get a simple transfer function as follows:

$$T_d(s) = \frac{K_{pd}(R + Ls) + \frac{K_{id}(R + Ls)}{s}}{(R + Ls)^2 + (wL)^2 + K_{pd}(R + Ls) + \frac{K_{id}(R + Ls)}{s}} \tag{3.127}$$

This closed-loop transfer function describes the dynamics of the system when a PI Controller is applied. For the second plant when we apply a PI Controller to the given transfer function, we need to integrate the controller into the system dynamics. The given transfer functions from Equation (3.116).

$$G(s) = \frac{i_q(s)}{V_q(s)} = \frac{-wL}{(R + Ls)^2 + (wL)^2} \tag{3.128}$$

- The PI Controller can be represented by

$$G_c(s) = K_{pq} + \frac{K_{iq}}{s} \tag{3.129}$$

- Combining the controller yields the closed-loop transfer function of the system with the PI controller. The transfer function in closed-loop($T_q(s)$) is represented by

$$T_q(s)=\frac{(K_{pq}+\frac{K_{iq}}{s})*(\frac{-wL}{(R+Ls)^2+(wL)^2})}{1+(K_{pq}+\frac{K_{iq}}{s})*(\frac{-wL}{(R+Ls)^2+(wL)^2})} \quad (3.130)$$

By rearranging this equation we get a simple transfer function as follows:

$$T_q(s)=\frac{-wL(K_{pq}+\frac{K_{iq}}{s})}{(R+Ls)^2+(wL)^2-wL(K_{pq}+\frac{K_{iq}}{s})} \quad (3.131)$$

In order to determine the value of K_i and K_p we have put the value of R and L designed from the LCL Filter designed and put it Equations (3.120) and (3.122)

- Assume R_f =R and $L_1=L$, then R=0.82Ω and L=0.000045H, w=2πf=314rad/sec.
- Then Equations (3.120) and (3.122) become the following equation:

$$T_d(s)=\frac{K_{pd}(0.82+0.000045s)+\frac{K_{id}(0.82+0.000045s)}{s}}{(0.82+0.000045s)^2+(0.01413)^2+K_{pd}(0.82+0.000045s)+\frac{K_{id}(0.82+0.000045s)}{s}}$$

(3.132)

- From the Equation (3.132) we can rewrite as follows

$$T_q(s)=\frac{-0.01413s(K_{pq}+K_{iq})}{2*10^{-9}s^3+3.7*10^{-5}s^2-(0.01413(K_{pq}+K_{iq})+0.67)s+2*10^{-4}(K_{pq}+K_{iq})}$$

(3.133) .

The Ziegler-Nichols method is a well-known heuristic approach for fine-tuning PID (Proportional-Integral-Derivative) controllers. Developed in the 1940s by John G. Ziegler and Nathaniel B. Nichols, this technique provides a systematic way to adjust a PID controller's parameters to achieve the desired system response in control systems. (Pramujati et al., 2015).

Table 3-4 : Tuning formulae of Ziegler Nichols (Pramujati et al., 2015).

Controller type	K_p	T_i	T_d
P	$0.5\,K_{cr}$	∞	0
PI	$0.45\,K_{cr}$	$\frac{1}{1.2P_{cr}}$	0
PID	$0.6\,K_{cr}$	$0.5\,P_{cr}$	$0.125\,P_{cr}$

The following steps very necessary in this method,

- Obtaining closed loop transfer function.
- Define characteristics equation from the given transfer function.
- Using Routh array to calculate K critical and w.
- Using w, calculate T critical.
- Using K critical and T critical determine K_i and K_p.

For d-axis and q-axis we have to determine separately from equation (3.133) and (3.130)

- **For d-axis: to** determine K critical assume ki, kd=0., Using Routh array.as follow

S^3	$2*10^{-9}$	$0.67+0.82K_p$	0
S^2	$3.7*10^{-5}$	$0.82K_p$	0
S^1	$\frac{2{,}5*10^{-5}-2.05*10^{-5}Kp}{3.7*10^{-5}}$	0	
S^0	$0.82K_p$		

From this range is $0<k_p<1.3$ then K critical is 1.3, so $K_p=0.45*1.3=0.59$ In order to determine value of K_i first we have to calculate value of T critical from frequency as follow

$$3.7*10^{-5}s^2+0.82K_p=0 \ ,$$

$$3.7*10^{-5}s^2+0.82(1.3)=0$$

$$3.7*10^{-5}(jw)^2+1.06=0 \ ,$$

$$-3.7*10^{-5}(w)^2+1.06=0$$

Then w=169, T Critical=0.04 from this $K_i=1.2*\frac{1.3}{0.04}=39$.

- **For q-axis:** to determine K critical assume ki, kd=0., Using Routh array.as follow

S^3	$2*10^{-9}$	$-0.01412K_p-0.009$	0
S^2	$3.7*10^{-5}$	$2*10^{-4}K_p$	0
S^1	$\frac{-0.05*10^{-5}k_p-2.97*10^{-7}}{3.7*10^{-5}}$		
S^0	$2*10^{-4}K_p$		

From this range is $0<k_p<0.59$ then K critical is 0.59, so $K_p=0.45*0.59=0.27$ In order to determine value of K_i first we have to calculate value of T critical from frequency as follow

$$3.7*10^{-5}s^2+2*10^{-4}K_p=0$$

$$3.7*10^{-5}s^2+2*10^{-4}(0.59)=0$$

$$3.7*10^{-5}(jw)^2+2*10^{-4}(0.59)=0$$

$$-3.7*10^{-5}(w)^2+1.18*10^{-4}=0$$

Then w =1.79,T critical=3.5 $K_i = 1.2 * \frac{0.59}{3.5} = 0.2$

Table 3-5 Specification of the Designed converter controller

Controller gain	For d-axis	For q-axis
K_p	0.59	0.27
K_i	39	0.2

3.8.3 Inverter Controller

A three-phase voltage inverter is mainly utilized to transform a steady DC voltage into an AC voltage with adjustable amplitude and frequency. To maintain a steady Voltage over a DC-link, power flow is regulated by the GSC. The control method is centred on managing line currents to manage the amount of power provided to the grid by the stator circuits and maintain a constant DC bus voltage. To address this, a filter was created and put in place intermediate the grid and the inverter. (Mahersi et al., 2013).

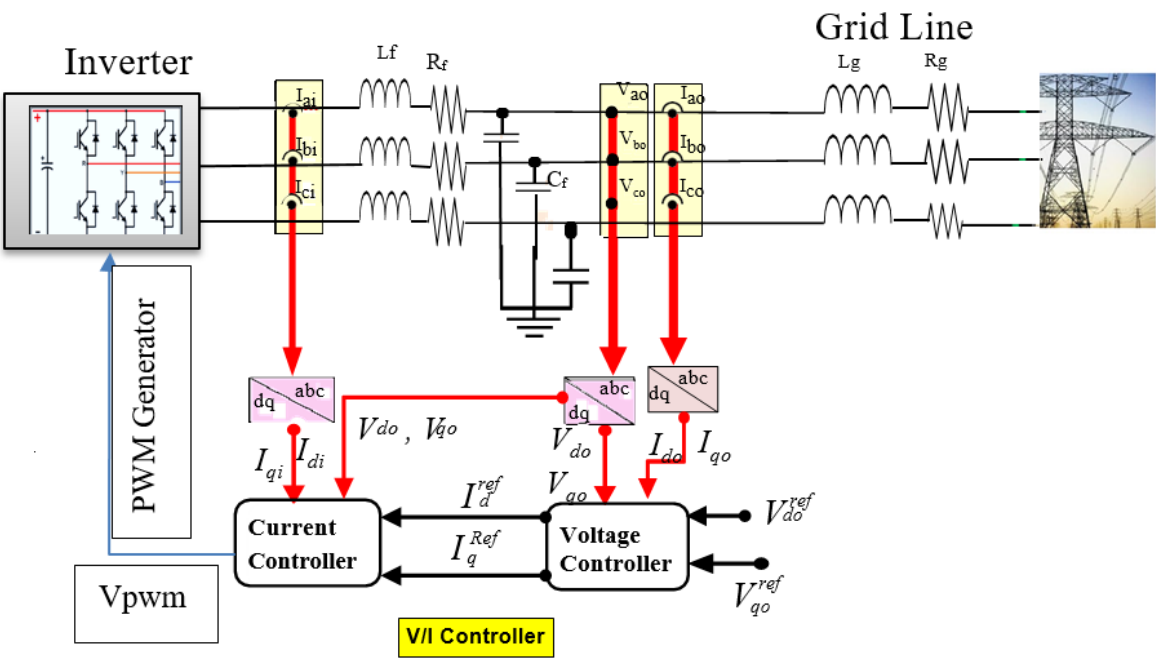

Figure 3-10 :Control diagram for three-phase voltage and current of GSC(Pavan Kumar & Bhimasingu, 2021).

Phase locked loop

The phase angle and frequency of the input voltage waveform are determined by the voltage and current controller using a phase-locked loop .This information is then utilized for the abc-to-d-q transformation, resulting in the q-axis and d-axis voltage components, v_{qo} and v_{do} .(Stecca et al., 2020)

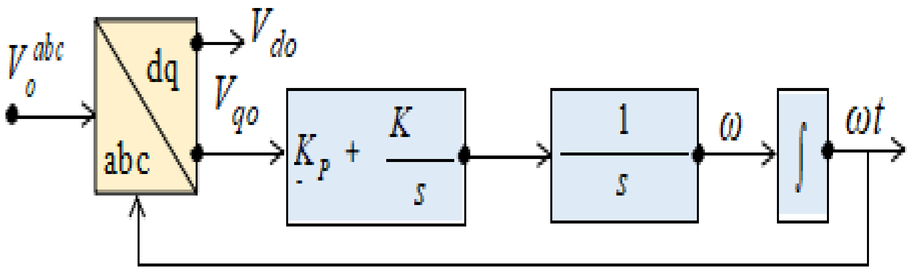

Figure 3-11: Phase Locked Loop (Pavan Kumar & Bhimasingu, 2021)

$$V_{ao} = V_0 \sin(\theta) \tag{3.134}$$

$$V_{bo} = V_0 \sin(\theta - \frac{2}{3}\pi) \tag{3.135}$$

$$V_{co} = V_0 \sin(\theta + \frac{2}{3}\pi) \tag{3.136}$$

Where wt= θ ,

The transformation abc-to- d-q axis is as the following manner;

$$\begin{pmatrix} V_{do} \\ V_{qo} \end{pmatrix} = \begin{pmatrix} \cos(\theta) & \cos(\theta - \frac{2\pi}{3}) & \cos(\theta + \frac{2\pi}{3}) \\ -\sin(\theta) & \sin(\theta - \frac{2\pi}{3}) & \sin(\theta + \frac{2\pi}{3}) \\ 0 & 0 & 0 \end{pmatrix} \begin{pmatrix} V_{ao} \\ V_{bo} \\ V_{co} \end{pmatrix} \tag{3.137}$$

to design the control loop with a damping ratio of 0.707 and a natural frequency of 100 Hz.

$$K_i = \frac{w^2{}_n}{vo} = \frac{(2*3.14*100)^2}{690} = 571.57 \tag{3.138}$$

$$K_p = \frac{2*\xi*w_n}{vo} = \frac{(2*0.707*3.14*100)}{690} = 0.64 \tag{3.139}$$

How the Voltage and Current Controller Works

In order to regulate the power converter's switches and, ultimately, the converter's electronics output, the voltage and current controller uses the inverse Park to create a three-phase reference signal (Pavan Kumar & Bhimasingu, 2021).

- **A Voltage Control Module is**;

$$I_{dref} = I_{do} + (V_{doref} - V_{do})(\frac{K_{pv}s + K_{iv}}{s}) - V_{qo}C_f w \tag{3.140}$$

$$I_{qref} = I_{qo} + (V_{qoref} - V_{qo})(\frac{K_{pv}s + K_{iv}}{s}) - V_{do}C_f w \tag{3.141}$$

- **A Current Control Module is**;

$$E_d = V_{do} + I_{di}R_f + (I_{dref} - I_{di})(\frac{K_{pa}s + K_{ia}}{s}) - I_{qi}L_f w \tag{3.142}$$

$$E_q = V_{qo} + I_{qi}R_f + (I_{qref} - I_{qi})(\frac{K_{pa}s + K_{ia}}{s}) - I_{di}L_f w \tag{3.143}$$

$$V_{PWM} = \begin{pmatrix} V_{aref} \\ V_{bref} \\ V_{cref} \end{pmatrix} = \begin{pmatrix} \sin(wt) & \cos(wt) & 1 \\ \sin(wt - \frac{2\pi}{3}) & \cos(wt - \frac{2\pi}{3}) & 1 \\ \sin(wt + \frac{2\pi}{3}) & \cos(wt + \frac{2\pi}{3}) & 1 \end{pmatrix} \begin{pmatrix} E_d \\ E_q \\ Eo \end{pmatrix} \tag{3.144}$$

- V_{PWM} reference voltage used for the PWM generator's input
- I_{dref}, I_{qref}, V_{dref} *and* V_{qref} Serves as the current and voltage controller's reference input current.
- I_{qo}, I_{do}, V_{qo}, *and* V_{do} is d-q related to I_{oabc} *and* V_{oabc}.
- I_{di}, I_{qi} Is $I_{iabc's}$ d-q component.
- E_d, E_q Is V_{PWM} 's d-q component.

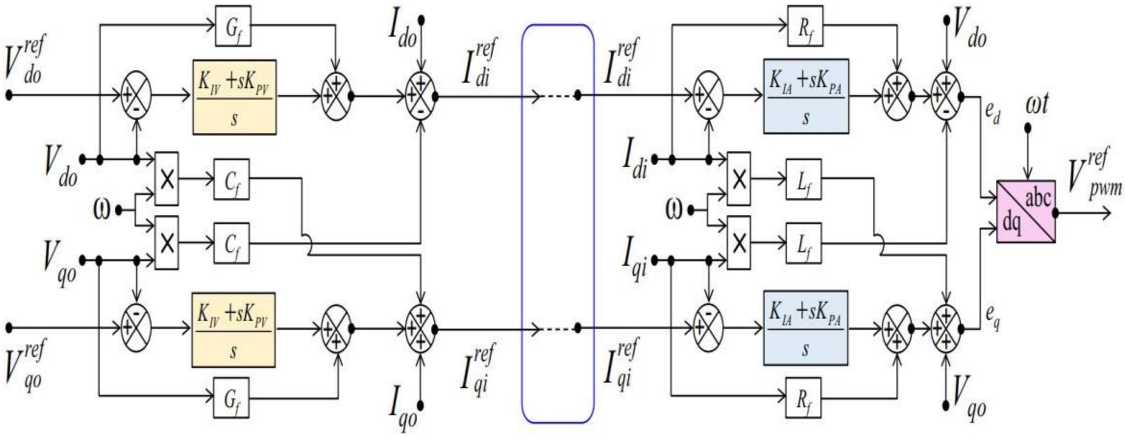

Figure 3-12: Diagram of voltage and current control (Kumar & Bhimasingu, 2021).

$$I_{is}(s) = I_{og}(s) + I_c(s) \text{ or } I_c(s) = I_{is}(s) - I_{og}(s) \tag{3.145}$$

$$V_{og}(s) = \frac{V_{\sin}(s) - (R_f + sL_f)I_{og}(s)}{1 + sC_f(sL_f + R_f)} \tag{3.146}$$

Where

V_{sin}, V_{og}, V_{il} are the single phase equivalents of V_{sinabc}, V_{ogabc}, V_{ilabc}, respectively

I_{il}, I_{og}, I_v are the single phase equivalents of I_{ilabc}, I_{ogabc}, I_{cabc}, respectively .

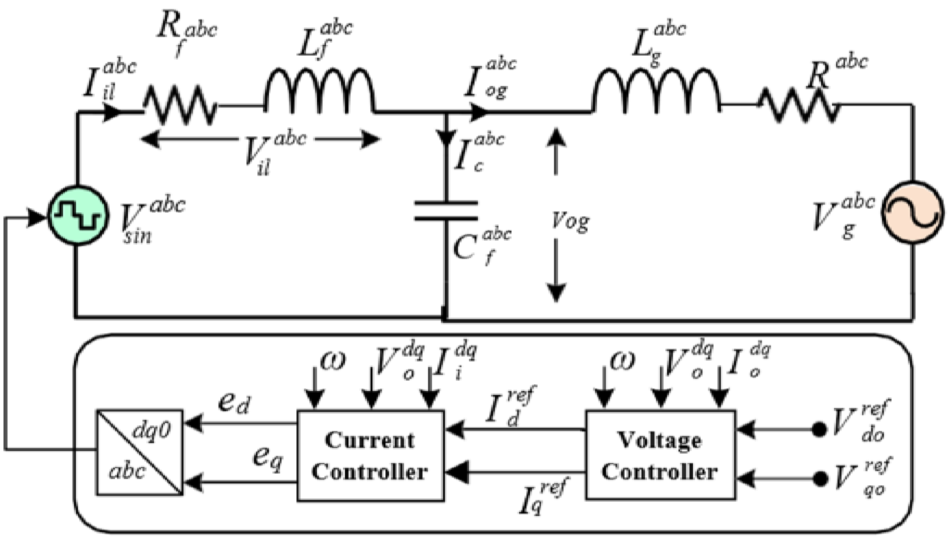

Figure 3-13: Equivalent Circuit of voltage and current control (Kumar & Bhimasingu, 2021).

Transfer function of internal current and external voltage controller

By simulating the inner current controlling loop and disregarding the voltage control outer loop, the current controller draws the system current. In contrast, the voltage controller models the control loop in order to control the voltage, ignoring the inner control loop. (Kumar & Bhimasingu, 2021).

$$\frac{I_{iL}(s)}{I_{il}(s)} = \frac{Kp_a s + Ki_a}{s^2 L_f + s(R_f + Kp_a) + Ki_a} \tag{3.147}$$

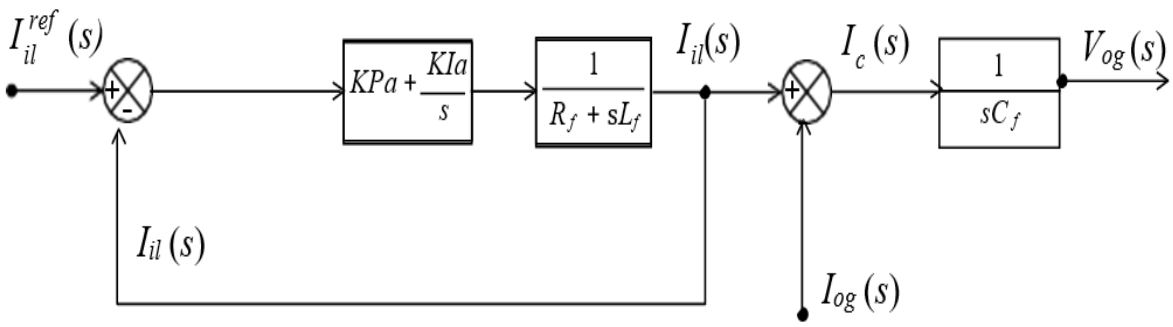

Figure 3-14: Diagram of the current control (Kumar & Bhimasingu, 2021)

to ascertain the current controller's proportional and integral gain values. With a second-order dynamic characteristic equation, the closed-loop current control system's characteristic equation is;

$$s^2 + 2\varsigma w_n s + w_n = 0 \tag{3.148}$$

$$s^2 L_f + s(R_f + Kp_a) + Ki_a = 0 \tag{3.149}$$

To achieve both transient stability and a satisfactory dynamic response, the closed-loop system's desired damping ratio (ζ) was determined to be 0.707.

- Proportional gain is computed as follows:

$$K_{pa} = 2\varsigma w_n - R_f = 2*0.707*11.94*1000 \; - 0.82 = 1.688*10^4$$

- Integral gain is computed as follows:

$$K_{ia} = 11.94*10^3*44.89*10^{-6} = 0.54$$

$$\frac{V_{og}(s)}{V_{oref}} = \frac{sKp_v + Ki_v}{s^2 C_f + Kp_v s + Ki_v} \tag{3.150}$$

Figure 3-15 shows the voltage control of the inverter connected to the grid .

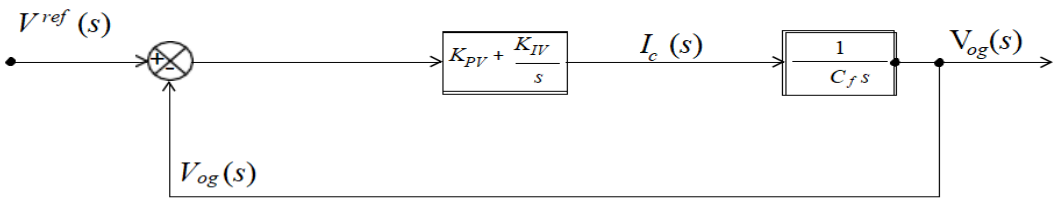

Figure 3-15: Block Diagram for voltage control

We need to determine the integral (K_{iv}) and proportional gain (K_{pv}) values for the voltage controller.

$$s^2 C_f + sKp_v + Ki_v = 0 \tag{3.151}$$

$$s^2 + 2\varsigma w_n s + w^2{}_n = 0 \tag{3.152}$$

- Integral gain is computed as follows

$$K_{iv} = w_n{}^2 * C_f = (11.94*10^3)^2 * 49.76*10^{-6} = 7.093*10^3$$

- Proportional gain is computed as follows

$$K_{pv} = 2*\varsigma*w_n = 2*0.707*11.94*10^3 = 16.9*10^3$$

Table 3-6: Specification of the Designed Inverter controller

Controller type	K_p	K_i
Voltage controller	$16.9*10^3$	$7.093*10^3$
Current controller	$1.688*10^4$	0.54

3.8.4 STATCOM Controller

This work employed MATLAB/Simulink's built-in STATCOM module to model the power system under study. A STATCOM architecture based on a VSC depicts in Figure (3-16).This is how the control principle is explained.

- The phase angle θ in PLL is integrated with the park transform to yield the system measured voltage V_m . In order to acquire the direct axis voltages and currents

$(V_d\ and\ I_d)$ and quadrature axis voltages and currents $(V_q and\ I_q)$, the three-phase system voltages and currents are decoupled to the d-q axis using synchronous rotary coordinates (AC voltage measurement and current measurement blocks).

- ➢ The AC and DC Voltage Regulator, respectively, are used to obtain the quadrature and direct axis reference currents $(I_{qref}\ and\ I_{dref})$, with I_{qref} in charge of managing reactive power and I_{dref} in charge of managing active power.
- ➢ By utilizing the differences between I_{qref} (I_{dref}) $and\ I_q$ (I_d), the current regulators is regulating the PWM phase angle and output voltage magnitude while also determining the magnitude and phase of the VSC terminal voltage V2.

A STATCOM has two modes of operation.

a.Mode of voltage control (keeping the voltage at a specific level).

b. Reactive power control mode: this modality sets a specific value for the STATCOM Reactive power output.

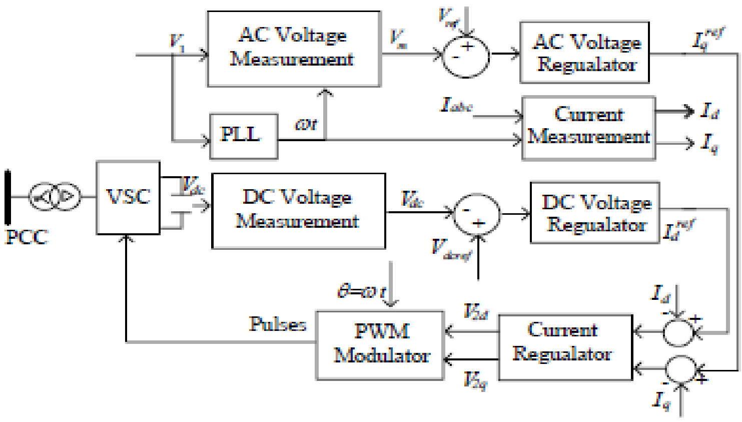

Figure 3-16 : VSC-based STATCOM architecture

The STATCOM output current functions as a current source and is voltage independent. The quick response time makes it appropriate for reducing voltage flicker. Generally, the STATCOM responds in less than 10 milliseconds. It takes only one millisecond to transition from the rated inductive reactive power to the rated capacitive reactive power. Figure 3-17 demonstrates the null k_d (derivative gain) PI regulator in the AC voltage regulator. The difference between the measured system voltage v_m and the reference voltage V_m serves as the input, and the reference current I_{qref} on the quadrature axis is the output.

Figure 3-18 shows the DC Voltage Regulator's PI regulator. The difference between the DC reference voltage, V_{dcref} , , and the DC link voltage, Vdc, is the input, and the direct-axis reference current, I_{dref} , is the output. Based on the Equation (3.94) and Equation (3.95) the transfer function of the voltage regulator is

$$\frac{V_{ref}(s)}{V_m(s)} = \frac{(sL+R)(sK_p+K_i)}{s^2L+sR+sK_p+K_i} \tag{3.153}$$

$$s^2 + 2\varsigma w_n s + w_n{}^2 = 0$$

$$s^2L + sR + sK_p + K_i = 0$$

$$K_i = w^2{}_n * L = (11.98*10^3)*8.98*10^{-6} = 1.3*10^3$$

$$K_p = 2\varsigma w_n - R = 2*0.707*11.98*10^3 - 0.82 = 16.9*10^3$$

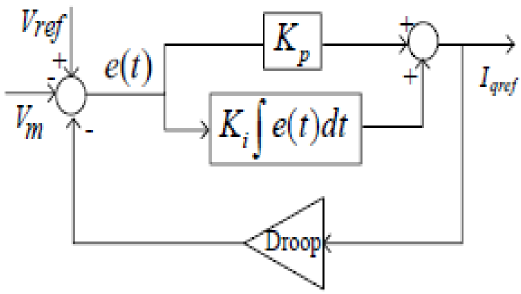

Figure 3-17: PI controller for the AC voltage regulator

Table 3-7 : Tuned PI controller gains

Controller gain	Value
K_p	$16.9*10^3$
K_i	$1.3*10^3$

Based on the equation (3.94) and equation (3.95) the transfer function of dc link is

$$\frac{V_{dcref}(s)}{V_{dc}(s)} = \frac{sC(sk_p+k_i)}{s^2C+sk_p+k_i} \tag{3.154}$$

$$s^2 + 2\varsigma w_n s + w^2{}_n = 0$$

$$s^2C + sk_p + k_i = 0$$

$$k_i = w^2{}_n * c_f = 11.98*10^3 * 49.75*10^{-6} = 7.14*10^3$$

$$k_p = 2*11.98*10^3 * 0.707 = 16.9*10^3$$

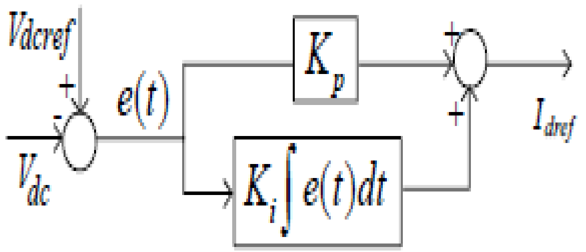

Figure 3-18: PI controller for the DC voltage regulator

Table 3-8: Tuned PI controller for the DC voltage regulator

Controller gain	Value
K_p	$16.9*10^3$
K_i	$7.14*10^3$

The current regulator shown in Figure 3-19 has two PI regulators that use the differences between I_{qref} *and* I_q, I_{dref} *and* I_d, respectively, to generate the direct and quadrature axis voltages, V_{2d} *and* V_{2q}, at the VSC terminal bus, which serve as the PWM modulator's input. For both axis the transfer function is given as follows based on the Equation (3.94) and Equation (3.95)

$$\frac{I_{dref}(s)}{I_d(s)} = \frac{(sL+R)(sK_p + K_i)}{s^2L + sR + sK_p + K_i} \tag{3.155}$$

$$s^2 + 2\varsigma w_n s + w_n{}^2 = 0$$

$$s^2L + sR + sK_p + K_i = 0$$

$$K_i = w^2{}_n * L = (11.98*10^3)*8.98*10^{-6} = 1.3*10^3$$

$$K_p = 2\varsigma w_n - R = 2*0.707*11.98*10^3 - 0.82 = 16.9*10^3$$

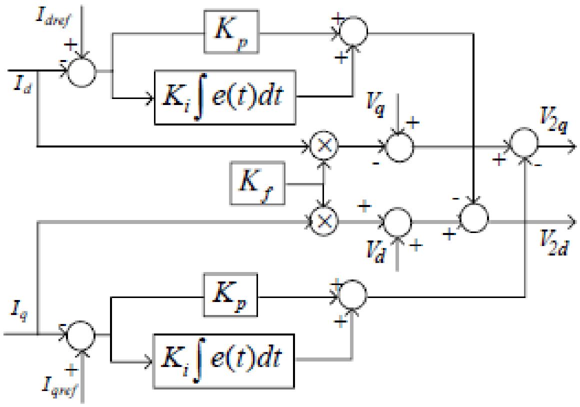

Figure 3-19: Current regulators with PI controllers

Table 3-9: Tuned Current regulators with PI controllers

Controller gains	**Value**
K_p	$16.9*10^3$
K_i	$1.3*10^3$

CHAPTER FOUR

RESULTS AND DISCUSSION

4.1 INTRODUCTION

In this chapter, a MATLAB/Simulink simulation is carried out to assess the PMSG based on wind energy conversion systems. PMSG based on a wind energy conversion system operating normally A rectifier is used to change the AC energy produced by a wind turbine into DC. The DC link functions as an energy storage component to reduce variations in the DC voltage, typically with the aid of capacitors. This smoothing is necessary because the rectified output from the wind turbine generator can be highly variable due to changes in wind speed. By stabilizing the DC voltage, the DC link provides a more consistent input for the inverter. This inverter converts DC to AC and 690V AC Voltage is generated. To connect this voltage to the grid we used two step-up transformers of 690V/33KV and 33KV/230KV to coordinate the voltage with the grid voltage. When different types of three-phase fault is applied to the system three phase voltage on the grid as well as the voltage from the inverter disrupted based on the types of faults happened to the system. During these disruptions occurred .in order to overcome these types of faults STATCOM is designed. STACOM injected reactive power into the system, effectively stabilizing voltage levels and restoring grid balance. The successful utilization of STATCOM in overcoming three-phase faults highlights its essential role in ensuring the stability of wind energy conversion systems linked to the grid. The figure 4-1shows that the overall of the system starting from wind turbines to the grid.

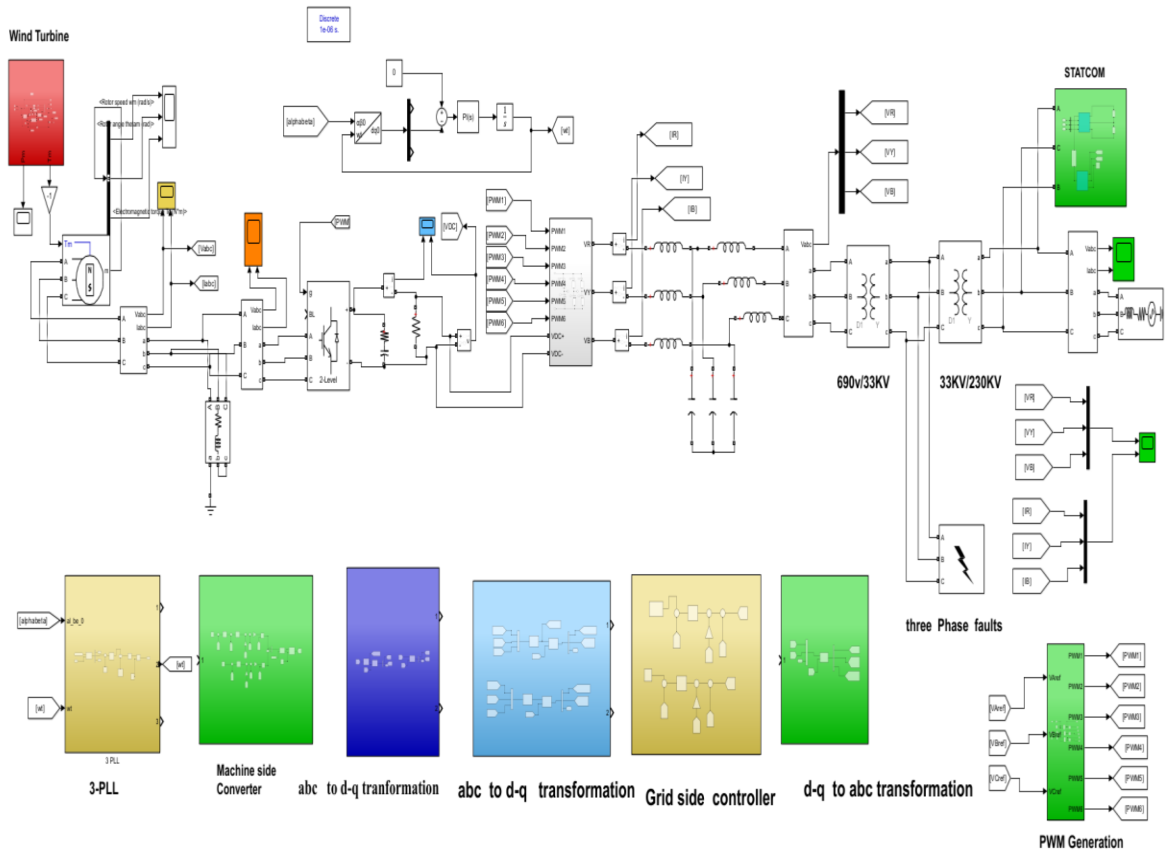

Figure 4-1: Block diagram of the overall system

4.1.1 Randomly generated wind speed

Wind speed is a critical factor in the operation of wind turbines because it directly affects their ability to produce electricity. Wind turbines operate by converting the kinetic energy of wind into electrical energy through a series of mechanical and electrical processes this figure is indicating that randomly wind speed is supplied to the system. This speed is used to generate mechanical power and the mechanical torque that is connected to the PMSG to generate stator voltage connected to the rectifier.

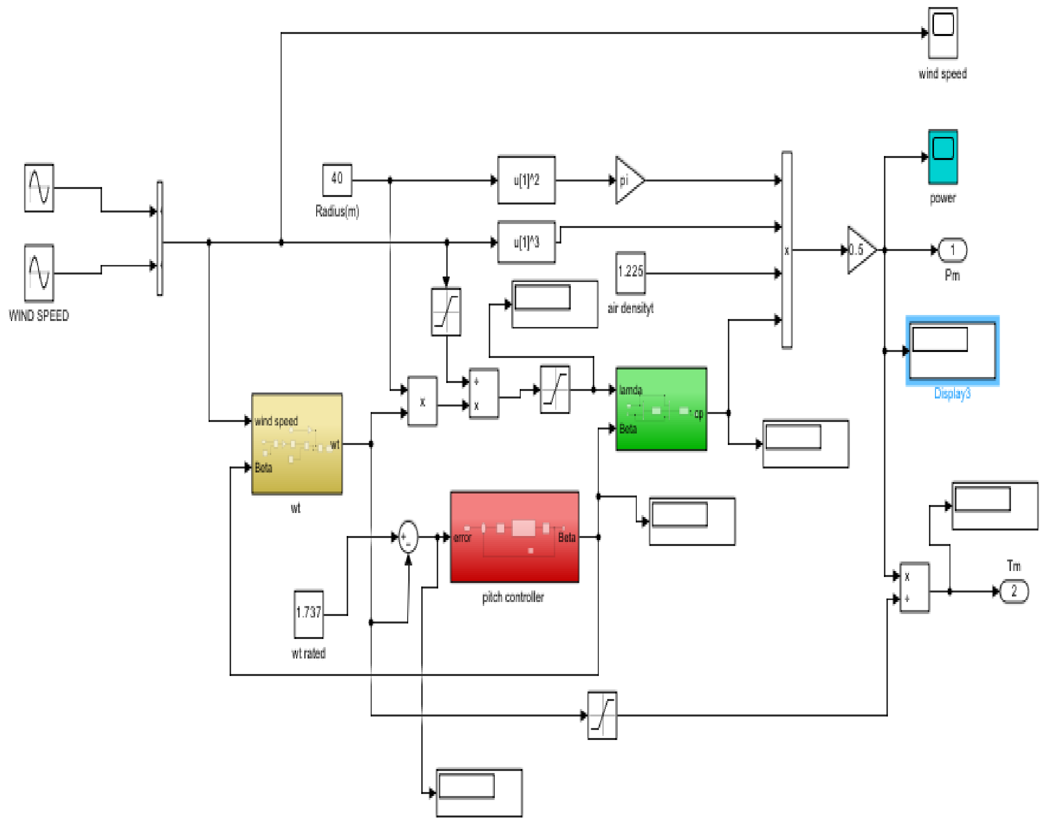

Figure 4-2: Wind turbine modelling

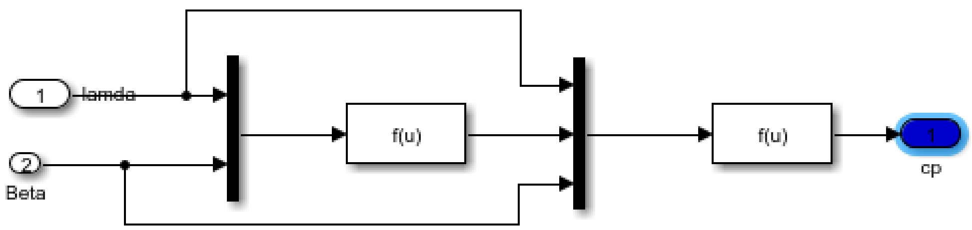

Figure 4-3 : Power Coefficient Simulink

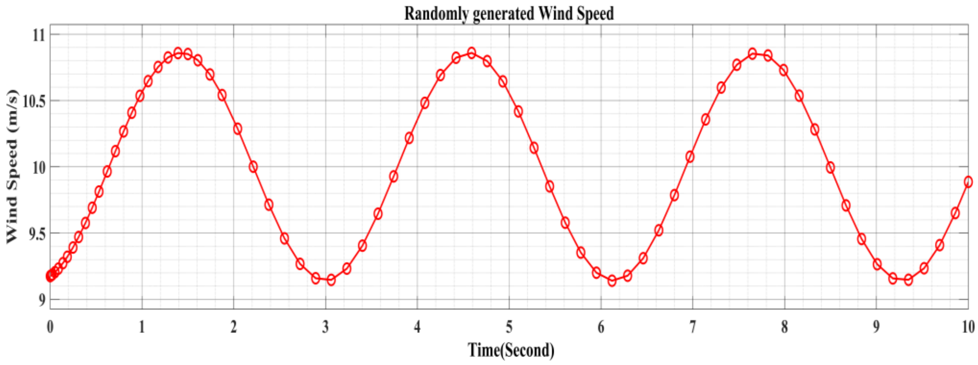

Figure 4-4: Wind Speed randomly generated

4.2 Wind Turbine and Pitch with Controller

4.2.1 Mechanical power

A wind turbine's mechanical power grows as a cube of wind speed and a square of the blade length (or radius). Turbines with longer blades are more effective at producing electricity because they can capture more wind energy, especially in regions with slower wind speeds. Figure indicates that mechanical power is generated in the given time based on the randomly generated speed, designed radius of blades, and constant density given.

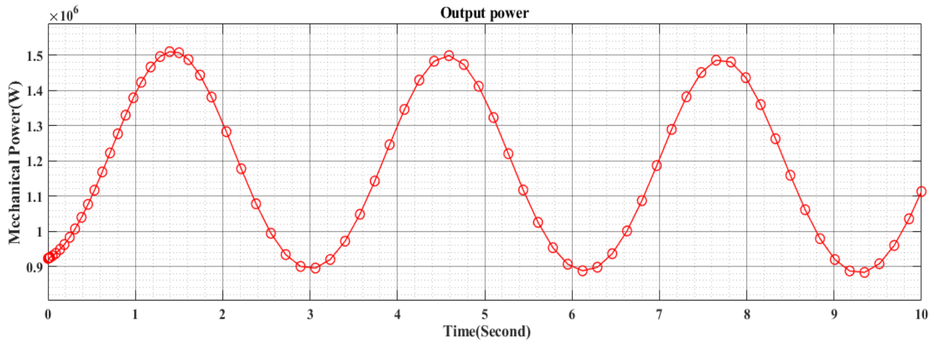

Figure 4-5: Mechanical power based randomly generated wind speed

4.3 Three -phase Stator Voltages and Current from the PMSG

Based on given the air density, wind speed, blade radius, and power coefficient you can calculate the mechanical power from the wind. Using the mechanical efficiency, you find the mechanical power generated through the turbine, then the torque produced. By applying the generator efficiency, you determine the electrical power output and, finally, the stator voltage produced by the PMSG. In a PMSG-based wind turbine, the mechanical energy from the turbine's rotating blades is converted into electrical energy by the generator. PMSGs produce three-phase alternating current (AC) electricity. The primary function of the rectifier is to convert the variable-frequency AC produced by the PMSG into direct current (DC). This is essential because DC is easier to control and stabilize than variable AC, making it more suitable for the next stages of power conversion. Figure 4-6 indicates the block diagram from wind turbines to rectifier.

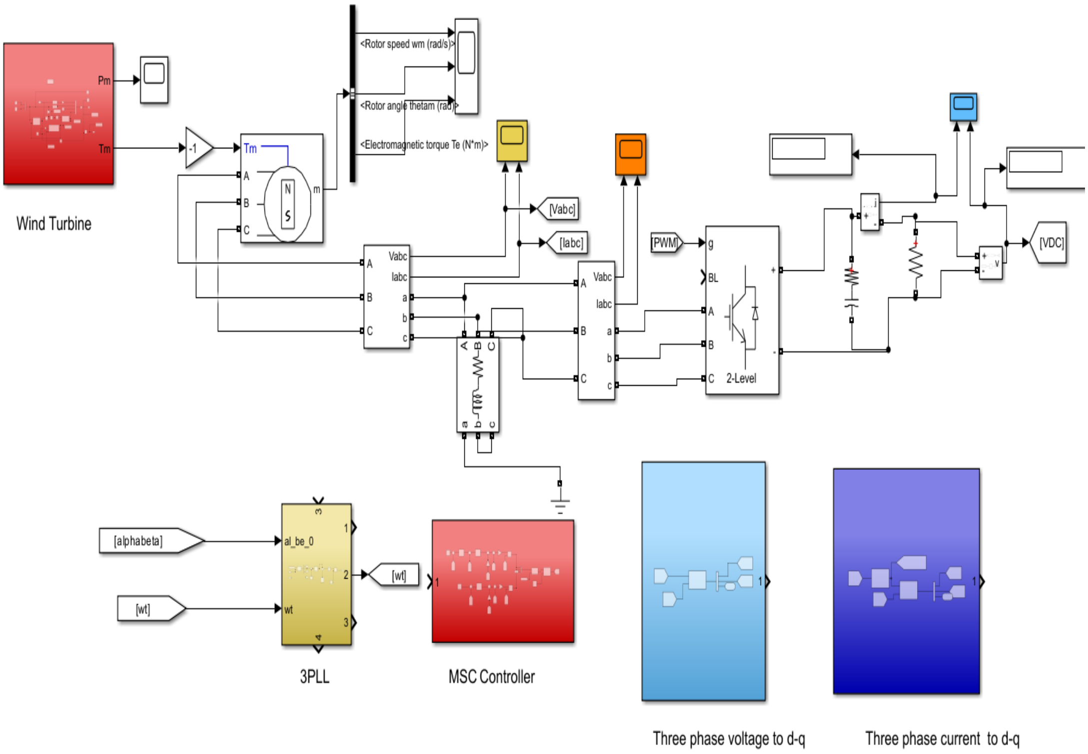

Figure 4-6: PMSG connected to Rectifier

4.3.1 DC Link voltage from the rectifier

Rectifiers and inverters are essential components of wind energy conversion systems that are connected to the grid because they guarantee that the electricity produced by the wind turbine can meet the grid's demands. The DC voltage between the rectifier and inverter often referred to as the DC link or DC bus**.** This DC link allows the rectifier (which converts variable AC to DC) and the inverter (which converts DC to grid-synchronized AC) to operate independently. This separation is essential for controlling each stage effectively. Also, it provides flexibility in managing different operating conditions and handling variations in wind speed without directly affecting the grid connection. In some systems, the DC link can incorporate energy storage elements (like capacitors) that help in maintaining voltage stability and improving power quality. 690V AC voltage is converted to 690V DC and this voltage is connected to the inverter. The following figure indicates the dc link voltage converter from rectifier and connected to the inverter.

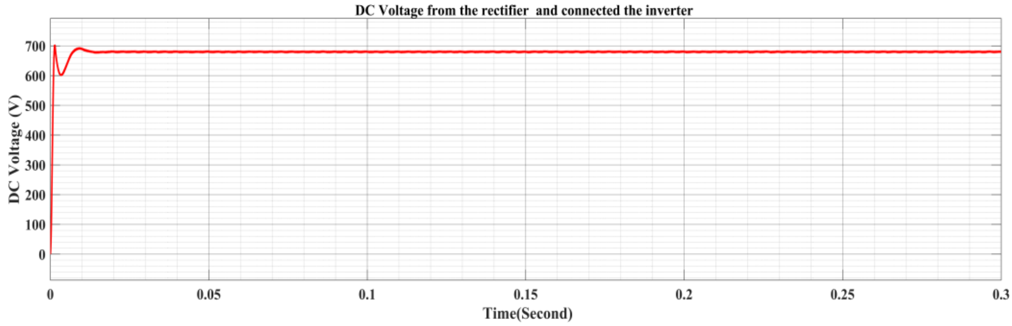

Figure 4-7: Dc Voltage from Rectifier and Connected to Inverter

4.4 Grid Side Convertor during Normal Operation and Its Result

The Grid-Side Converter is a part of the power electronics system, typically found after the inverter (which converts DC to AC) in the power conversion chain. It's responsible for interfacing the generated power with the grid. The GSC converts the AC power produced by the inverter into a form that is compatible with the grid's requirements. This involves ensuring the correct voltage level, frequency, and phase alignment. During the regular operation of the system 690V is generated from the inverter and by using two step-up transformers which means 690V/33KV and 33KV/230KV then connected to the grid.

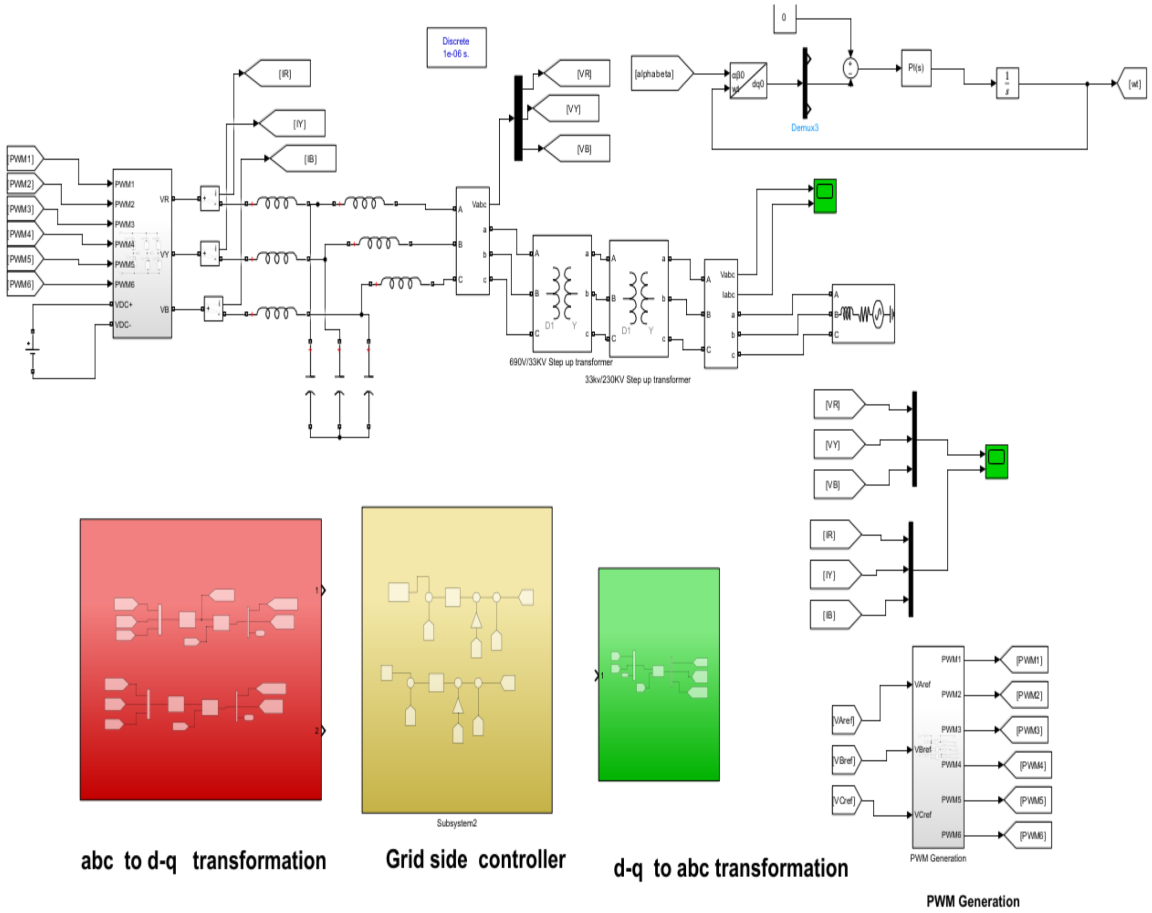

Figure 4-8: Grid Side Convertor during Normal Operation

4.4.1 Three -phase Voltage and Current from Inverter before the three -phase Faults.

During normal operation system 690V DC Voltage connected to the inverter and converted to the 690V AC Voltage. Figure 4-9 shows that the three phases AC Voltage and Current generated from Inverter without three phase faults .i.e. while the system is operating normally and without the application of STATCOM.

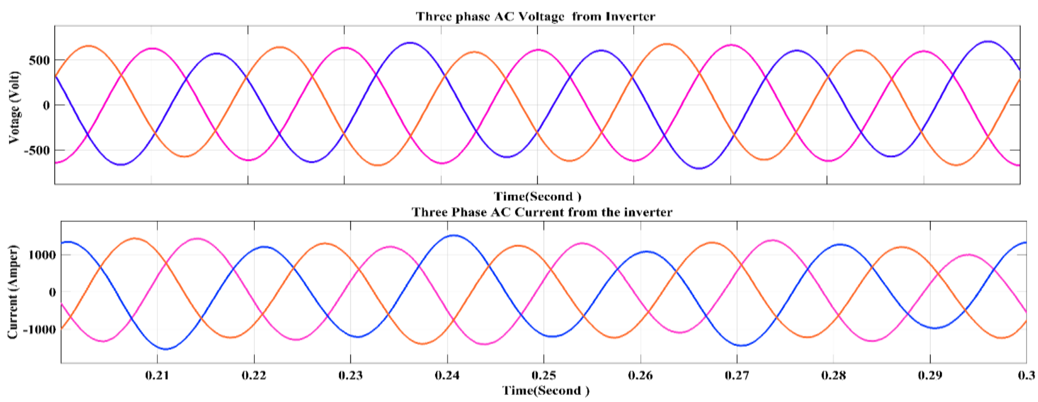

Figure 4-9:Three-phase AC voltage and current from the Inverter

4.4.2 Three-phase Voltage and current from the grid before the Three-phase Fault.

At normal operation the grid voltage is 230KV, however the voltage from the inverter is 690V that means it is not synchronized .in order to synchronise this voltage step-up by two transformers of 690V/33KV and 33KV/230KV. On The figure below indications that the three-phase AC Voltage and Current generated from the grid without three-phase faults .While the system is operating normally and without the application of STATCOM.

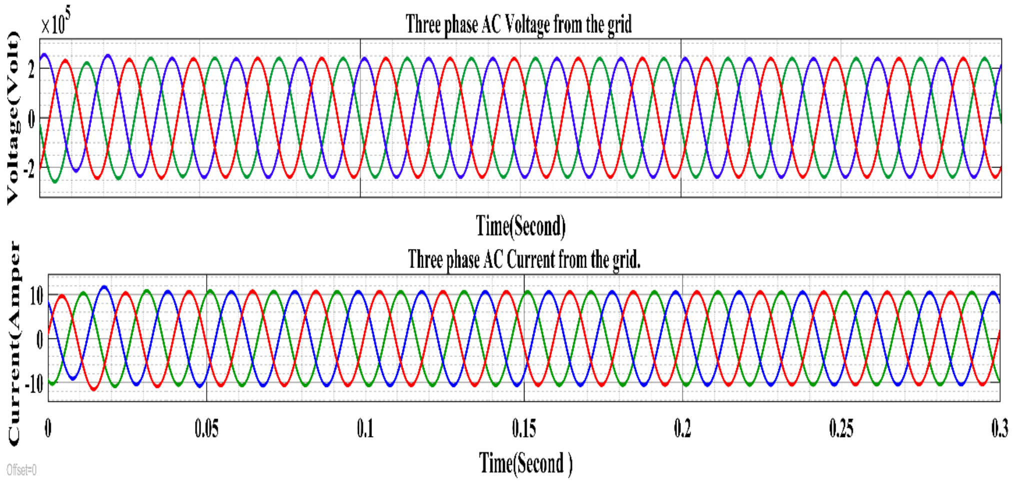

Figure 4-10 :Three phase AC voltage and current from the grid

4.5 Grid Side Convertor During different types of faults Operation and Its Result

When the fault happened in to normal operation the voltage and current is disturbed. based on different types of faults is voltage instability is happened, this instability A three-phase fault can cause a significant reduction in voltage levels in the affected part of the grid. This voltage dip can propagate through the system, affecting sensitive equipment and causing disruptions in operation. Also, when a fault occurs, there's typically a sudden increase in fault currents flowing through the system. These currents can be several times higher than normal operating currents, potentially damaging equipment and causing further system instability

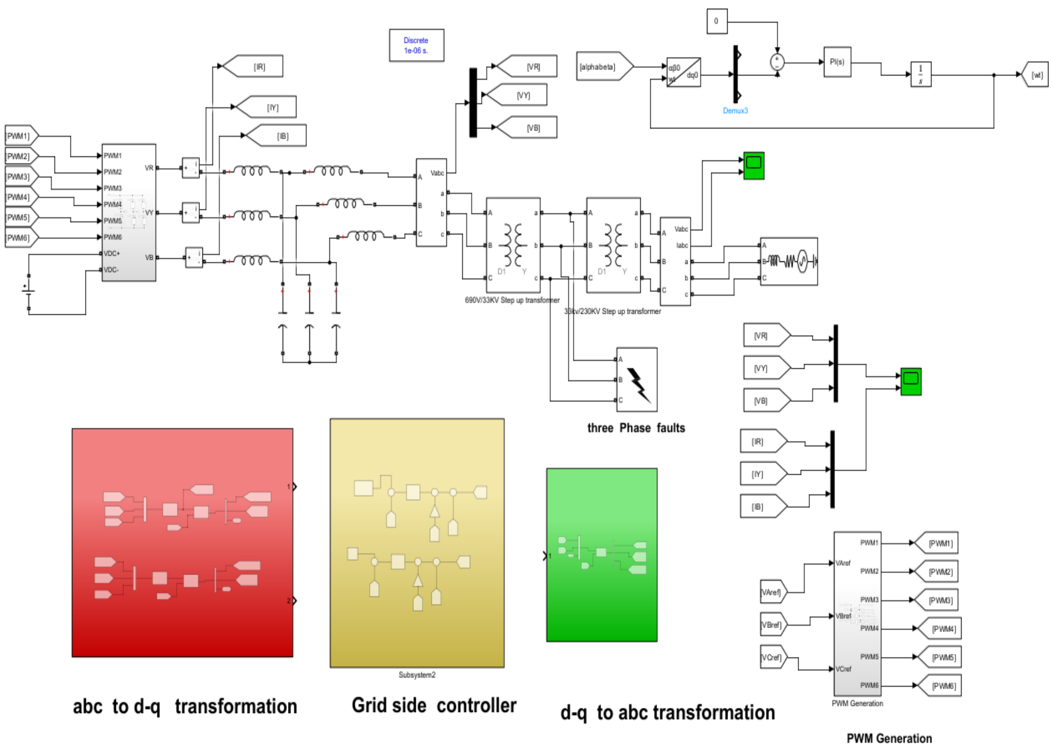

Figure 4-11: Grid Side Convertor during different types of faults Operation

4.5.1 Three- phase Voltages and Current from Inverter with L-G three -Phase Faults.

L-G fault (Line-to-Ground fault) is one of the most common types of electrical faults that occur in power systems. It happens when one phase conductor comes into contact with the ground or a grounded component. The figure below shows that the three-phase AC Voltage and Current generated from Inverter with L-G types of faults. i.e during the fault operation of the system and without the application of STATCOM.at this the inverter voltage is very low from 690V to 50V and the current from the inverter is high (100A to 500A). This low voltage can lead instability, also causing fluctuation in voltage levels, which may disrupt the operation of sensitive electronic equipment and cause malfunction and damage.

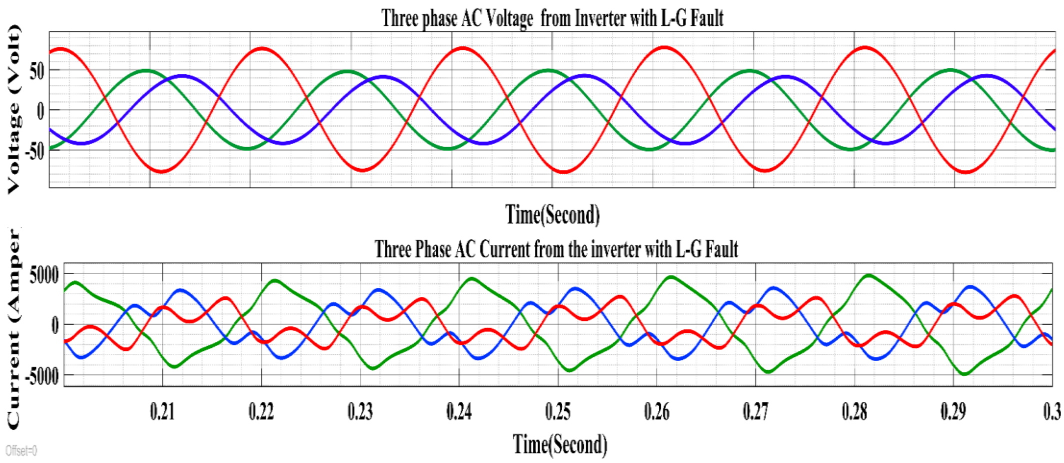

Figure 4-12: three phase AC voltages and current from the inverter with L-G Fault

4.5.2 Three-phase Voltages and current from grid with L-G Three- phase Fault.

The figure below is show that the three-phase AC Voltage and Current generated from grid with L-G types of faults .i.e during the fault operation of the system and without the application of STATCOM.at this grid voltage is very low and special two-line voltage is very low and the current from the grid is higher than normal operation. This causes also instability and fluctuation within the system. This can result in equipment malfunction, reduced the efficiency and potential damage of sensitive devices. Due to higher current electrical component such as transformer, generators, cables are subjected to higher stress and heat.

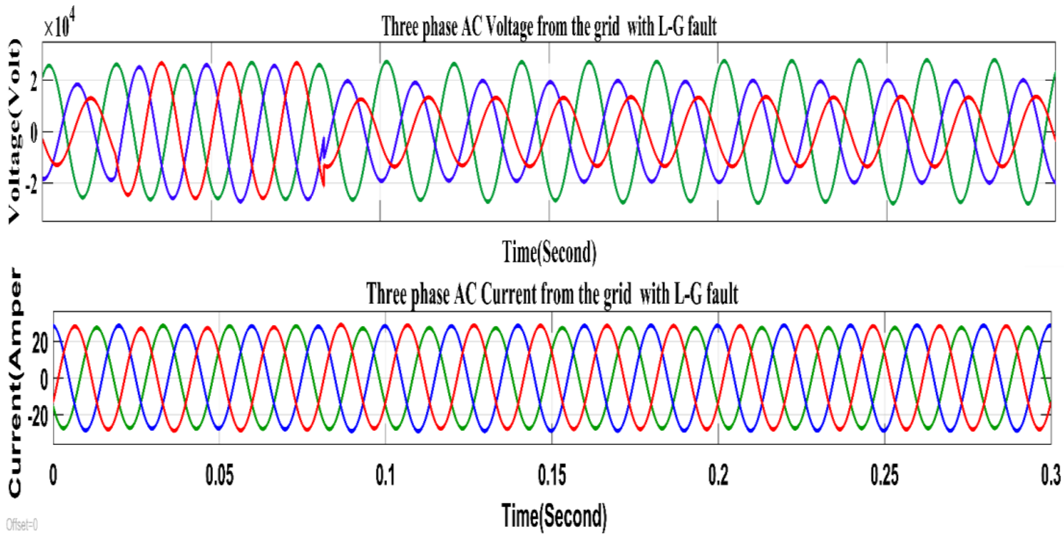

Figure 4-13: Three phase AC voltages and current from the grid with L-G Fault

4.5.3 Three -phase Voltages and current from Inverter with L-L-G three-phase Faults.

The figure below is show that the three-phase AC Voltage and Current generated from Inverter with L- L-G types of faults. I.e. during the fault operation of the system and without the application of STATCOM.at this inverter voltage is very low and special two-line voltage is very low and the current from the inverter is much higher than normal operation. This causes also instability and fluctuation within the system. This can result in equipment malfunction, reduced the efficiency and potential damage of sensitive devices. Due to higher current electrical component such as transformer, generators, cables are subjected to higher stress and heat. This can be accelerated wear and tear, reduce the lifespan of equipment, and increase risk of failures.

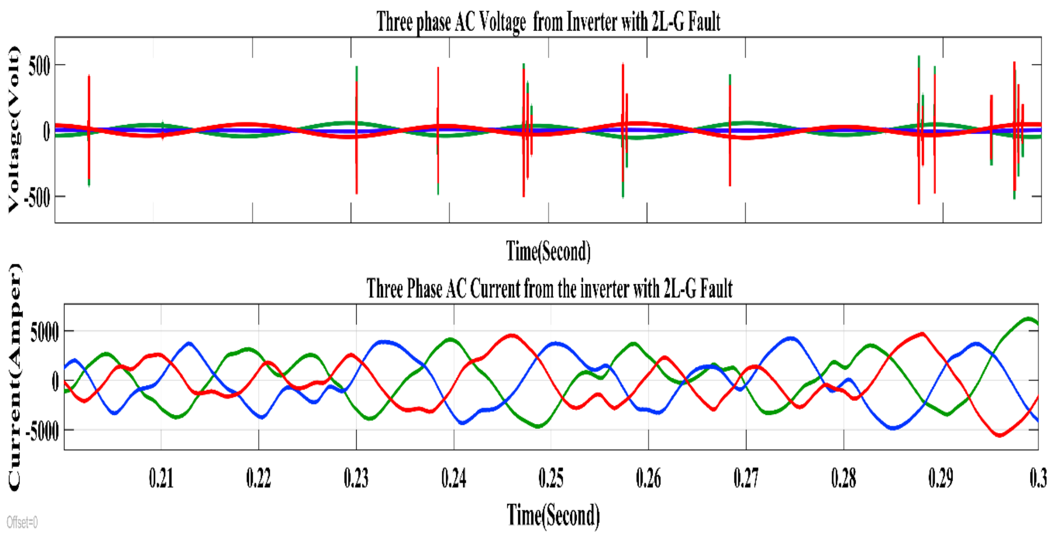

Figure 4-14:Three phase AC voltage and current from the inverter with L-L-G Fault

4.5.4 Three-phase Voltages and current from grid with L-L-G Three-phase Faults.

The figure below is show that the three-phase AC Voltage and Current generated from grid with L- L-G types of faults. I.e. during the fault operation of the system and without the application of STATCOM.at this grid voltage is very low and special two-line voltage is very low and the current from the inverter is much higher than normal operation. This causes also instability and fluctuation within the system. This can result in equipment malfunction, reduced the efficiency and potential damage of sensitive devices. Due to higher current electrical component such as transformer, generators, cables are subjected to higher stress and heat. This can be accelerated wear and tear, reduce the lifespan of equipment, and increase risk of failures.

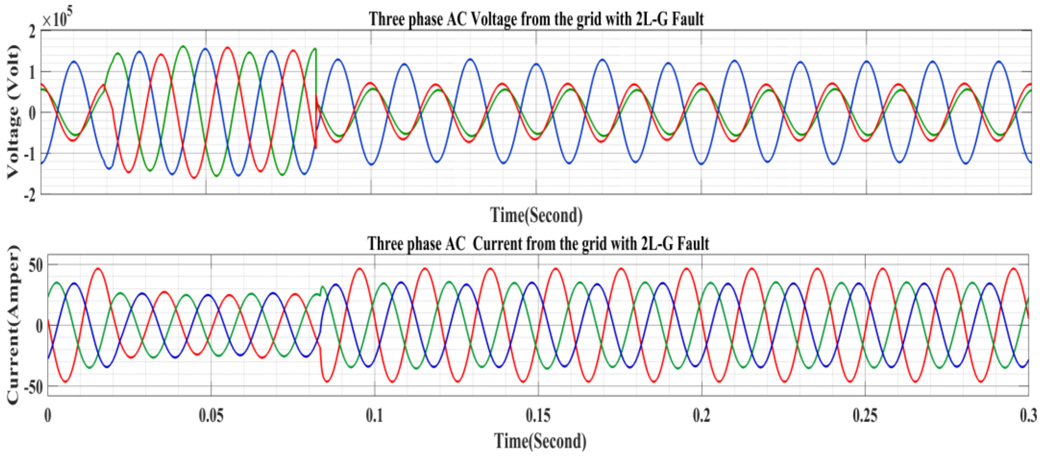

Figure 4-15: Three phase AC voltage and current from the grid with L-L-G Fault

4.5.5 Three -phase Voltage and current from Inverter with 3L-G Three -phase Faults.

Figure 4-16 shows that the three-phase AC Voltage and Current generated from Inverter with 3 L-G types of faults. i.e., during the fault operation of the system and without the application of STATCOM.at this Inverter voltage is very low and special one line voltage is very low and the current from the inverter is much higher than normal operation. This causes also instability and fluctuation within the system. This can result in equipment malfunction, reduced the efficiency and potential damage of sensitive devices. In these types of fault current from the inverter is very high. Due to higher current electrical component such as transformer, generators, cables are subjected to higher stress and heat. This can be accelerated wear and tear, reduce the lifespan of equipment, and increase risk of failures.

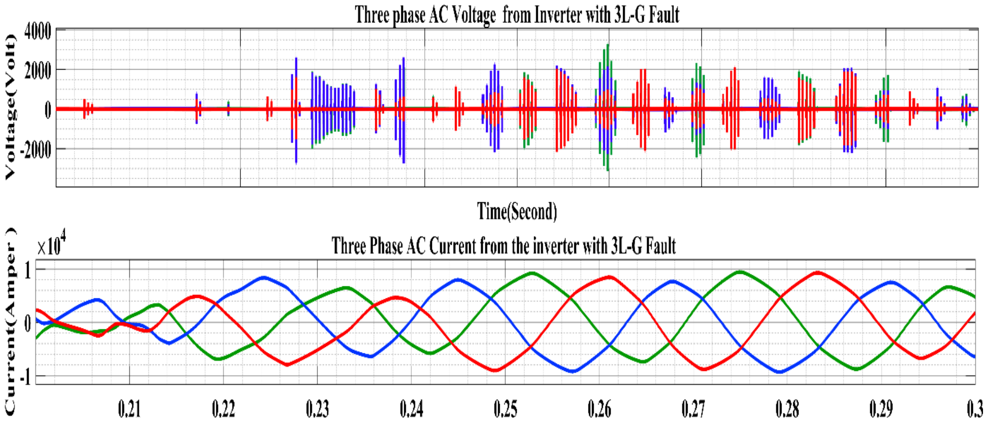

Figure 4-16: Three-phase AC voltage and current from the inverter with 3L-G Fault

4.6 Three -phase Voltages and current from grid with 3L-G Three -phase Faults.

Figure 4-17 shows the three-phase AC Voltage and Current generated from grid 3 L-G types of faults. I.e. during the fault operation of the system and without the application of STATCOM the grid voltage is very low and special one-line voltage is very low and the current from the grid is much higher than in normal operation. This causes also instability and fluctuation within the system. This can result in equipment malfunction, reduced efficiency, and potential damage to sensitive devices. Also, in these types of faults current from the grid is very high. Due to higher current electrical components such as transformers, generators, and cables are subjected to higher stress and heat. This can accelerate wear and tear, reduce the lifespan of equipment, and increase the risk of failures.

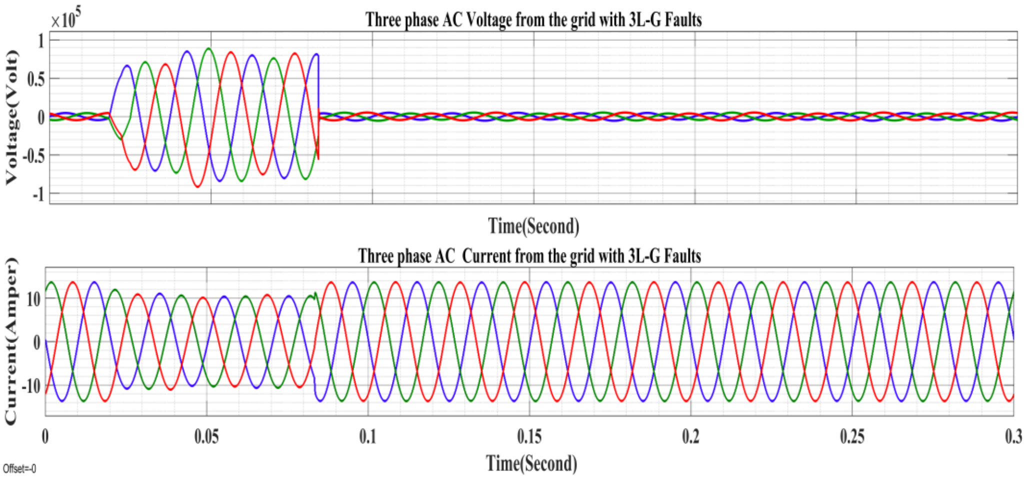

Figure 4-17:Three-phase AC voltage and current from the grid with 3L-G Fault

4.7 Grid Side Converter during Different types of faults with STATCOM

During the fault, the system is automatically isolated from the normal operation due to instability of the Voltage. During this fault through capability is required. To fulfil this requirement STATCOM is designed. Due to the natural and man-made when different types of faults are happened different result of instability happened on the grid voltage and inverter side voltage. In this thesis, L-G, L-L-G, and 3L-G types of faults are considered and result in different types of instability during this voltage from the grid is minimized to 200kv, 150kv, and 80kv respectively. When the faults happened then STATCOM automatically on and regulating the voltage and return to its normal operation until the fault is recover by adjust their output to inject or absorb reactive power, addressing sudden voltage drops or rises caused by faults. When the fault is recovered STATCOM is automatically off and its returns to normal operation. After STATCOM is applied to the system three types of faults are solved and the system acts as a normal operation.so enhancing fault ride through capability of wind energy conversion system is obtained.

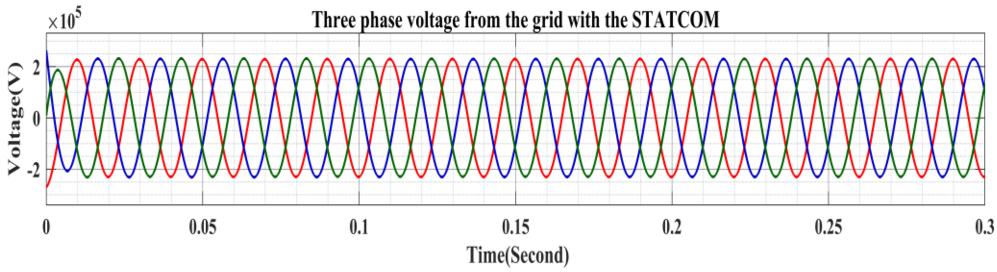

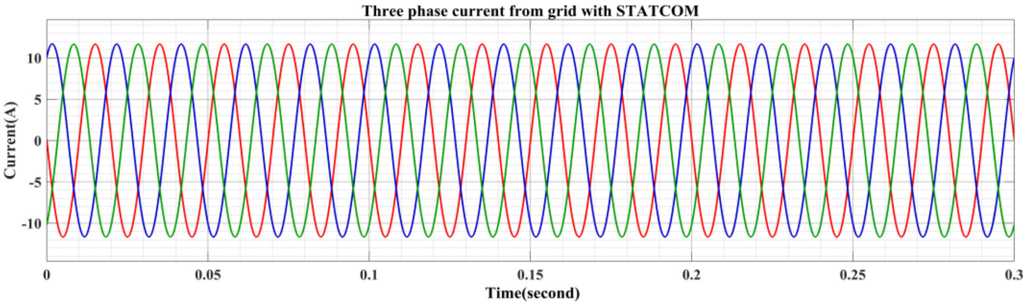

Figure 4-18: Three phase voltage and current from the grid with STATCOM

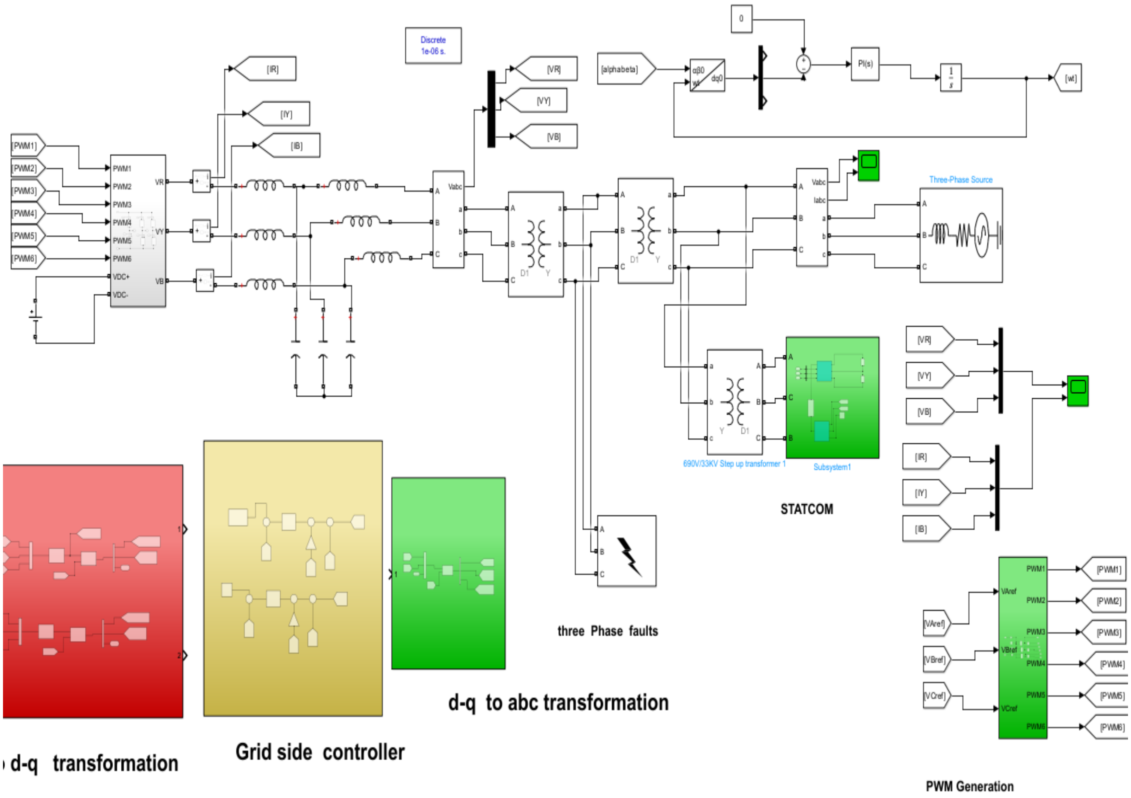

Figure 4-19: Grid Side Convertor during different types of faults with STATCOM

CHAPTER FIVE

CONCLUSION AND RECOMMENDATION

5.1 Conclusion

In this thesis, three types of fault is considered such as L-G .2L-G and 3L-G .When this fault is happens to the system at normal operation, the voltage at the grid is minimized from 230kv to 200 kv, 150 kv ,80 kv respectively . Due to the voltage sag system is being unstable, fault ride through capability is necessary. In this thesis, the design of a PI controller for enhancing the fault ride-through capability of a grid-connected PMSG-based wind energy conversion system has been investigated comprehensively. Through the examination of various types of faults, including grid disturbances and system faults, coupled with the utilization of a fault-tailored STATCOM, significant strides have been made in mitigating the adverse effects of faults on system performance. When the faults happened STATCOM automatically turned on and regulated the voltage and returned to its normal operation (230kv) until the fault is recovered by adjusting their output to inject or absorb reactive power, addressing sudden voltage drops or rises caused by faults**.** When the fault is recovered, STATCOM is automatically off and its returns to normal operation. After STATCOM is applied to the system, three types of faults are solved, and the system acts as a normal operation**.**so enhancing fault ride through capability of wind energy conversion system is obtained.

5.2 Recommendation

For future research endeavours focusing on enhancing the fault ride-through capability of grid-connected PMSG-based WECS with the integration of fault-designed STATCOM and optimal controllers, several recommendations can be proposed:

- Investigate the application of advanced control strategies, such as model predictive control (MPC), adaptive control, and nonlinear control techniques, to further improve the fault ride-through capability of the system. These strategies can offer enhanced performance and robustness under diverse fault scenarios and operating conditions
- Explore the integration of multi-agent systems (MAS) to enable decentralized control and coordination among various components within the WECS and the

grid. MAS can facilitate dynamic decision-making and communication among distributed controllers, enhancing system resilience and adaptability to fault events.

By pursuing these recommendations, researchers and practitioners can contribute to advancing the state-of-the-art in fault ride-through enhancement for grid-connected PMSG-based WECS, ultimately facilitating the integration of renewable energy resources into the grid and enhancing grid resilience and stability

REFERENCE

Akter, P., Uddin, M., Mekhilef, S., Tan, N. M. L., & Akagi, H. (2015). Model predictive control of bidirectional isolated DC-DC converter for energy conversion system. *International Journal of Electronics*, *102*(8), 1407–1427. https://doi.org/10.1080/00207217.2015.1028479

Alabdali, Q. A., Bajawi, A. M., Fatani, A. M., & Nahhas, A. M. (2020). Review of Recent Advances of Wind Energy. *Sustainable Energy*, *8*(1), 12–19.

AlGhamdi, S. A. (2023). Improvement of Fault Ride-Through Capability of Grid Connected Wind Turbine Based on a Switched Reluctance Generator Using a Dynamic Voltage Restorer. *Sustainability (Switzerland)*, *15*(14). https://doi.org/10.3390/su151411061

Algaddafi, A., Alshahrani, J., Hussain, S., Elnaddab, K., Diryak, E., & Daho, I. (n.d.). *6 1*, *2*, *3*. 2144–2150.

Alhammad, H. I., & Habiballah, I. O. (2021). Fault Ride Through for Solar Photovoltaic and Wind-Turbine Integrated Distribution Network: A Systematic Review. *International Journal of Engineering Research & Technology (IJERT) Www.Ijert.Org*, *10*. www.ijert.org

Babu, B., & Divya, S. (2017). Comparative study of different types of generators used in wind turbine and reactive power compensation. *IOSR Journal of Electrical and Electronics Engineering*, 2320–3331. www.iosrjournals.org

Berhanu, M., Mekonnen, Y., Leidhold, R., Mamo, M., Muluneh, Z., & Sarwat, A. (2018). Analysis of a Doubly Fed Induction Generator Through Modeling and Simulation. *2018 IEEE PES/IAS PowerAfrica, PowerAfrica 2018*, 652–657. https://doi.org/10.1109/PowerAfrica.2018.8521094

de Azevedo, I. A., & Barros, L. S. (2021). Comparison of control strategies for squirrel-cage induction generator-based wind energy conversion systems. *2021 14th IEEE International Conference on Industry Applications, INDUSCON 2021 - Proceedings*, *August*, 790–796. https://doi.org/10.1109/INDUSCON51756.2021.9529574

El Kassoumi, A., Lamhamdi, M., Mouhsen, A., & Mouhsen, A. (2022). Maximum Power Generation and Pitch Angle Control of a PMSG-Based WECS Connected to the Grid.

Lecture Notes in Networks and Systems, *455 LNNS*(December), 696–705. https://doi.org/10.1007/978-3-031-02447-4_72

Gambhir, J., Thakur, T., & Chawla, P. (2015). *Modeling and Analysis of DFIG Based Wind Power System Using Instantaneous Power Components*. *9*(8), 908–913.

Gatavi, E., Supervisor, M., Co-supervisors, A. H., & Rizk, J. (2019). *Voltage Regulation and Reactive Power Compensation to Improve Low Voltage Ride-Through Capability for Doubly Fed Induction Generator-based Wind Turbine*. *August*.

Hamdan, I., Ibrahim, A. M. A., & Noureldeen, O. (2020). Modified STATCOM control strategy for fault ride-through capability enhancement of grid-connected PV/wind hybrid power system during voltage sag. *SN Applied Sciences*, *2*(3), 1–19. https://doi.org/10.1007/s42452-020-2169-6

Han, C., Huang, A. Q., Baran, M., Bhattacharya, S., Litzenberger, W., Anderson, L., Johnson, A., & Edris, A. A. (2006). STATCOM impact study on the integration of a large wind farm into a weak loop power system. *2006 IEEE PES Power Systems Conference and Exposition, PSCE 2006 - Proceedings*, 1266–1272. https://doi.org/10.1109/PSCE.2006.296488

Hong, Y., Nguyen, M., Zeng, H., Chang, Y., Lee, Y., & Lin, C. (2018). *Studies on Optimal Controller Design of STATCOM in Power System with Large Wind Farms*. *1*, 708–714.

Hwas, A., & Katebi, R. (2012). Wind turbine control using PI pitch angle controller. *IFAC Proceedings Volumes (IFAC-PapersOnline)*, *2*(PART 1), 241–246. https://doi.org/10.3182/20120328-3-it-3014.00041

Mahersi, E., Khedher, A., & Mimouni, M. F. (2013). The wind energy conversion system using pmsg controlled by vector control and smc strategies. *International Journal of Renewable Energy Research*, *3*(1), 41–50.

Moness, M., & Moustafa, A. M. (2016). A Survey of Cyber-Physical Advances and Challenges of Wind Energy Conversion Systems: Prospects for Internet of Energy. *IEEE Internet of Things Journal*, *3*(2), 134–145.

Muisyo, I. N., Muriithi, C. M., & Kamau, S. I. (2022). STATCOM Controller Tuning to Enhance LVRT Capability of Grid-Connected Wind Power Generating Plants. *Journal* *of Electrical and Computer Engineering*, *2022*. https://doi.org/10.1155/2022/2873053

Muisyo, I. N., Muriithi, C. M., & Kamau, S. I. (2022). Enhancing low voltage ride through capability of grid connected DFIG based WECS using WCA-PSO tuned STATCOM controller. *Heliyon*, *8*(8), e09999. https://doi.org/10.1016/j.heliyon.2022.e09999

Navarrete, E. C., Trejo Perea, M., Jáuregui Correa, J. C., Carrillo Serrano, R. V., & Moreno, G. J. R. (2019). Expert Control Systems Implemented in a Pitch Control of Wind Turbine: A Review. *IEEE Access*, *7*, 13241–13259. https://doi.org/10.1109/ACCESS.2019.2892728

Ofualagba, G., & Ubeku, E. U. (2008). Wind energy conversion system-Wind turbine modeling. *IEEE Power and Energy Society 2008 General Meeting: Conversion and Delivery of Electrical Energy in the 21st Century, PES*, *October*. https://doi.org/10.1109/PES.2008.4596699

Pavan Kumar, Y. V., & Bhimasingu, R. (2021). Design of voltage and current controller parameters using small signal model-based pole-zero cancellation method for improved transient response in microgrids. *SN Applied Sciences*, *3*(11). https://doi.org/10.1007/s42452-021-04815-x

Pramujati, B., Nurhadi, H., & Patriawan, D. A. (2015). *A-Study-on-the-Effect-of-an-Attractive-and-a-Repulsive-Forces-with-Feedback-Control.docx*. *August*.

Shuaibu, M., Abubakar, A. S., & Shehu, A. F. (2021). Techniques for ensuring fault ride-through capability of grid connected dfig-based wind turbine systems: A review. *Nigerian Journal of Technological Development*, *18*(1), 39–46. https://doi.org/10.4314/njtd.v18i1.6

Syahputra, R., & Arrozak, L. F. (2017). Power Transformer Loading Analysis in Order to Improve the Reliability of a Substation. *Journal of Electrical Technology UMY*, *1*(4), 165–175. https://doi.org/10.18196/jet.1422

Tarafdar Hagh, M., Roshan Milani, A., & Lafzi, A. (2008). Dynamic stability improvement of a wind farm connected to grid using STATCOM. *5th International Conference on Electrical Engineering/Electronics, Computer, Telecommunications and Information Technology, ECTI-CON 2008*, *2*(June), 1057–1060. https://doi.org/10.1109/ECTICON.2008.4600614

Tamaarat, A. (2019). Active and Reactive Power Control for DFIG Using PI, Fuzzy Logic and Self-Tuning PI Fuzzy Controllers. *Advances in Modelling and Analysis C*, *74*(2–4), 95–102. https://doi.org/10.18280/ama_c.742-408

Vijayaprabhu, A., Bhaskar, K. B., Jasmine susila, D., & Dinesh, M. (2021). Review and Comparison of Various Types of Generation Using WECS Topologies. *IOP Conference Series: Materials Science and Engineering*, *1177*(1), 012004. https://doi.org/10.1088/1757-899x/1177/1/012004

Zebraoui, O., & Bouzi, M. (2018). Comparative study of different MPPT methods for wind energy conversion system. *IOP Conference Series: Earth and Environmental Science*, *161*(1). https://doi.org/10.1088/1755-1315/161/1/012023

Zheng, X., Qiu, K., Hou, L., Liu, Z., & Wang, C. (2018). Inverter with a Passive Damped LCL Filter. *2018 13th IEEE Conference on Industrial Electronics and Applications (ICIEA)*, 739–744.

Zorich, R., & Garberville, P. O. B. (2023). *Brief communication : Betz ' s Law : the Zorich Derivation*. *1*, 1–9.

Zouheyr, D., Lotfi, B., Thierry, L., & Abdelmadjid, B. (2021). Grid Side Inverter Control for a Grid Connected Synchronous Generator Based Wind Turbine Experimental Emulator. *European Journal of Electrical Engineering*, *23*(1), 1–7. https://doi.org/10.18280/ejee.230101

Document ID: 66eae2560205d05849cfe3b7
Document Name: Gutema Gudunfa thesis after defence
Document Pages: 104

Document Status: Completed
Document Completion Date: September 18, 2024, 14:25 UTC

Signer: almaz (almaztekle24@gmail.com)

Signer	Signature	Timestamps
almaz almaztekle24@gmail.com Using IP: 196.189.127.157 IP Location: Ethiopia, Addis Ababa Authentication method: Email		Viewed: September 18, 2024, 14:25 UTC Signed: September 18, 2024, 14:25 UTC